

Physical and Numerical Modelling of The Dam-Break Evolution in an area with Vegetation



Dipartimento di Ingegneria dell'Ambiente, del Territorio e delle Infrastrutture
POLITECNICO DI TORINO

Universidade de Vigo

Departamento de Física Aplicada – Área de Física de la Tierra
UNIVERSIDADE DE VIGO

Supervisors

Prof. Eng. Davide Poggi
Dr José Manuel Domínguez Alonso
Eng. Silvia Cordero

Candidate
Marco Accoto

*Se cerchi la tua strada verso Itaca
spera in un viaggio lungo,
avventuroso e pieno di scoperte.
I Lestrigoni e i Ciclopi non temerli,
non temere l'ira di Poseidone.
Pensa a Itaca, sempre,
il tuo destino ti ci porterà.
Non hai bisogno di affrettare il corso,
fa' che il tuo viaggio duri anni, bellissimi,
e che tu arrivi all'isola ormai vecchio,
ricco di insegnamenti appresi in via.
Non sperare ti giungano ricchezze:
il regalo di Itaca è il bel viaggio,
senza di lei non lo avresti intrapreso.
Di più non ho da darti.
E se ti appare povera all'arrivo,
non t'ha ingannato.
Carico di saggezza e di esperienza
avrà capito cos'è Itaca.*

Abstract

The importance of collecting water has always represented an interesting topic for all the populations throughout years. The possibility to catch and store it has represented a necessary thing for different reasons: crops, fauna, flood control and in the last century a valid alternative for the generation of electricity and recreational uses. The most common way to store it are the dams, from small to the bigger ones.

This work deals with the study of the behaviour in case of failure of dams, and in particular focusing on the smaller. What is interesting in this is that for big dams the wave generated by the collapse of the weir does not take into account the presence or not of elements in the valley area. In fact, what generally happens is that the wave carries everything with it, due to the high head of the free surface and the high velocities reached along the way.

In the case of small dams, the behaviour of the wave is completely different and the presence of elements in the downstream area can affect its development in a proper way. This is proved by the experimental work conducted at the Giorgio Bidone Hydraulics Laboratory at the Politecnico di Torino using the physical model built for the purpose. In fact, four different experiments using two types of roughness were done in the month of March 2019. The setup of the panels representing roughness could be used with an inclination of 0 degrees or 45 degrees.

The second part of this work is related to the description and use of SPH (*Smoothed Particle Hydrodynamics*), a numerical model used to simulate the experiments under study. All the data collected from the physical model are compared with SPH in order to validate SPH. This model is based on a mesh-less method in which the fluid is described as a group of particles. SPH is based on the solution of Navier-Stokes equations, continuity equation and momentum equation, using information of the neighbouring particles to detect all the quantities searched.

The aims of the study are: validation of SPH and evaluation of the hazard related to dam-breaks event for small reservoirs.

Table of Contents

1	Introduction	1
1.1	Small and medium dams: the case of USA	2
1.2	Small and medium dams: the case of Australia.....	4
1.3	Small and medium dams: the case of Italy (ALCOTRA-RESBA project).....	5
1.3.1	Risk assessment.....	6
1.4	Aim of the thesis	8
2	Status Report	9
2.1	Dam-Break Flows: Acquisition of Experimental Data through an Imaging Technique and 2D Numerical Modeling	10
2.2	Numerical simulation of dam-break flows using depth-averaged hydrodynamic and three-dimensional CFD models	12
2.3	Experimental validation of a 3D SPH model for the simulation of a dam-break event involving multiple fixed and mobile bodies.....	15
2.4	Modeling flood shock wave propagation with the smoothed particle hydrodynamics (SPH) method: an experimental comparison study	19
3	The experimental Model	23
3.1	Physical Model.....	24
3.1.1	Framework of the model.....	25
3.1.2	Reservoir and tank	26
3.1.3	Water	26
3.1.4	The Ultrasonic Probes	27
3.1.5	The Sluice Gate.....	28
3.1.6	The Led Lightning	30
3.1.7	The high-resolution Cameras	30
3.1.8	The downstream area	33
4	The experimental tests.....	35
4.1	How to deal with the physical model	36
4.2	Wave front analysis.....	38
4.3	Velocity analysis.....	41
4.4	Lambert-Beer law and the evaluation of heights	47
4.5	Theoretical analysis of the upper part of the free surface profile in proximity of a rectangular orifice	50
5	The numerical model.....	55
5.1	Smoothed Particle Hydrodynamics Method	56
5.1.1	The smoothing kernel.....	57
5.1.2	Momentum Equation	59
5.1.3	Continuity Equation.....	60
5.1.4	State Equation	60
5.1.5	Time Stepping.....	61
5.1.6	Boundary Conditions	62
5.2	DualSPHysics code	63

5.3	Initial Conditions & Pre-processing.....	65
5.4	Running DualSPHysics & Post-processing	68
5.4.1	PartVTK	69
5.4.2	MeasureTool	69
5.4.3	Flow computation (FlowTool)	69
5.5	Validation	71
5.5.1	Experiment.....	71
5.5.2	Numerical setup.....	71
5.5.3	Results.....	73
6	Numerical study of the Dam-Break	77
6.1	Test with Flat Bottom.....	78
6.1.1	Numerical setup.....	78
6.1.2	Results (VALIDATION)	80
6.1.3	Improving efficiency.....	82
6.1.4	Evaluation of the water depth	86
6.2	Tests with different roughness	88
6.2.1	Numerical setups	88
6.2.2	Results of the wave fronts	89
6.2.3	Comparison of the upper part of the free surface profile in proximity of the gate for experiment and different numerical models.....	95
6.3	Evaluation of the vulnerability for flat bottom test	97
7	Conclusion and future perspective	99
	Bibliography	105

Chapter 1

Introduction

The importance of water for the human being is known since day one and the methods through people catch and store it are various. One of the main, particularly in the mountain and hill-side areas is the water catchment conveyed to dams.

Most of the existing dams have been built in the twentieth century, starting from the 1950¹. According to the increasing of the worldwide population it all started from a need to storage water, generate electricity, irrigation, control the downstream flowrate after high intensity rainfall and last but not the least for navigation and to recreate a new habitat for fish and plants. The nature of dams depends on the purpose of the construction itself.

In fact, four major families can be identified:

- Storage dams: realized where there is a high flow of the river (or rivers) that goes (go) to the reservoir. These dams are supplied by the high rainfall of the area. Their aim is to produce electricity through hydroelectric power station, crops, flood control, generation of artificial snow, creation of a new habitat regarding fish life and plants, etc. Volumes stored are quite high.
- In the previous family can be added the coffer dams, which are smaller dams built upstream in order to help the construction of the main dam.
- Diversion dams: their main purpose is to reduce the flow rate downstream in case of high intensity rainfall and the water is gradually released with a controlled flow. This is necessary to prevent from inundation, according to the flow rate of the downstream channel. These dams are generally small or medium with a small volume stored. In this case free surface canals are used to divert water.
- Detention Dams: used to reduce the flood at downstream with a gradual release of the water stored. It is necessary to protect the downstream channel natural floor from excavation, due to the water jet, through unshaped rocks placed just under the dam.

Another way to consider dams is the material whom they are made of. This led to a new major classification: earthfill dams and concrete dams.

The Italian territory is extremely various, from mountainside to seaside, and consequently the variety and the number of dams is really high. And again, in this variety it is necessary to distinguish between three types of dams.: there are small, medium and large dams. In fact, after the publication of the: Circolare Ministero dei Lavori Pubblici 19 aprile 1995, n. us/482 “Dighe di ritenuta - Competenze in materia di vigilanza sulla progettazione, la costruzione e l'esercizio” and “Decreto Legislativo 31 marzo 1998, n. 112 “Conferimento di funzioni e compiti amministrativi dello Stato alle regioni ed agli enti locali, in attuazione del capo I della legge 15 marzo 1997, n.59. Ecologia”, there has been a new way to identify dams. Starting from the 1998 and thereafter, large dams are the ones whom the height, starting from the lowest point of the downstream face to the top of the

¹ ICOLD World Registers of Dams (2013)

dam, is equal or over 15 meters and the volume is at least equal to one million cubic meters.

These splitting is due to the fact that, in Italy, small and medium dams are under the regional control, whether for the larger ones, the region in which the dam has been built, lose the jurisdiction above it. In fact, for big dams there is a national competence.

However, the most dangerous aspect related to dams is their collapse. There are different kinds of collapse: overtopping, piping, earthquake's consequence or failure of the substructure. This is related to the material which composes the dam: there can be earth dams or concrete dams.

1.1 Small and medium dams: the case of USA

The case of the study for dams in the USA has been covering an interesting topic in the second part of the XX century. In particular, starting from the 1994 a database on all the dams in the USA has been released from the Stanford University in the National Performance of Damns Program (NPDP). In this database are collected all the information about the dams all over the world and focusing just upon the American ones, there are 85,225 damns (Up-to-date list at 2015-10-12 in the official site of the Stanford University http://npdp.stanford.edu/dams_database).

Dams have been always considered as a getaway to industrialization, urbanization and agriculture expansion.

The two main categories are the small and large dams. A dam can be considered as large dam if the height is equal to 15 meters or over. All the others are considered as small dams. As can be seen in the following image, the owners of the dams are various and:

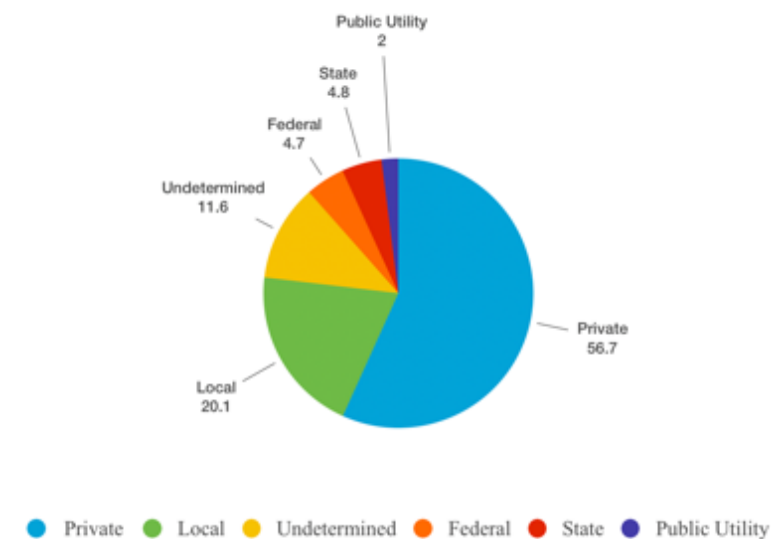


Figure 1.1: Nature of dam ownership in the USA. Data taken from the FEMA.

“Given the diffuse nature of dam ownership versus regulation in the United States, it is apparent that dam safety and security are often not solely a federal, state or local issue.” As stated by the FEMA (<https://www.fema.gov/dam-ownership-united-states>)



Figure 1.2: Main uses of the American Dams documented by the FEMA.

In fact, most of the them are private dams reaching a value of 57%. The use of these dams is various: from the hydroelectric, flood control, recreational service, mine tailings service and in some cases navigation. A single use for a dam is considered rare. In particular, as documented by the FEMA, the most powerful use of dams in the USA is represented by the recreational service. All over the world and in the United States as well, these artificial lakes are recording a more and more tourist traffic, representing a valid alternative to the overcrowded seashore regions. After this kind of use, flood control and fire and farm ponds are the main uses of the widespread reservoirs in this country.

Focusing just upon the small dams (*height < 15m*), the NPDP database has recorded 72,265 of them, showing an enormous gap between the United States and the other countries all over the world as can be seen in the following image.

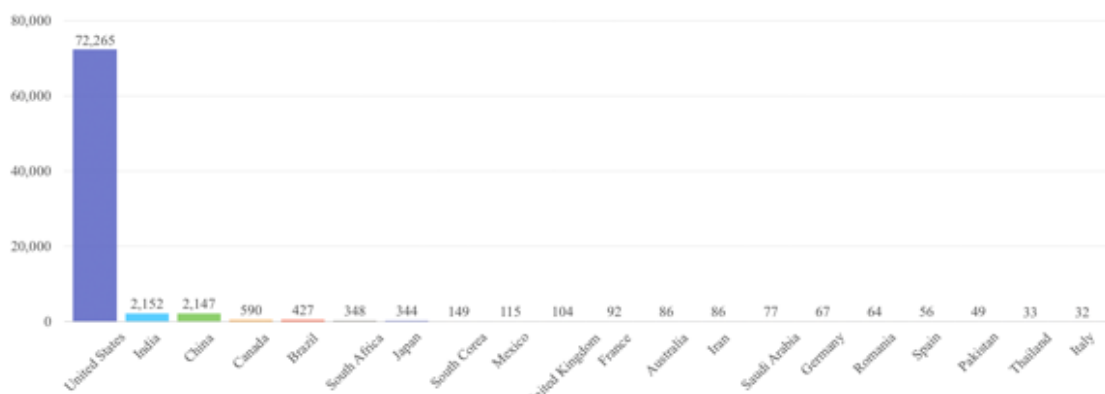


Figure 1.3: Database of the NPDP of main twenty countries in number of dams.

The other countries represent the main countries in number of dams and there can be noticed the enormous difference. But the government of the United States is the supporter to the creation of the database by NPDP, and this leads to consider as reliable the number of small dams just in their own country; instead for the others, the number cannot be considered as real.

Moving now to the larger dams, 5680 are detected and they are owned by the state, federal and local organization, although they share the same purpose as the smaller ones.

In this case the ownership plays an important role because, as suggested by Mark Ogden in an interview by the New York Times in the February of 2017:

“The larger dams are being watched very carefully. The smaller dams don’t enjoy that level of scrutiny”.

This could mean that most of the small dams in the United States have not been analyzed as they should or not been analyzed at all. This leads to the consideration that if the considered dam has not faced any problem till the moment in which is analyzed, then it could have no need of maintenance or surveillance. Furthermore, in the article is stressed the fact that most of the dams in the United States, 70%, are now passing the half of the years of the operating life in accordance to the American Society of Civil Engineers analysis.

1.2 Small and medium dams: the case of Australia

Different is the case for Australia. Apart from the larger dams, small and medium ones are farm dams: this means that private owners, usually contractors, should provide a good maintenance but more often they tend to neglect the need for reviewing their dams. Moreover, they usually are farmers and landowners and they do not have the competence and knowledge necessary to build a safe construction. They believe that if their dam is not failed up till that moment, it will never fail. Must be considered the fact that for larger dams there is a worldwide spread news and more attention is paid on it. But it is true that small and medium dams have a higher probability of failing than the others, due to a lack of maintenance, surveillance and in some cases an inappropriate design. This leads to a high probability of failure throughout years with a considerable damage in terms of human lives and environmental disasters in the downstream area.



Figure 1.4: Two Australian States with contrasting dam management practices: Tasmania and South Australia
Source: Tingey-Holyoak et al., 2012.

Furthermore, it is obvious to consider all the problems related to the wildlife habitat upstream too. It is well known that no construction can be realized one-hundred percent safe because of the non-perfect human work, materials behaviour and construction processes, with no exception for dams.

In Australia, there are about 480'000 farm dams. Focusing on only two main areas, South Australia and Tasmania, there can be seen the different behaviour in terms of policy. Just in Tasmania, there is over the 30% of the water storage capacity and more than 8'000 farm dams.

But in Tasmania there is a policy that consists in:

- Having an update list of all dams;
- A specific regulation that imposes control in the construction, maintenance and inspections;
- Recording all the information above one dam.

Different is the case for South Australia and there is no regulation about small dams. A follow up of the existing dams recorded a worse and worse situation with lack of maintenance, with an increasing percentage of failure.

All of this, lead to the consideration that there is a great gap between nations of the same continent. This is not the only case existing and a greater attention should be paid on it.

1.3 Small and medium dams: the case of Italy (ALCOTRA-RESBA project)

Moving back to Europe, it necessary to say that the situation in quite the same. Every nation has its own laws and rules above the reservoirs. Every nation maintains and inspects them in its own way. Common base rules should be introduced.

Following this path, a case is represented by the ALCOTRA-RESBA project. It has been developed starting from the 2014 in a project between Italy and France. The project is one of the studies in the main RESBA project developed by the Politecnico di Torino (DIATI department). Its aims are to:

- Create a trait d'union, based on technical knowledge and good manners between the two nations;
- Define technical rules for design, implementation, use and maintenance of these small and medium reservoirs built by the frontier line;
- Help the local communities in the creation of emergency plans.

A brief consideration on large dams is necessary. In fact, they are in mountain-side area and the dam-break wave generated can be approximated as a one-dimensional wave with a growth along the valley. In this case the modelling of the wave is easier and good solutions are already developed, one of them is the Ritter analysis (Ritter, 1892).

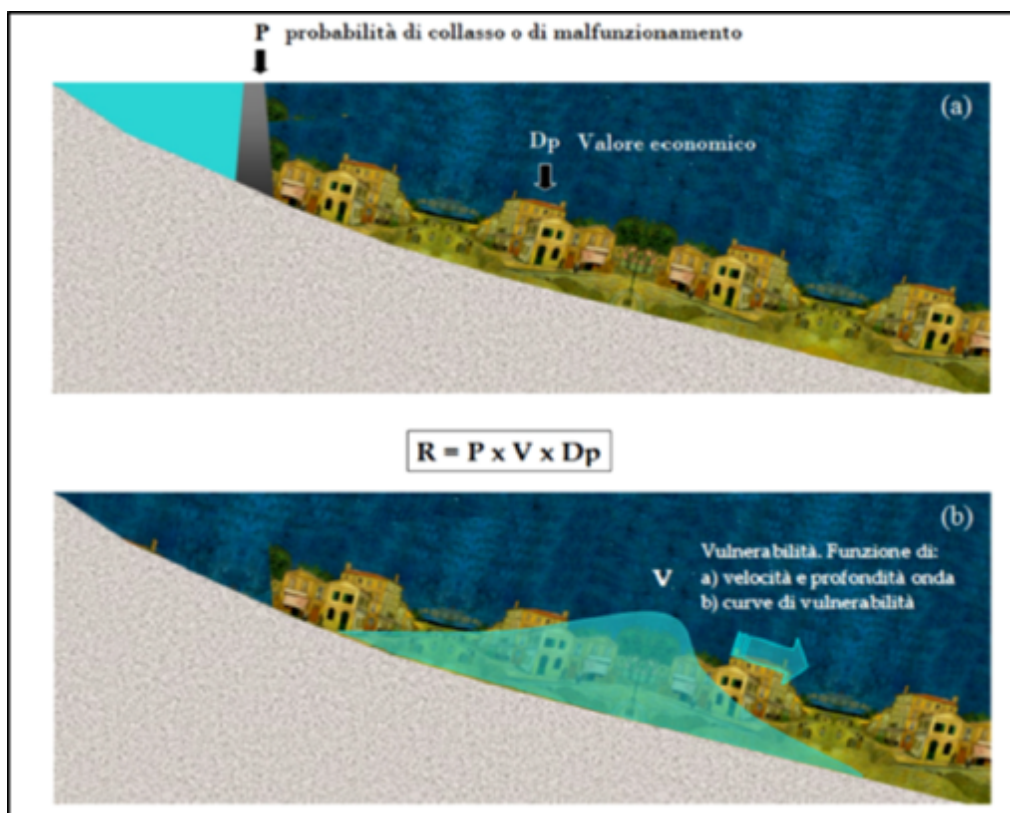
But this project, ALCOTRA-RESBA, focuses on small and medium dams, which are often used for irrigation, production of electricity or for the production of artificial snow. They usually are in hill-side areas or in open valleys and the boundary conditions are different: the wave grows up on the transversal direction too and the one-dimensional analysis cannot be used. Furthermore, the downstream area is, in most of the cases, represented by the crops and in general by vegetation. It has an important role in the development of the wave, its front and the velocity based on the density of the vegetation.

The volume stored is quite low but considering the fact that the wave could propagate along the transversal direction means that those are different than the ones generated by large dams. The damage, compared to their dimensions, could be quite high instead.

One of the main tasks of RESBA is the quick method for the evaluation of the wet areas, down to the small and medium regional dams. In fact, the evaluation of the risk needs the knowledge of the wet areas, the damage related to the elements and the associated probability.

1.3.1 Risk assessment

The risk assessment analysis started since the development of the evaluation of the probability. It represents the loss in terms of money related to the vulnerability of the objects, the hazard of an event and the potential adverse consequences. Stressing the fact that the economic analysis is function of the objects and, in general, of the place considered, each case must be analyzed.



As stated in Poggi et al., 2015, in 1984, Varnes edited a report UNESCO in which the definition of the risk is given. It is made up of three terms: the hazard P , vulnerability V and the potential adverse consequences D_p .

In symbols:

$$R = P \cdot V \cdot D_p \quad 1.1$$

And now every single term of the previous equation is analyzed.

- P is the hazard of a certain event of a given intensity happens in an area and in a certain moment. Generally, it is evaluated on an annual scale.
- V is the vulnerability of the object related to a particular event. It is a coefficient that represents the effect of the destroying event on the object considered. Its evaluation is quite difficult because of the elevate number of different factors. In order to overcome the assessment of the factors, value is between 0 and 1. The maximum value is often taken. In the case of a flood event the vulnerability V is described through two terms: the height and the local velocity of the water. These terms allow to consider the different forces that interest the object considered, the floating and drag forces, neglecting the erosion phenomenon, sediment transport, floating elements and deposition on the bed. In this case the evaluation of the vulnerability is given by the following equation:

$$V = u \cdot y \quad \left[\frac{m^2}{s} \right] \quad 1.2$$

Where:

u is the velocity of the water that covers the object considered;

y is the height of the water of the wet area in the nearby of the object considered.

Throughout years different studies and statistics, like Sangrey et al., 1975, Black, 1975, Clausen and Clark, 1990, on masonry building and Federal Emergency Management Office 1979 related to the human being and demonstrating the bad effects of the flood on the objects considered. Focusing on the goods, thanks to the Clausen and Clarks 1990 analysis, threshold values are used:

Simple inundation if the value of uy is less than $3 \text{ m}^2/\text{s}$; local structural damage if the value is between 3 and $7 \text{ m}^2/\text{s}$. If the value of the velocity is less than 2 m/s , it is considered simple inundation.

- D_p is the potential adverse consequences related to the number of objects interested and the value in terms of money loss. The impossibility of giving an economic value to the human life, led to the splitting between human life and objects. For every object a value is assigned and in function of the number of objects the economic loss is evaluated. There are different approaches that let the evaluation of the D_p like the discretized single value, utility functions, empiric formulas, the aggregated approach and the use of a thematic map named CORINE.

As a consequence of this analysis and to evaluate the risk, an estimation of hazard, damage and vulnerability must be done. In particular, per each dam a probability of failure should be evaluated; the dam-break wave intensity must be known considering the distance from the weir; the sensitivity of the elements is a function of the dam-break wave; the economic value of the downstream elements should be easily evaluated. It is necessary to say that all of these data load is not always available. For a quick evaluation analysis, the only hazard or vulnerability evaluation are considered enough adequate as an indicator of the risk of a specific area. This assumption leads to bias that, if it is possible, it is fine to evaluate.

In this case, the equation used is different from the previous and it is:

$$R = P \cdot V \cdot E \quad 1.3$$

In this equation the potential adverse consequences indicator (D_p) is changed with the exposure grade E . Considering the goods a study of the interested area, linked with aerial photo, digital mapping, urban planning, let to evaluate the loss assessment in a qualitative way.

Focusing on a quick evaluation the exposure grade E can be:

- $E1$: no living or non-productive area;
- $E2$: dispersed population, small infrastructures and facilities, farming area;
- $E3$: built-up area, industrial/small business/commercial and tourist area, infrastructure.

A quick way to evaluate the risk index leads to the consideration of three destruction rates: total, significant, partial. Considering a built-up area, for example, it is:

- V_{100} : total destruction which means a 100% loss ($uy=7 \text{ m}^2/\text{s}$);
- V_{70} : significant destruction which means a 70% loss ($uy=3 \text{ m}^2/\text{s}$);
- V_{30} : partial destruction which means a 30% loss ($uy=1 \text{ m}^2/\text{s}$).

Crossing the vulnerability rate with the exposure grade the value of $E \cdot V$ can be multiplied by the hazard P , obtaining the qualitative value of the risk for the considered weir.

1.4 Aim of the thesis

This thesis deals with the main project of the ALCOTRA-RESBA developed by the Politecnico di Torino (DIATI department) in the RESBA project.

The dam-break analysis will be studied in this work using both physical and numerical modelling. One of the aims of the work is to prove the capabilities of the numerical modelling to reproduce the phenomenon under study.

The physical modelling took place at “Giorgio Bidone” Hydraulics Laboratory at the Politecnico di Torino and it is a scale model 1:30, more or less, built as a medium of all the reservoirs that are in the Piemonte Region (only small and medium ones). All the experiments carried out are described in Chapter 4.

On the other hand, the numerical model called Smoothed Particle Hydrodynamics (SPH) model was employed to perform the simulations as stated in Chapter 5.

The experimental results were reproduced with the SPH model and the numerical results in terms of wave front and discharge ratio were compared with the information from the physical tests (Chapter 6).

Chapter 2

Status Report

In general, dams have always represented a sort of hazard in people mind and this is why it has been widely studied throughout years. In each case the boundary condition may be varied in order to simulate different cases in accordance to the experiment considered. For example, the setup may change in each case and both the upstream conditions and the downstream can change. The aim of these experiments is the evaluation of the behaviour of the dam-break wave as soon as the water gushes through the sudden opening of the sliding gate. As a result of the studies the evaluation of the risk is searched with an aim to reduce and minimize to the lowest value of the same.

As already said several studies have been made, but in the variety of experiments is difficult to find one with three-dimensional study of the wave in a vegetated area.

A brief analysis of the status report is given in the following pages. It starts with a bi-dimensional analysis of the reports and then a three-dimensional analysis. To close the status report part a brief description of the analysis made on numerical models on SPH is given.

List of the main papers on the dam-break simulations:

1. Dam-Break Flows: Acquisition of Experimental Data through an Imaging Technique and 2D Numerical Modeling – Aureli et al., 2008.
2. Simulation of dam-break flows using depth-averaged hydrodynamic and three-dimensional CFD models – Rob et al, 2015.
3. Experimental validation of a 3D SPH model for the simulation of a dam-break event involving multiple fixed and mobile bodies – Albano et al., 2014.
4. Modeling flood shock wave propagation with the smoothed particle hydrodynamics (SPH) method: an experimental comparison study – Turhan et al., 2019.

2.1 Dam-Break Flows: Acquisition of Experimental Data through an Imaging Technique and 2D Numerical Modeling

In this paper Aureli et al., 2008, four experiments are described, dealing with the sudden removal of a sluice gate. The analysis is a 2D, considering the fact that the height of the water is not evaluated during the tests. Analytical solutions are not available for the 2D dam-break analysis and so a physical model can lead to results based on evidence.

Four tests have been done:

1. Dam-break on horizontal plane in dry conditions;
2. Dam-break on horizontal plane in wet conditions (0.1 m downstream water);
3. Dam-break on horizontal plane in dry conditions with a submersible obstacle;
4. Dam-break on horizontal plane in dry conditions with a unsubmersible obstacle;

The facility is represented by a rectangular tank divided in two zones, in which the first one is the reservoir and the second one is the downstream plane. After the sudden opening of a sluice gate the water covers up the downstream plane. The height of the water at the starting condition in the reservoir is 0.15 m. The analysis of the wave is done through the use of a high-resolution camera in RAW mode and an imaging technique (similar to the one described in the following pages for the case of this thesis), converting the 16-bit RGB photos into the 8-bit grey space. The fluid was given by water blended with methylene and the bottom of the facility was backlighted. At the end all the experimental data were compared with a 2D finite volume numerical model that belongs to the MUSCL-Hancock centred slope limiter (SLIC). This model is based on the integral form of the 2D shallow water problem.

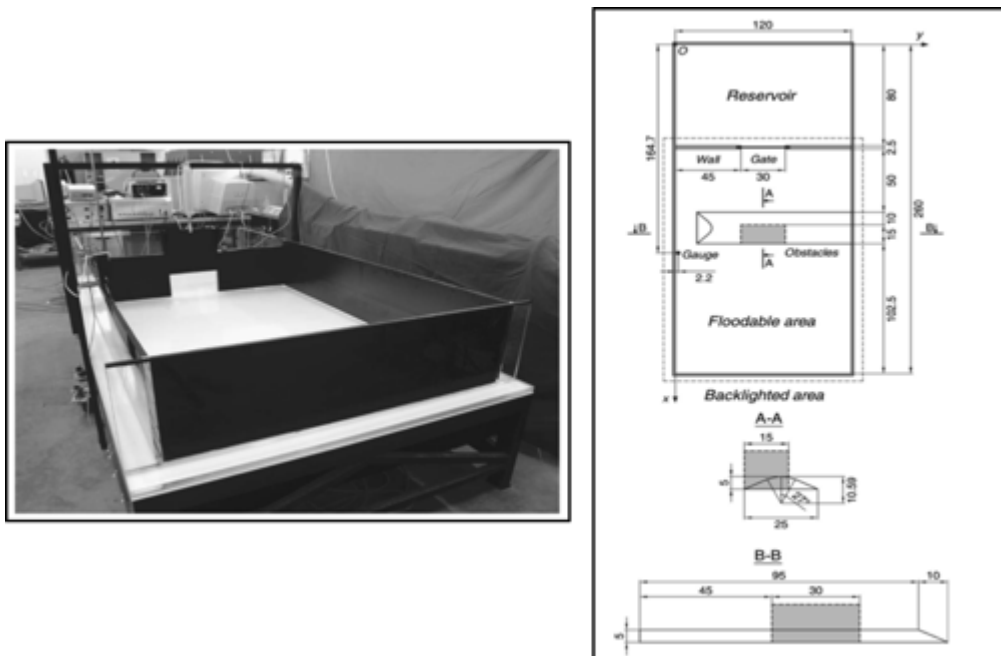


Figure 2.1: Picture of the facility built at the University of Parma and a reconstruction of the facility with the main dimensions. Source: Aureli et al., 2008.

Aim of the analysis is the identification of the values of the water throughout the time of the tests, the evolution of the wave front and the identification of velocity.

The result with a comparison between one of the experimental tests and the numerical model is given below (Figure 2.2).

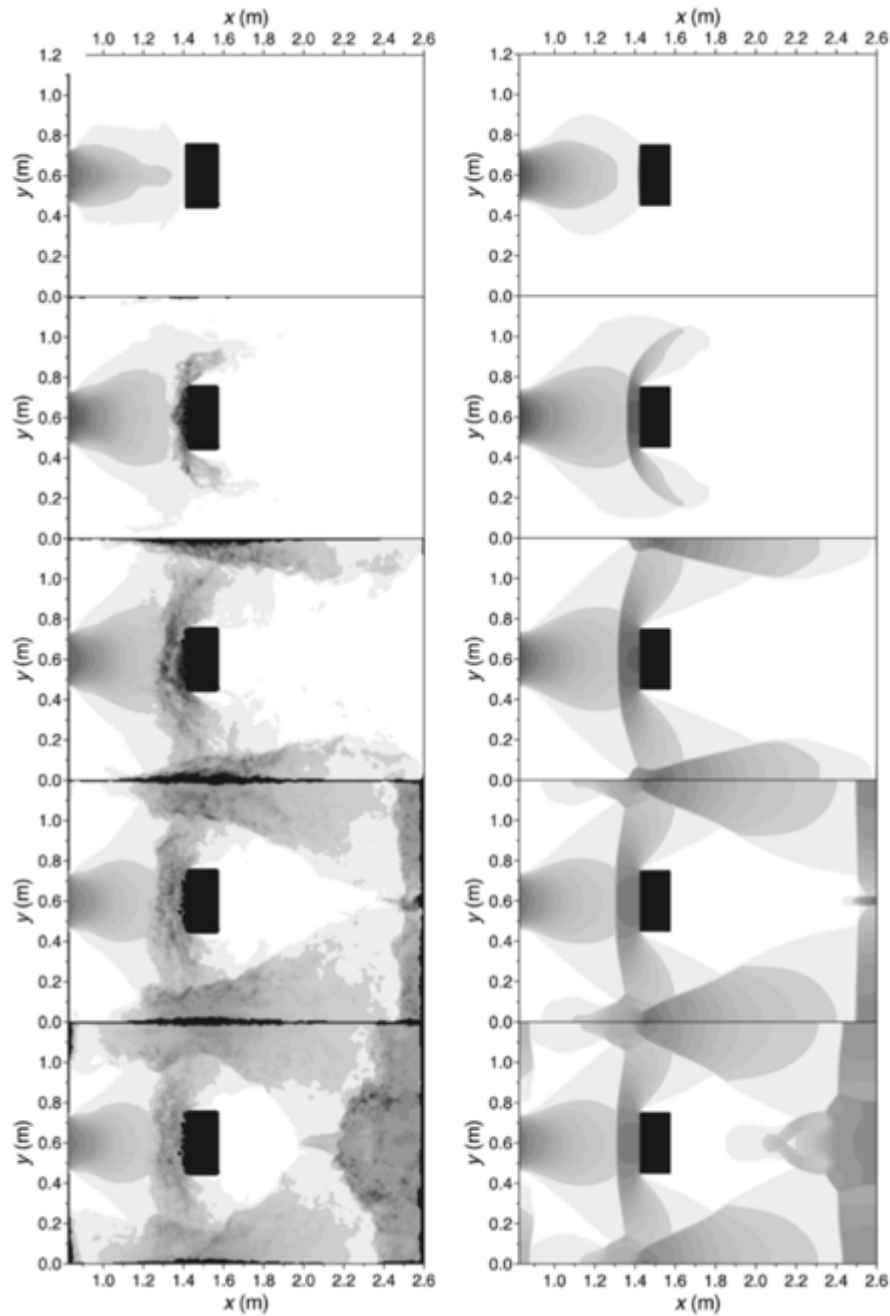


Figure 2.2: Experimental (left) and numerical (right) water depths for test n° 4 at $t=0.40$ s; $t=0.75$ s; $t=1.45$ s; $t=2.16$ s and $t=2.86$ s. Source: Aureli et al., 2008.

The result leads to the conclusion that the numerical model can fit quite good the experimental solution, although an underestimation of the water depths. But in the end the 2D model, with the classical shallow water approximations, can reproduce the main characteristics of the flow.

2.2 Numerical simulation of dam-break flows using depth-averaged hydrodynamic and three-dimensional CFD models

In this paper (Robb et al., 2015), an analysis of the dam-break has been investigated using three different numerical models and compared to the experimental data. In particular, the experimental tests were conducted by Soares-Frazão (2007) and Soares-Frazão and Zech (2007) at the experimental facility of the Hydraulic Laboratory at the Université Catholique de Louvain in Belgium. The first one deals with the analysis of the evolution of the dam-break wave over an irregular topography in dry conditions. The second one has a fixed obstacle rotated by 64° along the side of the flume in wet condition ($h=0.02$ m of water). The aim of this work was to validate the results of numerical models that act in a different way. The models used were: TELEMAC-2D, FLOW-3D and OpenFOAM.

Considering the equations used for the models, there is:

- TELEMAC-2D that is based on the solution of the shallow-water equations, neglecting the vertical velocity and acceleration.
- FLOW-3D is based on the solution of the Navier-Stokes equations along with the volume of fluid (VOF) method, to follow the free-surface at the air-water interface.
- Open-FOAM, same as the previous.

The facility used for the first experiment is in the following figure. All the sizes are in metres and the only existing water downstream is the one in the pool.

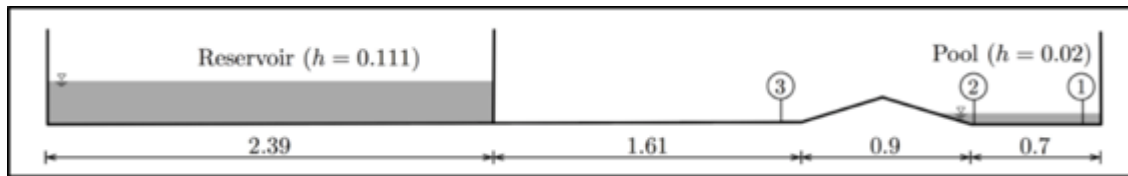


Figure 2.3: Set-up of the experimental test and initial conditions for the Dam-break wave over a triangular bottom sill. The pieces of information about the experiment are evaluated at the gauges 1-3. Source: Robb et al., 2015

The sudden removal of the gate generates a wave moving along the dry bed. Once the wave reaches the bump, a part of it finishes in the pool, whether the other part is just reflected generating a bore that tries to move upstream.

The TELEMAC-2D model uses a triangular mesh and a Manning coefficient of $0.011 \text{ s/m}^{1/3}$, whether both FLOW-3D and OpenFOAM use a hexahedral mesh. For the last two numerical models both a coarser and finer mesh were used, generating the same results: so, the solution can be considered mesh independent.

The results of the numerical models are the propagation of the wave during the experiment, the water level at the three-gauge locations and they are in described in the figure below.

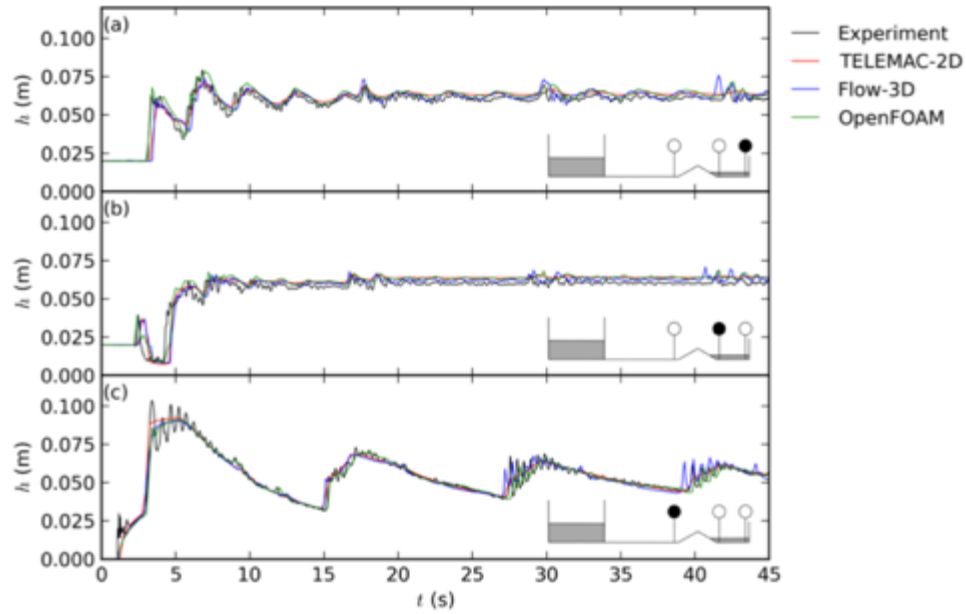


Figure 2.4: Comparison between the experimental and numerical results, for the case of a Dam-break over a dry bed and over a triangle bottom sill. Source: Robb et al., 2015

The second test deals with the analysis of the dam-break wave, flowing over a fixed obstacle. After the impact, the flow changes its behaviour from supercritical to subcritical, forming moving hydraulic jumps. As soon as the wave interacts with the obstacle and the side wall waves, it generates further hydraulic jumps.

The pieces of information about the facility are in the figure below. There are six different points of measurement, with five gauges downstream and one gauge upstream in the reservoir. The initial height downstream is $h=0.02$ m. The water depth evolution was measured using resistive gauges and the velocity is being measured with Acoustic Doppler Velocimeters (ADV). In order to have a complete surface velocity field a high-resolution digital camera was placed above the channel to capture the flow; indeed, the camera has the capability to take 38 frames per seconds. To catch the water velocity a certain quantity of tracers was mixed in the water. The gate opening is about 0.23 s, that can be stated as a sudden opening.

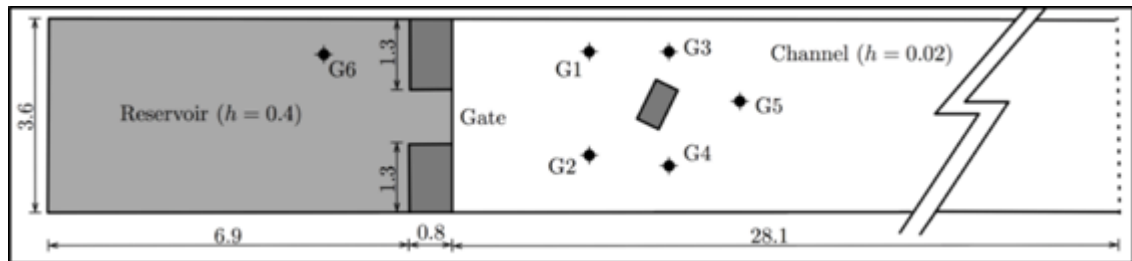


Figure 2.5: Experimental setup in the dam-break wave simulation with an isolated rotated obstacle. All the pieces of information are evaluated at the gauges 1-6. Source: Robb et al., 2015

Different meshes are used between all the numerical models. For the 2D model a roughness coefficient of $0.010 \text{ s/m}^{1/3}$ is used, whether for the 3D models a roughness of 0.0002 m was adopted for the bottom. Furthermore no-slip condition is used.

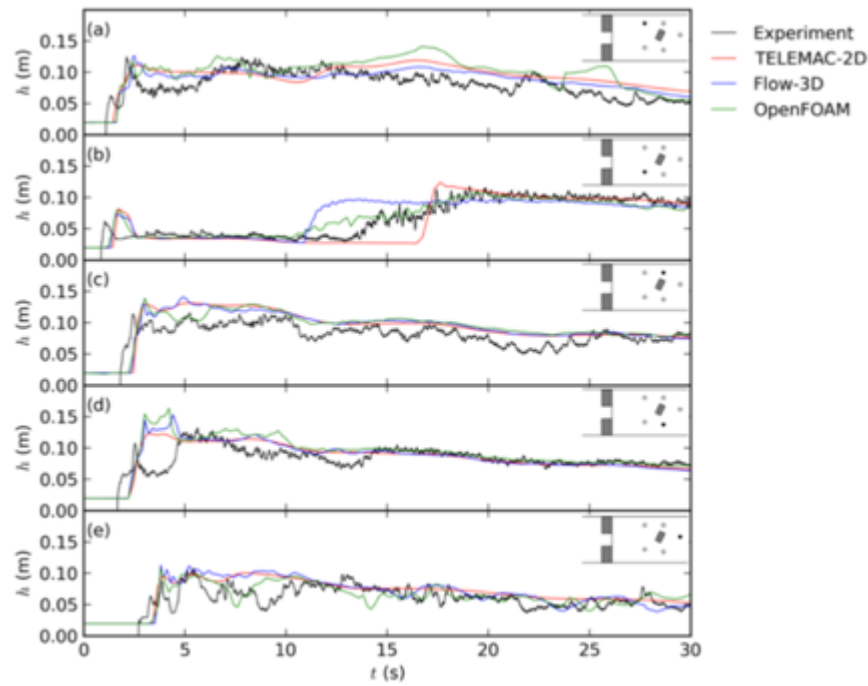


Figure 2.6: Comparison of the results between the numerical and experimental data at the five gauges downstream.
Source: Robb et al., 2015

In the end, as a conclusion of the numerical tests compared to the experimental ones, the numerical solution can reproduce in an optimal way the behaviour of the dam-break wave. In particular the 2D shallow-water model can be enough to predict the water level data. Instead, the 3D models can be used when the obstacles are in the nearby of the gate: this means that an abrupt vertical acceleration is caused by the present of the objects and only a 3D model can detect it.

Some images from the numerical analysis are given below at different times.

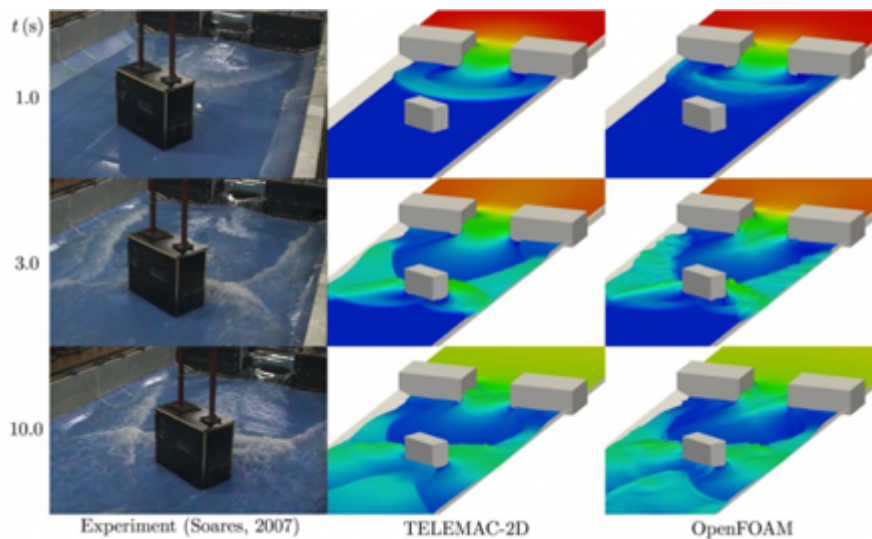


Figure 2.7: Information about the free-surface elevation from 0 m (blue) to 0.4 m (red) at different times: $t=1.0$ s, $t=3.0$ s, $t=10.0$ s. Source: Robb et al., 2015.

2.3 Experimental validation of a 3D SPH model for the simulation of a dam-break event involving multiple fixed and mobile bodies

This paper deals with the validation of the experimental data with a 3D numerical model using *Smoothed Particle Hydrodynamics* (the one used to try to confirm the results of this thesis). Talking about the experimental model, several tests were done and all of them were trying to simulate a dam-break through the opening of a mobile gate. Furthermore, the downstream area was filled with fixed and mobile objects in order to simulate the downstream behaviour. In fact, large debris are influenced by the presence of mobile objects that can amplify the hazard of the event.

The facility was built at the Università degli Studi della Basilicata in the Hydraulics Laboratory. The scale of the model was 1:40 and the size of the experimental model is given in the figure below.

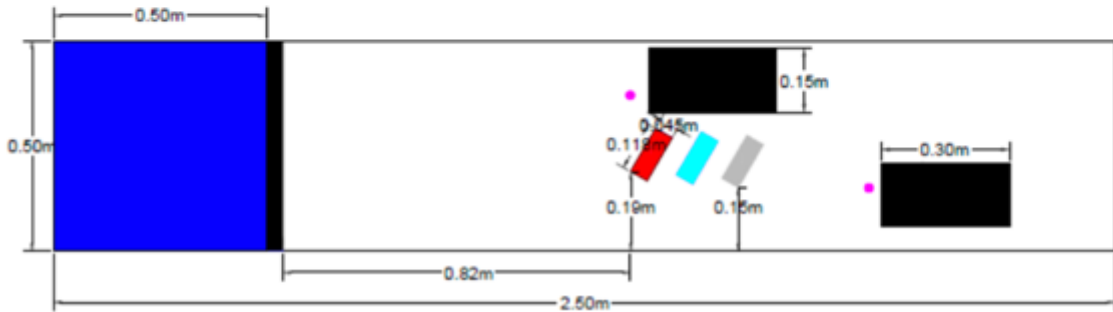
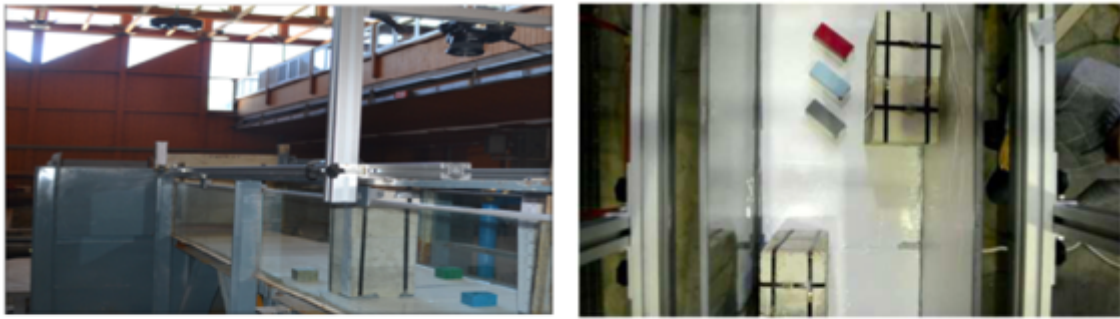


Figure 2.8: Facility of the experimental model, scale 1:40, made at the Università degli Studi della Basilicata in order to simulate the downstream behaviour after a dam-break event. Source: Albano et al., 2014.

The results of the analysis were looking for the water depths time evolution through two resistive gauges located upstream the fixed structures (the magenta points) and the 3D floating bodies displacements. The second result is given by the image analysis of two Charge Couple Device camera (CCD), focused on a limited area that is from 1.4 m to 2.1 m along the main direction. The movements were searched through two algorithms: the object extractor and the object tracker. With them, they had the possibility to follow the floating bodies during the experimental analysis and recognizing the positions on each image.

In order to validate the experimental data, a numerical model was built in scale 1:1. The gate had an opening time that goes from $t_0=0.00$ s to $t=2.00$ s with a velocity of

$w=0.11\text{m/s}$, that is a gradual opening. The solution is given through the resolution of the balance equation for 3D dynamics of rigid bodies. They deal with all the interactions between fluid-body and body-body. For the fluid-body interactions a free-slip condition is posed; whether for body-body and body-boundary, a different approach that the one used from SPH was used in order to manage the problems due to the low velocity impingements of entire solid bodies. The results of the numerical model can represent quite good the experimental data as can be seen in the next figures.

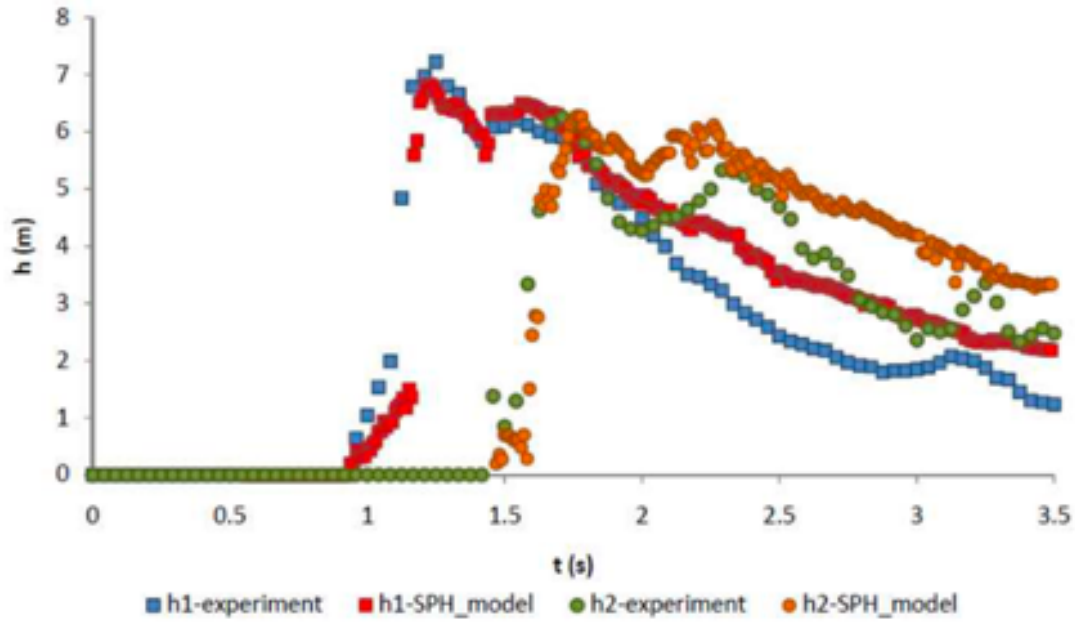


Figure 2.9: Time evolution for the up-stream height of the fixed body (h1) and the same for the down-stream body (h2). Source: Albano et al., 2014.

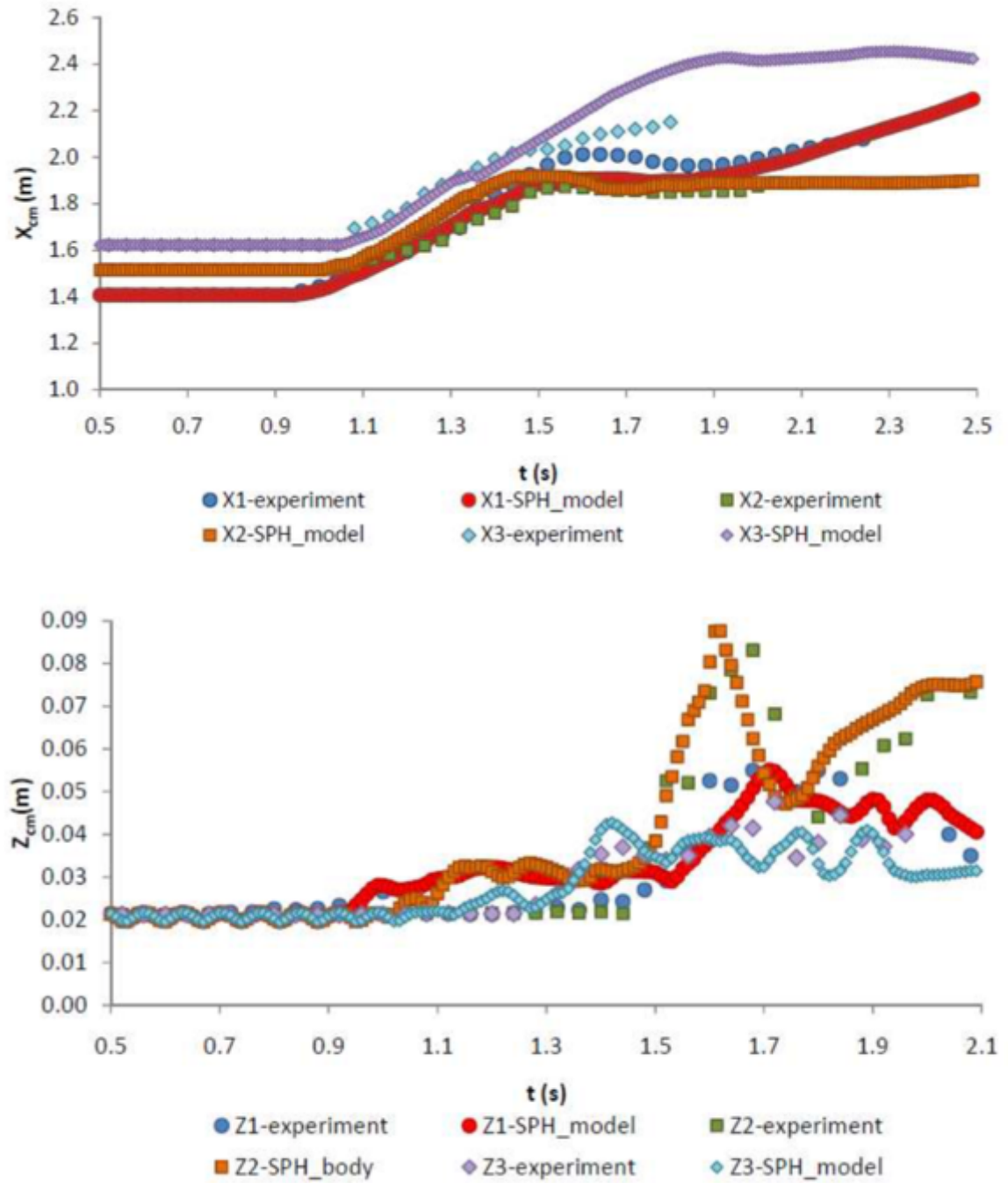


Figure 2.10: Time evolution of the x-coordinate for the centre of mass of the bodies (up) and the evolution on the z-coordinate of the centre of mass of the bodies (down). Source: Albano et al., 2014.

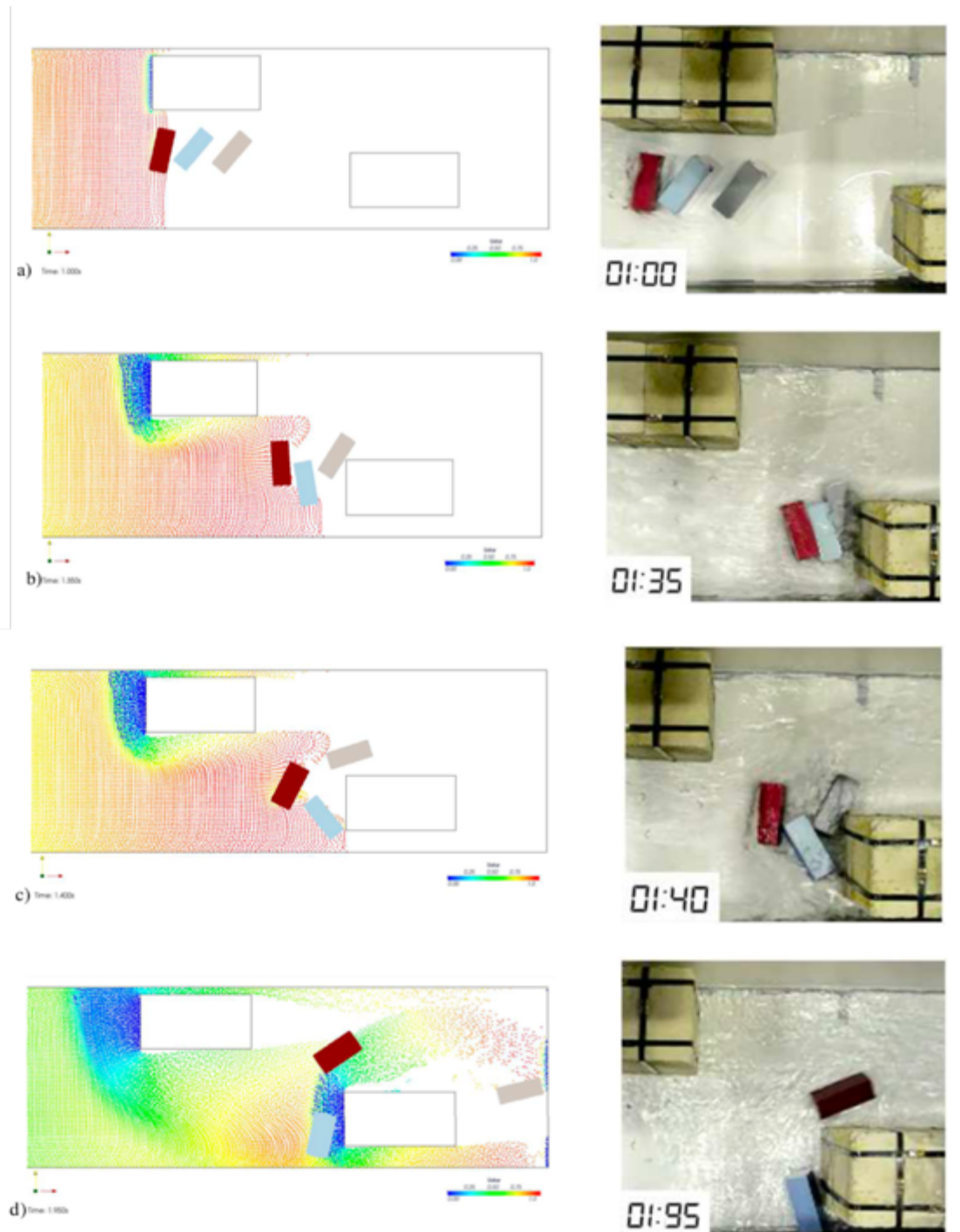


Figure 2.11: A brief comparison between the numerical model and the experimental test at the time $t=1.00$ s, $t=1.35$ s, $t=1.40$ s and $t=1.95$ s. Source: Albano et al., 2014.

The simulation on the SPH can represent a good alternative instead of the experimental tests, which are always expensive and last a lot. But as already said in the previous pages, a comparative with an experimental data must be done and it is necessary. Talking about the SPH, it can solve problems that the standard approaches usually fail, like the linear and second order wave diffraction theory.

2.4 Modeling flood shock wave propagation with the smoothed particle hydrodynamics (SPH) method: an experimental comparison study

This paper (Turhan et al., 2019) deals with the applicability of numerical models to the simulation of a dam-break, with particular attention to RANS (Reynolds Averaged Navier-Stokes equation) and SPH (Smoothed Particle Hydrodynamics). The dam-break simulated takes into account the nature of the water during the real event: in fact, to consider that the water is characterized by the presence of different elements, salt water was used.

The physical scale model used has been built at the faculty of Engineering in Adana, Turkey. It has a rectangular shape with a downstream area of 0.2 m x 0.30 m. The height of the reservoir is 0.15 m and the reservoir is filled with salt water. The gate has a height of 0.32 m and it simulates the sudden removal through a wire system linked to a 12 kg load.

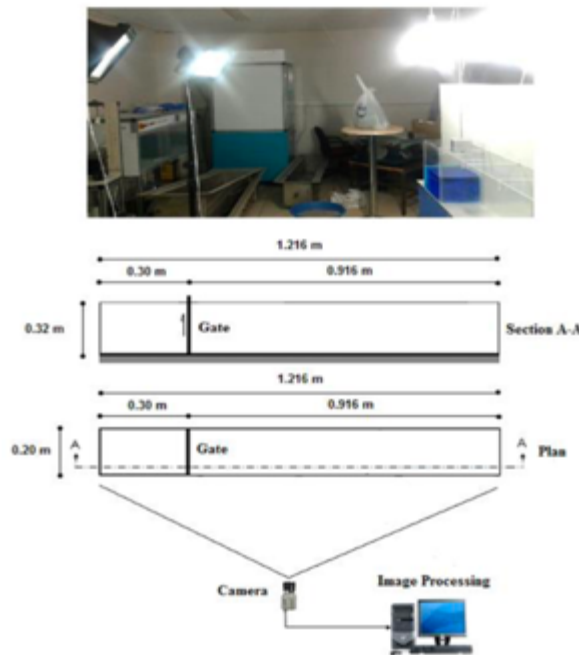


Figure 2.12: Experimental set-up for the dam-break analysis. Source: Turhan et al., 2019

The downstream area has a rectangular shape with a length of 0.916 m, and it is in dry condition at the beginning of the test. The width is the same as the reservoir and equal to 0.20 m.

The position of the camera, on a side of the physical model, lets to collect images throughout the experimental test and helps in the detection of the wave front development. In this way it is possible to compare the evolution of the wave. The camera was set to 60 fps and a resolution of 1280x720 pixel, with shooting options like 1/125 snapshot, 85 mm, f3.5 lens and 1250 ISO proof.

The water level is evaluated in four different points, one in reservoir and the other three in the downstream area. The representation of the results is made with dimensionless quantities H and T , which are the height and the time respectively.

In the following image the position of the probes is described.

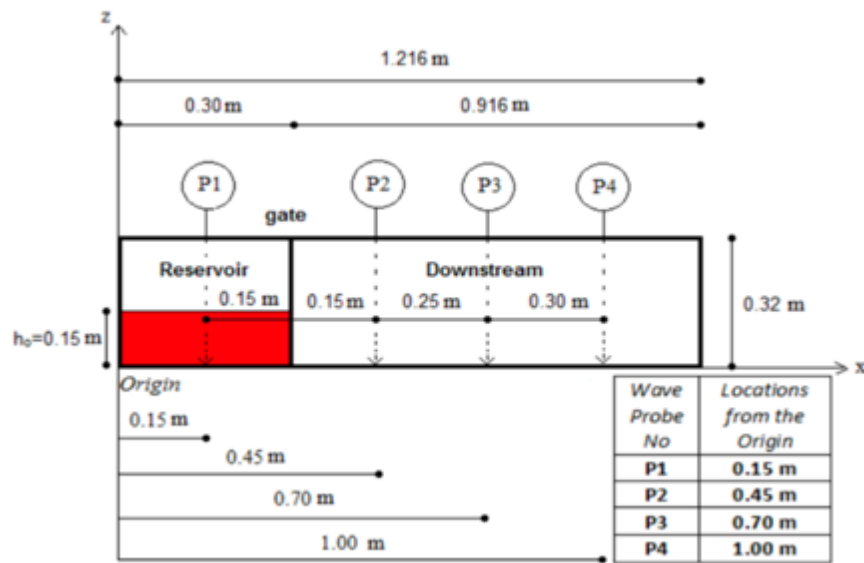


Figure 2.13: Measure points in the experimental setup. Source: Turhan et al., 2019.

The two numerical models used are RANS and SPH.

RANS is the acronym of Reynolds Averaged Navier-Stokes, and it uses the equations of Navier-Stokes for an incompressible Newtonian fluid. The solution for RANS is obtained using a Flow-3D software CFD program based on the VOF method.

In the case of SPH equations of momentum and mass conservation. A detailed description of this method is given in Chapter 5.

Talking about the results of this analysis of the wave propagation in a dry bed condition, the evolution of the free surface is obtained both in the experimental and numerical models. In the following images all the results are given.

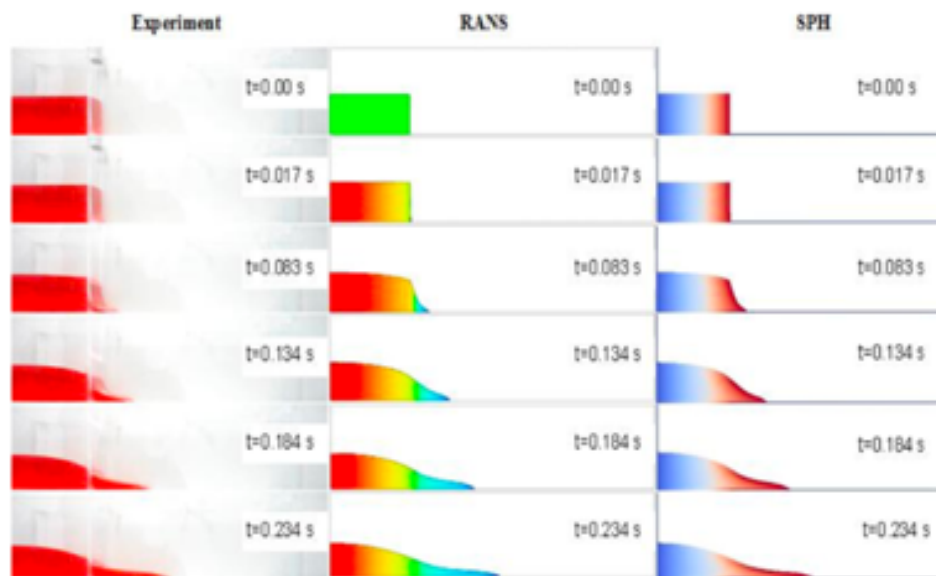


Figure 2.14: Evolution of the free surface at different instants for experiment, RANS and SPH. Source: Turhan et al., 2019.

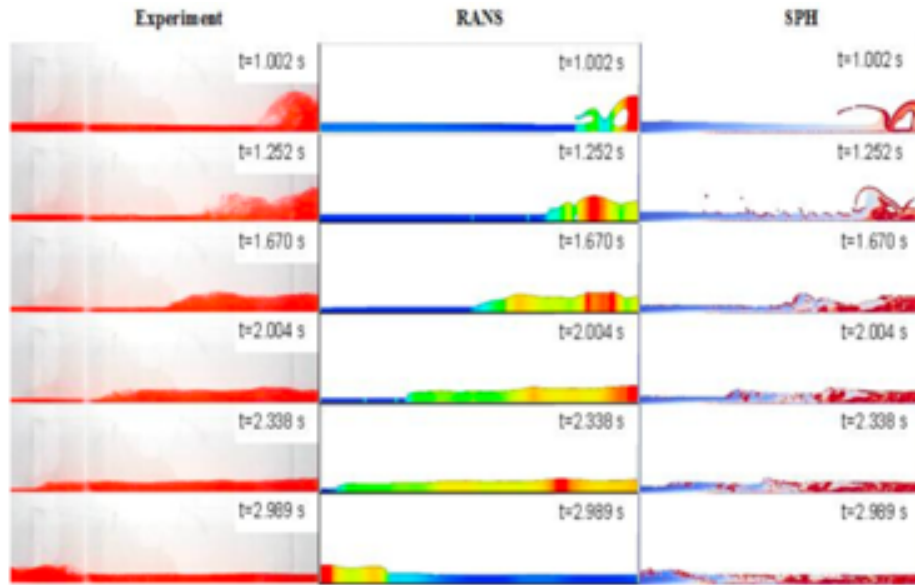


Figure 2.15: Evolution of the free surface in case of reflection of the wave at different instants for experiment, RANS and SPH. Source: Turhan et al., 2019.

As a conclusion of this analysis, the numerical models can reproduce the experimental data, although at a certain moment when the turbulence is high there is a gap between the results. RANS results are in agreement with the experimental results, whether in the case of SPH the results are a little different in the case of graph and profile. Anyway, the results collected lead to consider both RANS and SPH as good numerical models to simulate the dam-break event.

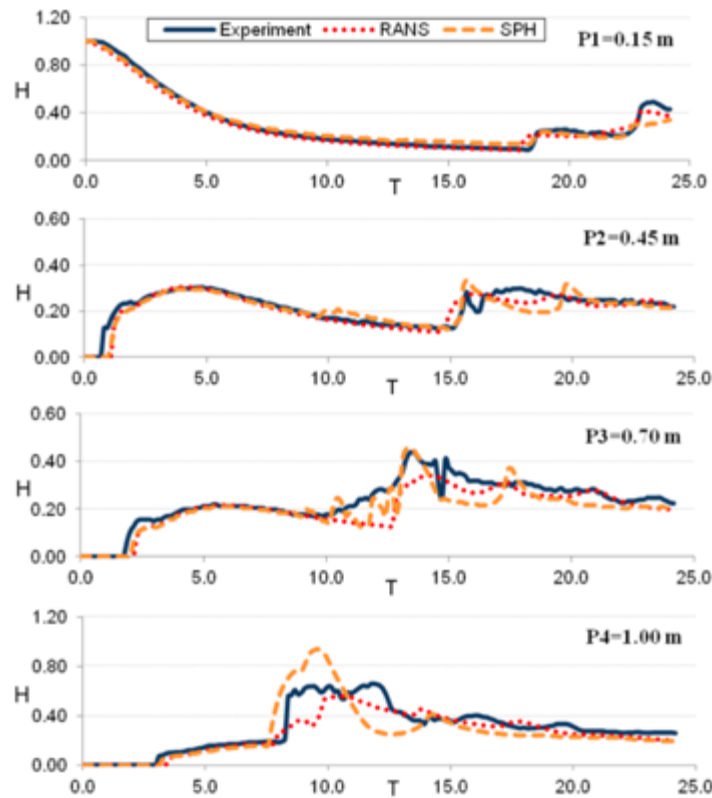


Figure 2.16: Flow depth variation during the 3 s of the experiment considered. Source: Turhan et al., 2019.

Chapter 3

The experimental Model

The status report deals with old technologies that are already been overcome. For instance, in the first case conducted by Aureli et al., 2008, the frame rate was only of 3 Hz, although they were high-resolution images. In the second case, a more recent analysis made by Soares-Frazão and Zech, 2007, the frame rate was higher and about 38 frames per second. But nowadays, digital cameras are reaching higher and higher resolution.

Furthermore, the analysis that will be described in the following pages has a strong difference from the others: all the pieces of information are not discrete, but continuous in the space. To do so, there is no need to use the technology mentioned above but considering an image processing through the photos given by the camera. In this way, every single cell has its own information that collects important data.

All the data collected are important both in the spatial and in time: the higher frame-rate adopted is necessary to let an evaluation for a temporal scope. In fact, there is a 10 factor between the frame-rate used in the experimental tests and the one used by Aureli et al., 2008. All the information about the instrumentation used, will be given in the following paragraphs.

The aim of this study are the characteristics of the dam-break wave (position, height and velocity), which are later compared with the ones by the numerical model (SPH).

This is possible thanks to the main camera, that is the Andor's Zyla 5.5 with the following preferences:

- High-resolution images with 2160 x 2560 pixel
- Grayscale dynamic range in 16-bit (0 - 65,536 intensity values)
- Frame-rate of the camera is 41.388 Hz
- A ratio pixel/mm about 0.995
- All the collected images and saved by default in .sif can be saved in .tif without losing any information

The other camera is the Nikon DSLR D810 that is just used for collecting coloured pictures during the tests.

Both of them are fixed on a portal at 3 meters of height above the downstream area, that is a horizontal plane covered with a waterproof polyvinyl chloride stratus. This model has taken place at the "Giorgio Bidone" Hydraulics Laboratory at the Politecnico di Torino. In the next paragraphs all the characteristics about the physical model will be described.

3.1 Physical Model

The physical model used for the experimental tests has been built in the Hydraulics Laboratory “Giorgio Bidone” of the Dipartimento di Ingegneria dell’Ambiente, del Territorio e delle Infrastrutture (DIATI) as can be seen in the figure 3.1.

This model’s purpose is to recreate a dam-break generated by the partial or total collapse of a compacted ground dam, typical in the south Piemonte region. As already said in the Chapter 1, this kind of dams are generally used for irrigation, generation of electricity and snow production. Generally, a lot of these dams are placed just up of vineyard crops.

The physical model needs to have a geometric and mechanic compatibility. This means that a group of dimensionless quantities remains unaffected.

Through the Buckingham π theorem is possible to define dimensionless quantities related to the physical quantities which describe the physical model. Two main possible paths can be followed: *Froude constant* or *Reynolds constant*. Considering that in a dam-break the velocity is quite high, can be noticed that viscosity does not play an important role. In this way the Froude constant is the one chosen. In this way, the velocity field can be reproduced, considering that the model has high velocity.

The model itself is a 3 x 4 m rectangular box in which the dam-break happens. This box is surrounded by black curtains in order to avoid the entrance of the natural light during the experimental tests. Out of them three monitors are placed to control all the instrumentation used for capturing the data.

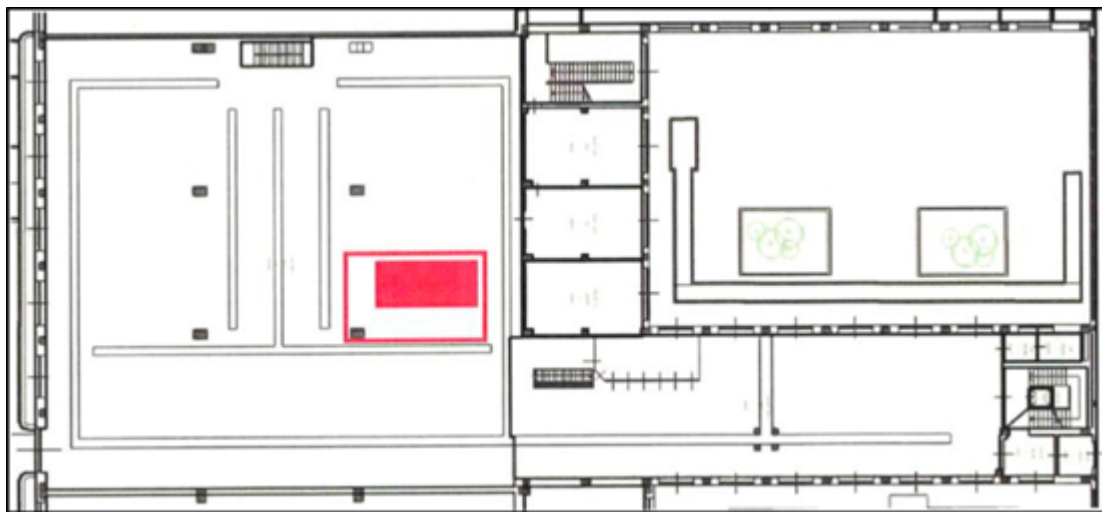


Figure 3.1: Position of the physical model in the Hydraulics Laboratory in Turin.

3.1.1 Framework of the model

All the elements of the model are now described singularly. The model has a scale around 1:30. It is not the exact scale factor because it has been built as a medium of the small and medium reservoirs spread all over the province of Cuneo.

The model is made up of two rectangular cases: the first one, on the left is the reservoir with a volume of $1.5 \times 1.5 \times 0.5 \text{ m}^3$, filled with fluid from a tank placed 3 meters far through a PVC pipe. It is not filled with water till the edge, but a maximum of 0.40 m is used for the experimental tests. As can be seen in the following image, the second rectangular area on the right side is the downstream wooden plane that represents the valley on which the wave develops during the tests. A PVC film of 0.003 m is placed on the wooden plane and two angle bars are placed along the main direction to fix it. At the end of the downstream area a reservoir collects all the water after the experiments.

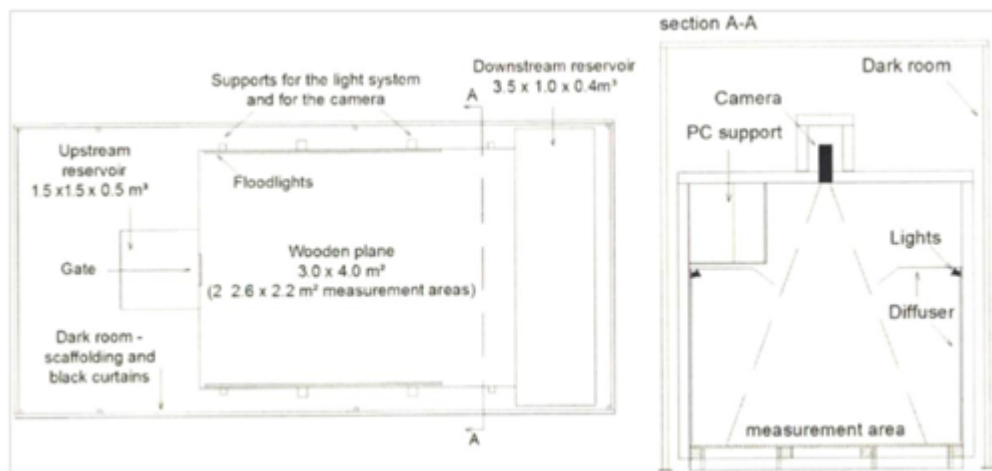


Figure 3.2: General overlook over the physical model with the correct dimensions (left) and a section of the model (right).

The upstream reservoir is separated from the downstream area thanks to a gate with a rectangular stainless-steel breach with a width of 0.03 m and a height of 0.5 m. During the experiments the gate is linked to two magnets welded on a stainless-steel panel and worked out to the facility. On the upper part, a welded stainless-steel ring is linked to a metallic wire which is linked to a 10 kg weight through a pulley. At the initial conditions, the metallic block is attached to a magnet positioned 3 meters high.

3.1.2 Reservoir and tank

In the upstream area, there is the reservoir that has the function of collecting water and releasing it after the sudden removal of the gate. The dimensions of the reservoir are $1.5 \times 1.5 \times 0.5 \text{ m}^3$. The upstream reservoir has a plane bottom with a drain in an angle controlled by a ball valve. On the main frame two wooden bars are placed. Their function is just to fix the metallic frame of the ultrasonic probes through clamps.

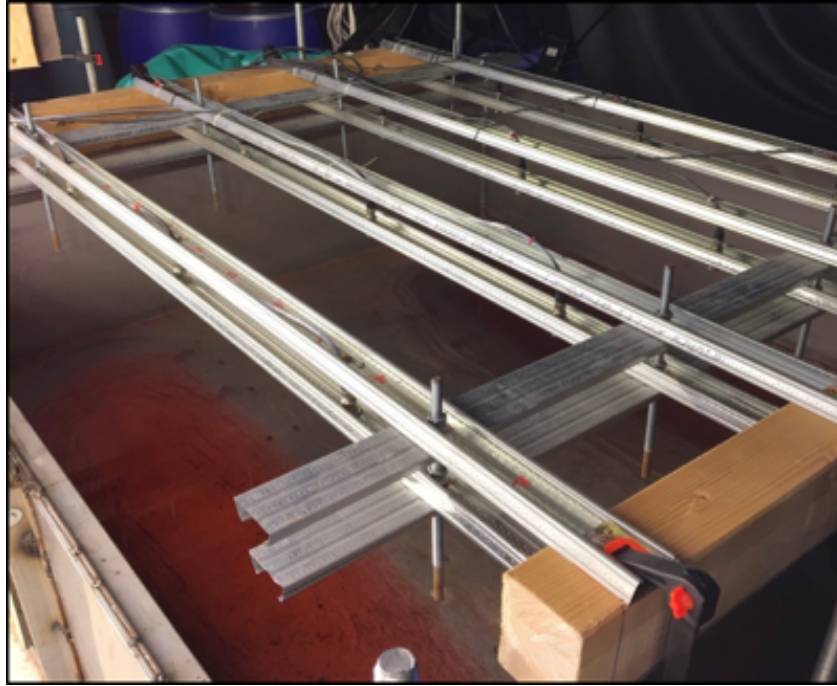


Figure 3.3: Upstream reservoir in the Hydraulics laboratory in Turin.

The square reservoir is filled through a PVC pipe that links the water tank and the reservoir itself. It is placed 3 meters far from the reservoir but thanks to pumps that are on the bottom of the tank it is possible to fill the reservoir till the height needed. To check the height of the water, there are not only the probes but a standard measuring rod in an angle of the reservoir too.

Talking about the water tank, the whole capacity is 1500 l, but it is filled till 1350 l. It is linear polyethylene. As already said, through the submersible pumps it is possible to fill the reservoir. After the experiments, the water collected in the downstream reservoir is sent to the tank again through submersible pumps.

3.1.3 Water

The water is collected in the linear polyethylene tank: it is a red water. Its colour is obtained after an experimental campaign with an adding of cochineal dye (E120). The concentration of cochineal is 0.0167 g/l and after that another addition of E124 with a concentration of 0.185 g/l (250 g on 1350 l).

At the beginning of the study of the colorant, the choice of the cochineal was a problem due to the fact that it tends to collapse on the bottom, although it takes too much time. Moreover, it is quite expensive, and this led to the choice of the colorant E124, which has advantages in terms of variability in time.

3.1.4 The Ultrasonic Probes

The ultrasonic probes used for the experimental tests are the Balluff BUS_18M1-07/035. Their aim is to evaluate the distance generating an acoustic signal and evaluating the returned analog signal. The output signal is proportional to the distance from the surface or from the object. The Balluff sensors are placed on a metallic framework that can be seen in the previous page and there are twelve of them. A brief description of the model used is taken from the manual.

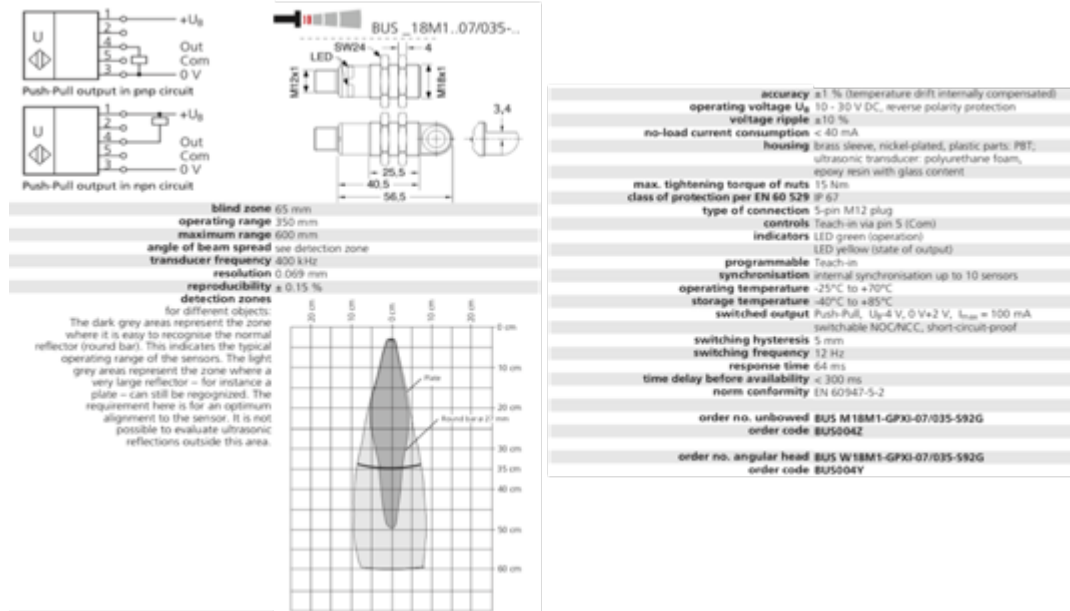


Figure 3.4: Technical description of the twelve Balluff sensors that are used in the physical model taken from the manual.

And now a focus on the main characteristics of the sensors is given:

- A maximum range of measuring value of 600 mm. Best measuring range by 350 mm. In the first 65 mm there is the blind zone with no visual cone.
- Reproducibility of the measurement of $\pm 15\%$.
- Frequency of measuring of 80 Hz, which means that for each second there are 80 measurements and the values are given as a multiple of the internal resolution that is equal to 0.069 mm.

The calibration of the ultrasonic probes was the one made by the group of students committed in the dam-break analysis of the same physical model and with the same instrumentation.

A calibration campaign was done by Jacopo Briano, Silvia Cordero and me in the downstream area. The aim was to put known heights of red water in the downstream area, evaluated with a needle diastimeter, and then compared to the measurements of the sensors. In this way a graph can be built, plotting the measured values for different heights. Through the tool of Excel, the linear trendline and the its equation that is in the form:

$$y = m_i x + q_i \quad 3.1$$

The m_i and q_i are the coefficient for a specific sensor.

Anyway, considering the high variability of the water during the experimental tests and the visual cone related to the sensors, it is not possible to use the ultrasonic probes in the downstream area to evaluate the height of the water.

So, the twelve sensors are placed on a framework in the upstream area, the reservoir, and are used to evaluate the amount of water released in every single step during the dam-break. It is also used to confirm the continuity between the volume in the reservoir and the water in the downstream area, through the well know continuity equation. All the data from the ultrasonic probes are then used in MATLAB to represent the water surface in a precise instant. The blue colour represents the part next to the gate.

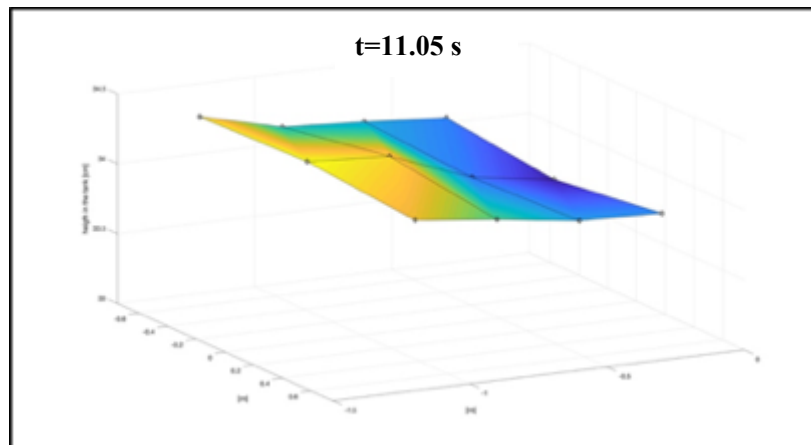


Figure 3.5: Variation of the water surface during an experimental test, obtained after processing the sensors' data. It represents just the variation of the water in the correct dimensions of the reservoir.

3.1.5 The Sluice Gate

On one of the sides of the reservoir a rectangular opening with dimensions of $0.03 \times 0.50 \text{ m}^2$ has taken place. Its aim is to simulate the breach, through the water flows after the opening of the gate. The gate is placed next to the reservoir and it is linked to it thanks to two magnets. In fact, two magnets are welded on the stainless-steel framework of the reservoir whether the other faces are on the gate. To avoid loss of water while the magnets are on, mastic is used to fill the gaps between gate and reservoir.



Figure 3.6: Picture of the sliding gate on which is possible to recognize the two magnets both on the reservoir and on the gate. Source: Natali, M., 2019.

On the upper part, a welded stainless-steel ring is linked to a metallic wire which is linked to a 10 kg weight through a pulley. At the initial conditions of a test, the metallic block is attached to a magnet positioned 3 meters high. As soon as the weight starts to fall down, the sluice gate abruptly moves up till it reaches the wooden dissipation blocks. In this way all the water collected in the reservoir starts to flow in the downstream area.

The time of the opening of the gate is $t_{\text{opening}} = 0.095 \text{ s}$.

This value can be compared with the evaluation criterion proposed by Vischer and Hager (1998), that lets to consider the dam-break as instantaneous if the opening of the sluice gate satisfy the following mathematical relationship:

$$t_{\text{opening}} = 1.25 \sqrt{\frac{h_0}{g}} \quad 3.2$$

where:

- h_0 is the height of the water in the reservoir before the opening in meters;
- g is the gravity and considered with the value of 9.81m/s.

Considering the fact that in this thesis are analyzed only the cases with a height of the water equal to 0.40 m , the opening of the sluice gate is: $t_{\text{opening}} = 0.25 \text{ s}$.

Another criterion is the one of Lauber and Hager (1998), that is less restrictive and satisfied for sure:

$$t_{\text{opening}} = \sqrt{\frac{2 \cdot h_0}{g}} \quad 3.3$$

According to equation 3.2, the $t_{\text{opening}} = 0.285 \text{ s}$.

In the end, the two criteria are both satisfied, and the opening of the gate can be considered as instantaneous.

3.1.6 The Led Lightning

The lightning of the physical model covers an important role in the experimental tests. In fact, it is important to consider that a correct lightning leads to the correct collection of the data taken by the cameras, avoiding problems like the reflection of the light upon the bottom. The two portal frames that are 3 meters long are positioned at a height of 1.80 m from the bottom of the model. They are inclined by 5° from the horizontal to avoid the problem of reflection. Furthermore, all the model is closed by a PVC matte white stratus in order to do not have problems with reflection and diffusion, leaving just the space to the breach and the cameras.



Figure 3.7: Photo taken into the physical model to show the led lightning and the PVC matte white stratus.

In fact, the PVC stratus covers the top of the box too but leaving the space to the visual cone of the cameras. In order to avoid the natural light pollution, the model is fully covered by black curtains: in this way the only light admitted is the one from the led lightning.

3.1.7 The high-resolution Cameras

The collection of all the information about the tests are taken through two high-resolution cameras that are held upright the bottom downstream area. They are placed on a portal frame that is linked to the main framework and maintain the position fixed. The objective lenses are perpendicular to the downstream. Two cameras are used with different features between each other: the Andor Zyla 5.5 sCMOS camera and the Nikon DSLR D810 camera. Both of them are described below.

3.1.7.1 The Andor Zyla 5.5 sCMOS camera

The first of the two cameras, and the one used during the experimental tests to collect all the photos is the Andor Zyla 5.5 sCMOS. It collects a high number of photos with a frequency of 41.3888 Hz (0.02416 s between each photo), with a resolution of 2560 x 2160 pixel.



Figure 3.8: Image of the Andor Zyla 5.5 sCMOS camera. Source: <https://andor.oxinst.com>.

In this thesis will be skipped the description to find the correct position and setup of the characteristics of the camera, but these pieces of information have already been detailed in other two master's thesis, as "Progettazione e verifica di un light-box per lo studio sperimentale di onde di dam-break", written by Guerra and "Metodi per la valutazione del rischio a valle delle dighe regionali: confronto tra i metodi in uso e semplificati" by Costa.

The Andor Zyla 5.5 uses a global shutter mode for collecting images during the experimental tests. It is known that in the digital cameras there is a A/D converter which allows to transform a light level to digital data. In this case two different ways can be chosen: Rolling Shutter and Global Shutter. But in the case of Zyla the Global Shutter has been selected and this allows to all of the sensor to be exposed at the light at the same time.

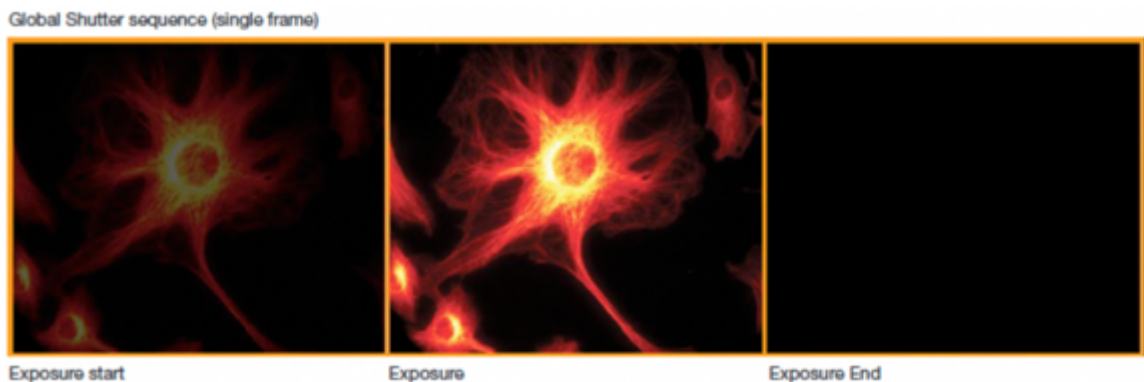


Figure 3.9: Global shutter mode. Source: <https://andor.oxinst.com>.

Different is the case for the Rolling Shutter, in which there is a temporal gap between the collection of information in the center of the sensor and the upper part of the same.

As already said the camera has a sCMOS sensor, which allows to collect with a high-frame rate and a low noise. The main difference is that the conversion from the signal to the image is made in the camera itself. Whether, in the CCD cameras the conversion happens out of the camera, that means that there is a higher post processing time.

This camera has a sensor APS-C, that is the basis for the half-frame camera. In this case, for the Andor Zyla, the size of the sensor is $16.6 \times 14.0 \text{ mm}$. The camera has a Sigma lens 18-35 mm, but it is always used at the minimum value because it represents a good compromise between the focal length and the distortion of the image. As already said, only a small part of the downstream area is taken into account, that is the $2.6 \times 2.2 \text{ m}^2$ more or less. All the photos collected are in greyscale.

3.1.7.2 The Nikon DSLR D810 camera



Figure 3.10: Images of the Nikon DSLRD810 camera and lens. Source: official website of Nikon <https://www.nikon.it>.

The second camera that is fixed on the portal girder is the Nikon DSLR D810, with an AF-S NIKKOR 24-120 mm f/4G ED lens. It takes video at 60 fps with a resolution of 1080p (1920 x 1080), with a dynamic interval of 8-bit (0-256) in the RGB channels. For the experimental tests a setup of f/4, ISO 200 and a temperature of 3000K has been used. This camera has been used only for the purpose of collecting coloured images for a better representation.

3.1.8 The downstream area

The downstream area is represented by a flat area of 3x4 m². The framework of the model is made up of wood, but it is covered by a 3mm white polyvinyl chloride stratus that makes it waterproof. Furthermore, it helps in the tests to diffuse light coming by the led and to detect the wave front generated by the sudden removal of the sluice gate.

This white layer is fixed to the framework through two angle bars that are placed at the angles along the main sides. They do not affect the experimental tests considering that, once the wave reaches the walls of the model, the analysis has already finished. The downstream area finishes in a downstream reservoir that collects the water released.

The Manning coefficient of the layer is $n_{\text{model}} = 0.0093 \frac{s}{m^{\frac{1}{3}}}$.

After an analysis of the roughness in the case of Froude constant in a scale model, the real value of the Manning coefficient is considered: $n_{\text{model}} = 0.016 \frac{s}{m^{\frac{1}{3}}}$. This leads to consider that this is a case of smooth surface. Further information about the detection of these values can be found in the work D'Oria, 2019.

For the aim of this thesis a study on the vegetated downstream area has been done. In fact, panels with different shapes were placed in the downstream area on which metallic rods are bolted. Two different configurations of panels are available:

- Mesh 100 mm x 100 mm
- Mesh 50 mm x 50 mm

Four possible configurations can be used in the simulations considering the angle given to the panels. It is possible to create the following simulations:

- Configuration with 100 mm x 100 mm with an angle of 0°
- Configuration with 100 mm x 100 mm with an angle of 45°
- Configuration with 50 mm x 50 mm with an angle of 0°
- Configuration with 50 mm x 50 mm with an angle of 45°

In the next figures it is possible to see the four configurations used for the experimental tests.

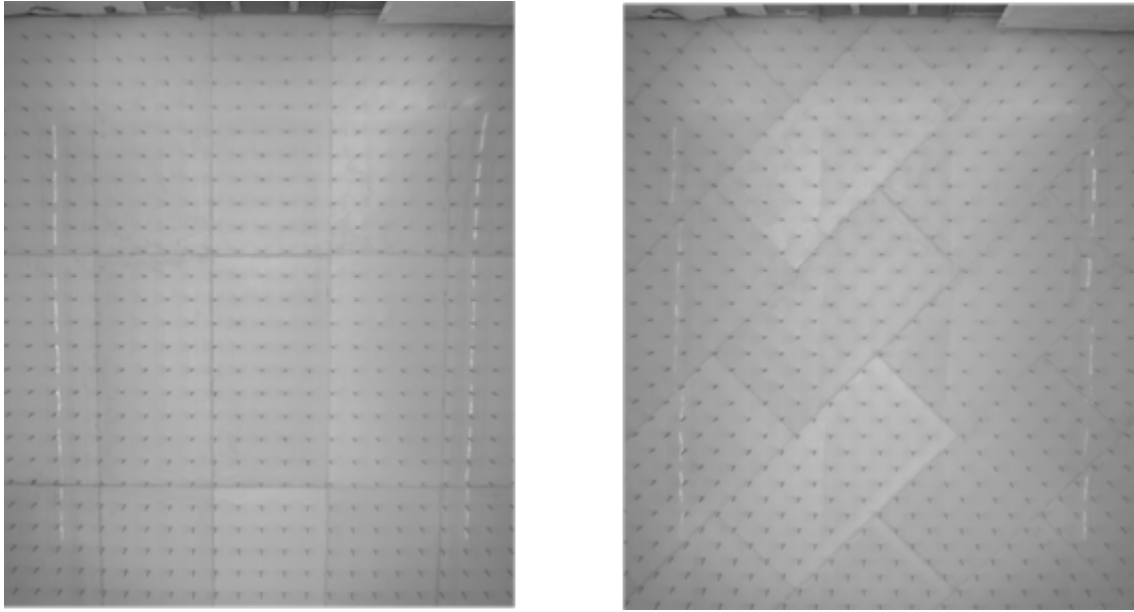


Figure 3.11: Photos taken in the configuration with panels 100 mm x 100 mm with angle of 0° (left) and 45° (right).

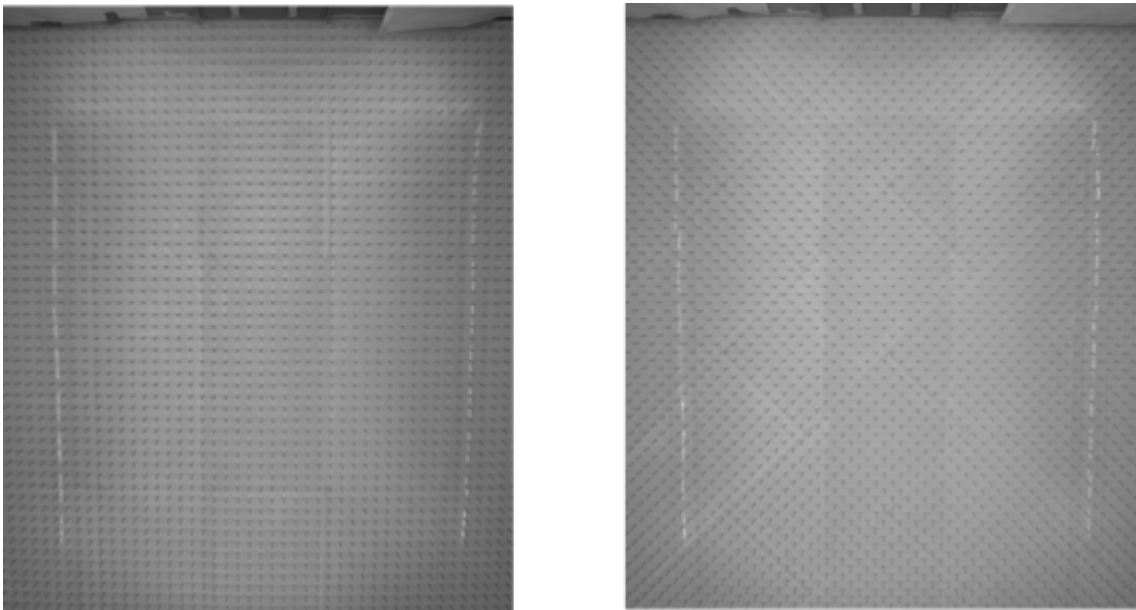


Figure 3.12: Photos taken in the configuration with panels 50 mm x 50 mm with angle of 0° (left) and 45° (right).

Chapter 4

The experimental tests

The analysis of the dam-break wave has been discussed a lot from the scientific community and the physical models built throughout years are various. The model described in this thesis has been built at the “Giorgio Bidone” Hydraulics Laboratory at the Politecnico di Torino. The possibility to simulate the dam-break in different conditions represents a good opportunity to obtain various results that can be validated in further occasions through numerical modelling.

In this case and for this kind of physical model the typology of the tests can be joint in two main categories: smooth surface and vegetated surface.

The smooth downstream surface is represented by the PVC layer of 0.003 m that covers the main framework. It will be briefly discussed in the next chapter, although it is not a part of the work made in the laboratory.

The vegetated area is realized thanks to polycarbonate panels of two different types considering the distance between the metallic rods: 5x5 cm and 10x10 cm. The importance of simulating the behaviour of the wave in the case of dam-breaks with vegetations in the downstream area, is stressed by the fact that for small and medium dams the presence of obstacles play a fundamental role. In fact, the behaviour of the wave is linked to the elements that cover the downstream area and the propagation of the wave is strictly related. For this reason, an increasing interest is now shown.

The main purposes are:

Detection of the free surface elevation in the downstream area

Search of the wave front and its evolution

Analysis of the velocity field during the tests

In the following paragraphs are described all the different steps to simulate a correct dam-break on the physical model, how to evaluate the height of the free surface and how to detect the wave front.

4.1 How to deal with the physical model

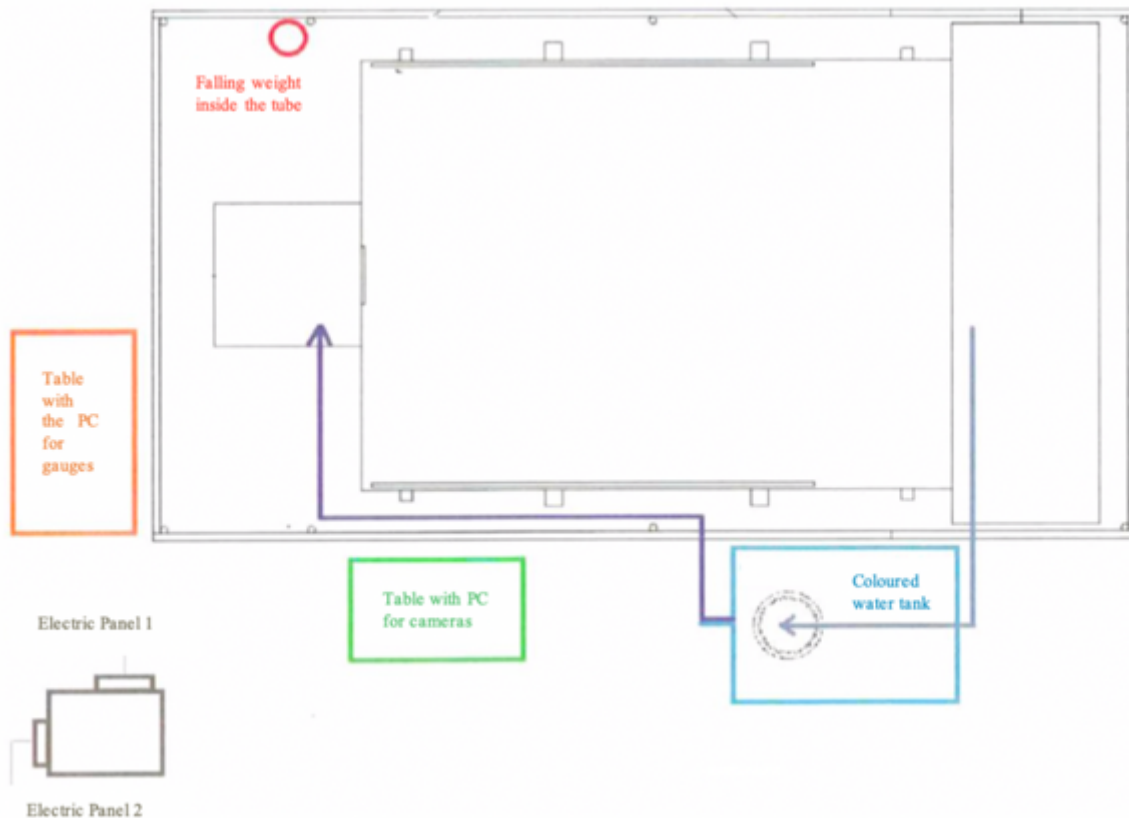


Figure 4.1: Overview of the layout of the physical model.

1. Check the right connection between the upstream and downstream areas

The first phase is about the check of the hydraulic continuity between the two different areas. In case of discontinuity, it can be used the mastic to resume the continuity.

2. Positioning of the discharge pipe in the reservoir and check of the anchorage

The check of the downstream area and the PVC layer ends with the creation of a depression in the last part, in which a submersible pump is placed. At the end of the experimental test the pump is placed again in the depression.

3. Check of all of the electric attachments to the electric panels

It is important to check the electric panel 1 before attaching the three magnets to the electricity. Two magnets are for the sluice gate and one for the falling weight. All the other instruments used for the test are attached at the electric panel 2.

4. Switch on the Led Lightning

From electric panel 1 it is necessary to flip the switch to turn on the led lightning.

5. Preparing the downstream area

In order to simulate the experiments with roughness, the different PVC panels are placed and linked each other with tape along the sides. This is necessary because in case the water passes under one of them, the buoyant force could lift the panels. This leads to reject the tests.

6. Switch on all the instruments

It is necessary to let the sensors start recording before the cameras, using the table with PC for gauges (Figure 4.1). Then it is necessary to check if the Zyla camera is working properly using the live view on the Andor SOLIS for Imaging. Once it is done, it is necessary to set all the frames needed during the experiment, frame rate and exposure time. The pc for the Zyla is along the main side of the downstream area.

In the end, it is necessary to set the Nikon camera and to check with a live view, using the pc next to the physical model.

7. Preparation of the sluice gate and the reservoir

The preparation of the setup for the tests starts with the positioning of the sluice gate down in the bottom. To fix the sluice gate in this position, it is necessary to stop the falling weight on the top of the pipe through the magnet. After this, it is possible to switch on the magnets and to link the sluice gate at the frame of the reservoir through the two magnets. To isolate the two different areas, upstream and downstream, mastic is used, and it is placed along the junctions on the sides and the bottom. It is important to check that the mastic is not invasive, otherwise it could affect the results.

8. Filling the reservoir with water and check of the tight

Before pumping the water in the reservoir, it is necessary to check that the drain is closed. Once all is closed, it is possible to start to pump the water inside the reservoir measuring the free surface elevation through the twelve gauges or the measure rod. The gauges must be at a maximum distance of 6.5 cm in order to avoid having the visual cone and to measure the height in that exact point. In this phase it is necessary to check that there are no water leaks from the reservoir.

To permit the motion of the gate, it is necessary to switch on the magnet of the falling weight.

9. Execution of the test

In this phase, there is the need to:

let the Zyla camera starts to record, checking that everything is working.

let the Nikon camera records.

switch off the electric panel 1, where all the magnets are attached.

10. Back to the initial conditions

After the experimental tests, it is important to switch on the submersible pump that is in the basin at the end of the downstream area. Then it is necessary to remove all the tape from the panels and to clean them through water outside of the facility.

These are all the mandatory passages, necessary to execute a successful test. During the months of March and April, eight tests were carried out on the physical model and they are summed in the next table.

Table 4.1: Experimental tests

Type	Date	Number of tests
10x10 - 0°	28/03/2019	2
	29/03/2019	
10x10 - 45°	26/03/2019	2
	27/03/2019	
5x5 - 0°	28/03/2019	2
	29/03/2019	
5x5 - 45°	01/04/2019	2
	02/04/2019	

4.2 Wave front analysis

The analysis of the experimental data is the main part of the work described in Briano, 2019. One of the aims of this thesis, related to the experimental tests, is the detection of the wave front. In each test hundreds of images are taken from the cameras. To reduce them, it is necessary to consider that the visual cone of the cameras is limited, but it represents a major part of the downstream area. This means that the only images needed are the ones that shows the variation in time of the wave front.

Considering the high number of frames created in each test, it is necessary to create an automatic routine. In every routine there are some steps that are described below. The software used for the wave front analysis is MATLAB R2018b.

The first step is the normalization of the images. Considering the variation of the brightness during the tests, due to the coloured water and the different position of the led lightning, the conditions are not uniform as they should be. To solve this problem, the matrix related to each image is normalized using the following formula:

$$im_{normalized} = \frac{background - im_{original}}{background} \quad 4.1$$

Where

- *background*: is an image taken before the water starts to flow on the downstream area.
- *im_{original}*: is the image of the considered instant during the test.
- *im_{normalized}*: is the normalized image, in which all the values related to its matrix are between 0 and 1. In this way there are two advantages: the reduction of the noise in the image and the spatial lightning variation.

The binary images are shown in Figure 4.2 and 4.3.



Figure 4.2: Binary images for mesh 10x10 0° (left) and 45° (right)



Figure 4.3: Binary images for mesh 5x5 0° (left) and 45° (right)

The second step is the de-distortion of the image. This is done using a command called *undistortImage*, in which it is necessary to insert the parameters of the camera and the source image. As a result of this command, the output image is a deformed but not distorted image: starting from a rectangular distorted image, then there is an irregular in shape, but with the right proportions in each pixel, image.

The third step is the masks application on the de-distorted image and the detection of the wave front. Through the application of masks, it is possible to make visible the wave in the downstream area. At the same time, the sluice gate and the PVC layer for the walls are hidden. In order to identify the wave front, it is necessary to convert the original photo into a binary image, apply the *imfill* command to cancel the noise in the binary image and then at this point it is possible to use some coefficients to detect the edge. The detection of these coefficients is possible running the code several times and checking the edge near the front.

In the next figures are shown the results of this analysis.

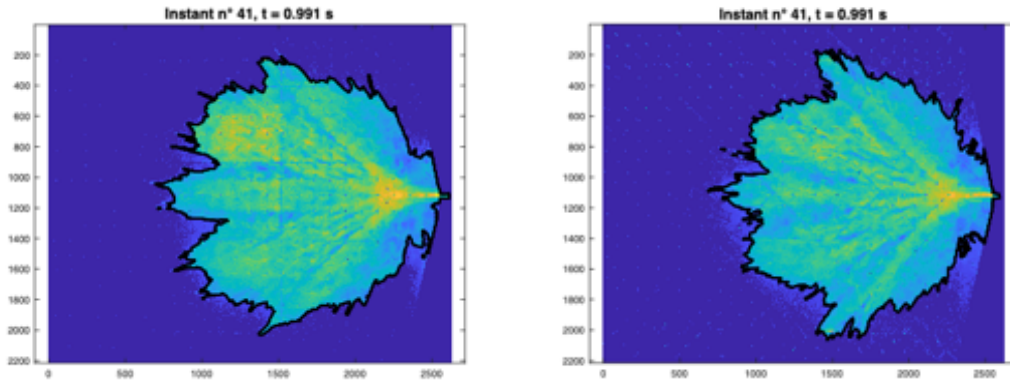


Figure 4.4: Wave front detection for mesh 10x10 at 0° (left) and 45° right at instant 41

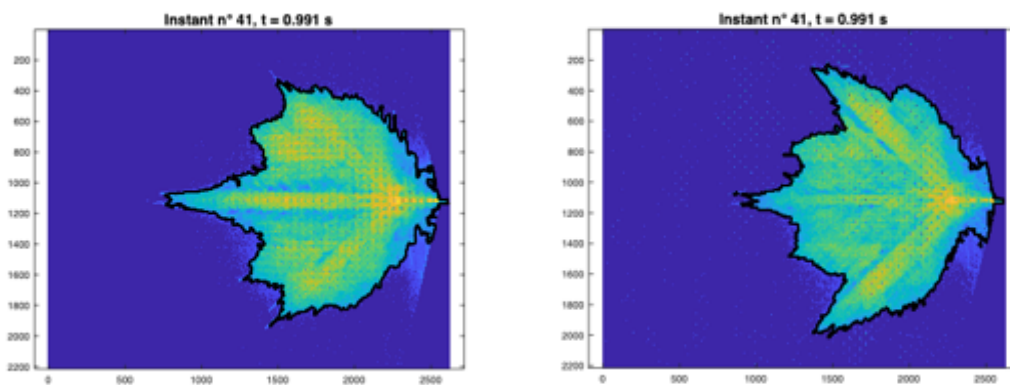


Figure 4.5: Wave front detection for mesh 5x5 at 0° (left) and 45° right at instant 41

The detection of the edge has to take into account a little percentage of error due to all the passages to arrive at the result. Moreover, in the wave fronts there are some elements, called fingers, which represent the growing direction of the wave.

The last step is the passage from pixel to metric coordinates using the command *pointsToWorld*. In this way, it is possible to save in a MATLAB structure all the metric coordinates of the wave fronts throughout the tests.

Furthermore, it can be shown the evolution of the wave front during the whole tests. It is necessary to consider that the experimental tests last 4 seconds, in the case of 10x10 mesh and 7.7 seconds in the case of the mesh 5x5.

The evolution of the wave fronts is represented in the Figure 4.6 and 4.7.

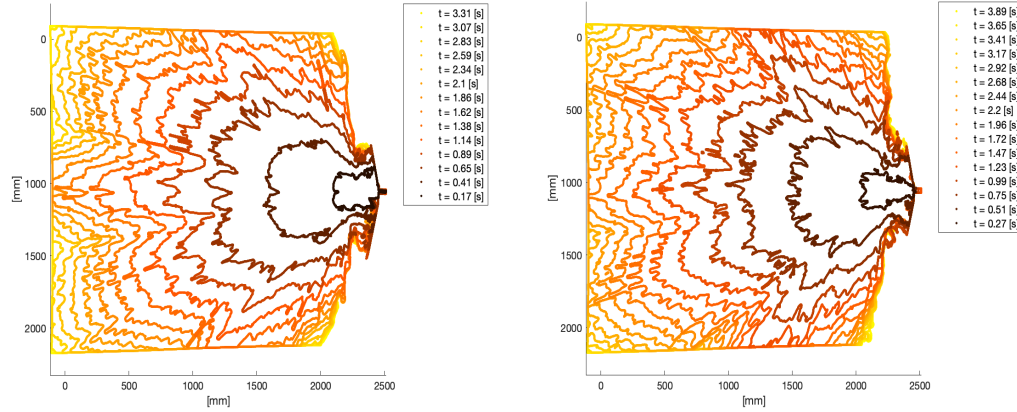


Figure 4.6: Temporal evolution of the wave front in the case of mesh 10x10 0° (left) and 45° (right)

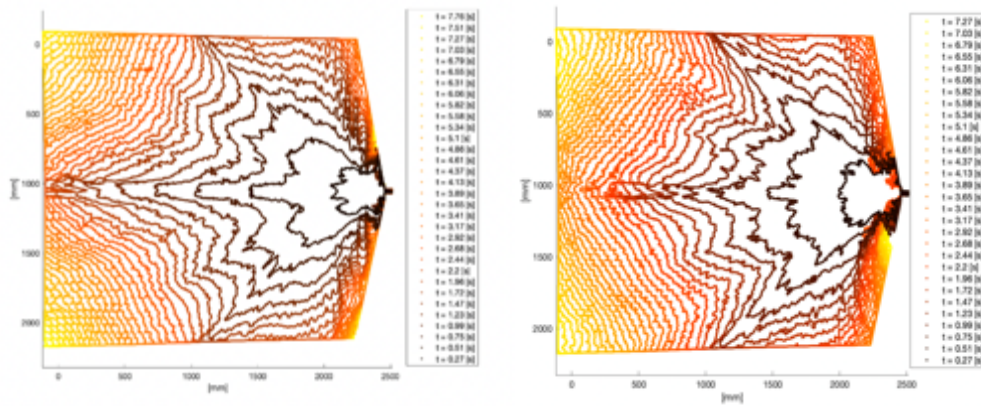


Figure 4.7: Temporal evolution of the wave front in the case of mesh 5x5 0° (left) and 45° (right)

4.3 Velocity analysis

The analysis of velocity is done considering the downstream area and dividing the area in eleven sectors. The angle of each sector is of 15°. The axis of the central sector corresponds to the axis of the breach. The starting point of the sectors between the different configurations is different and it depends on the impact point of the water: in the case of dam-break of 40 cm the impact points are the same. In the next table are written the centre points.

Table 4.2: Coordinates of the impact point

Case name	x [pixel]	y [pixel]
10x10 0°	2334	1127
10x10 45°	2334	1127
5x5 0°	2334	1127
5x5 45°	2334	1127

Once the centres are found it is possible to draw the sectors. All the sectors for the four different cases are represented in Figure 4.8 and 4.9.

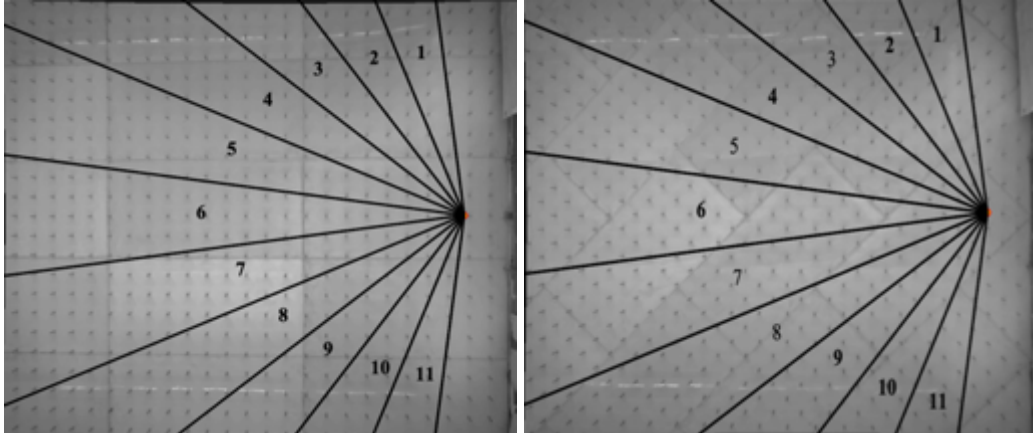


Figure 4.8: Representation of the eleven sectors in the tests with mesh 10x10 with 0° (left) and 45° (right)

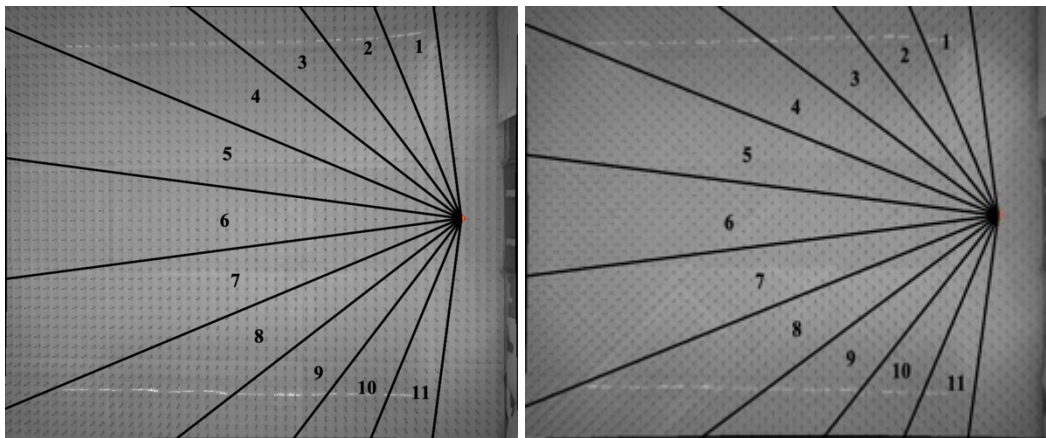


Figure 4.9: Representation of the eleven sectors in the tests with mesh 5x5 with 0° (left) and 45° (right)

The first analysis regards the cumulative distance in all the sectors. The results are shown in Figure 4.10, 4.11, 4.12, 4.13.

The results regarding the velocity analysis are represented only for the central sectors (number 6) in each case.

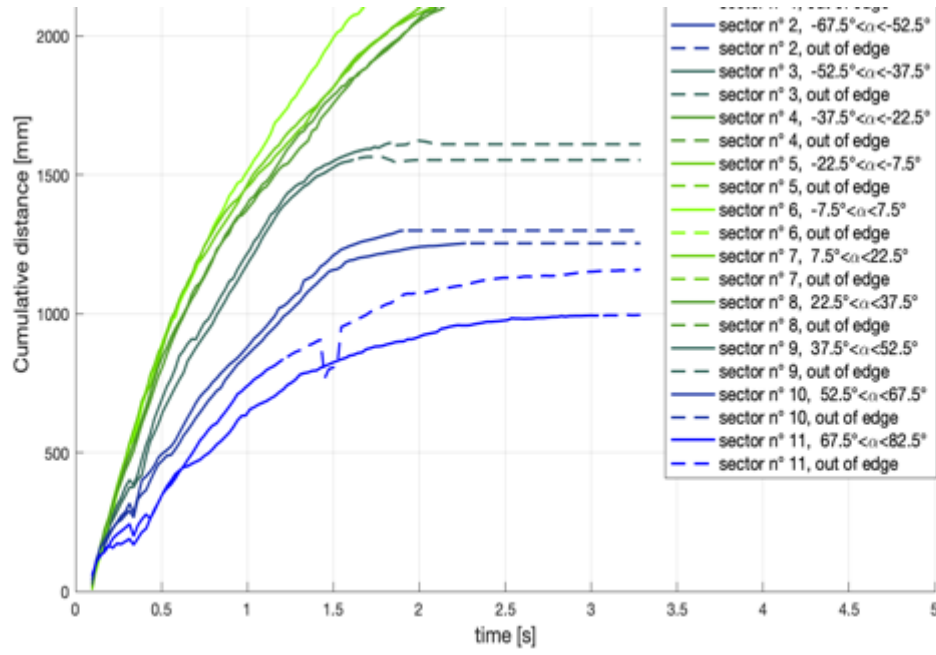


Figure 4.10: Comparison of cumulative distance in all sectors for test with mesh 10x10 with 0°

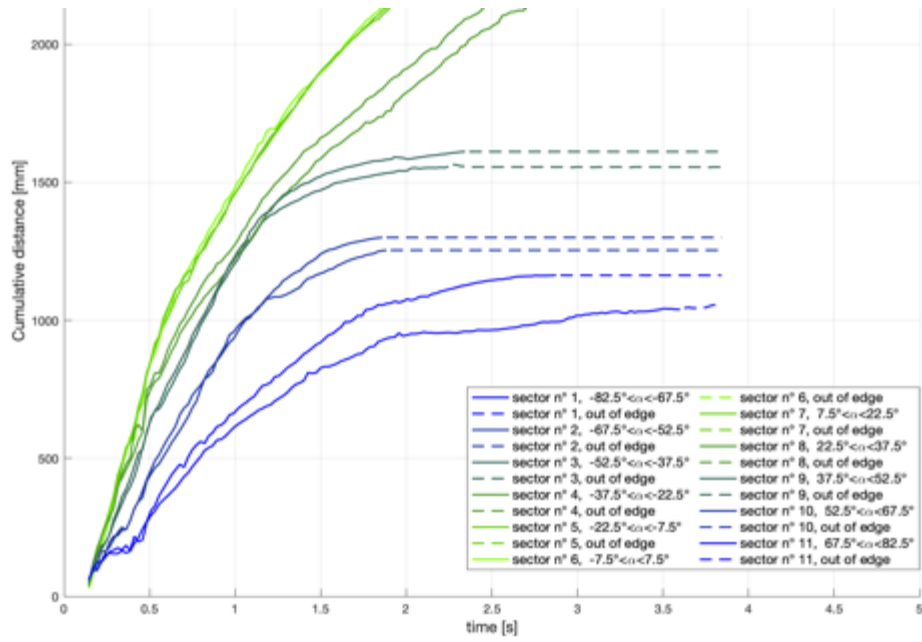


Figure 4.11: Comparison of cumulative distance in all sectors for test with mesh 10x10 with 45°

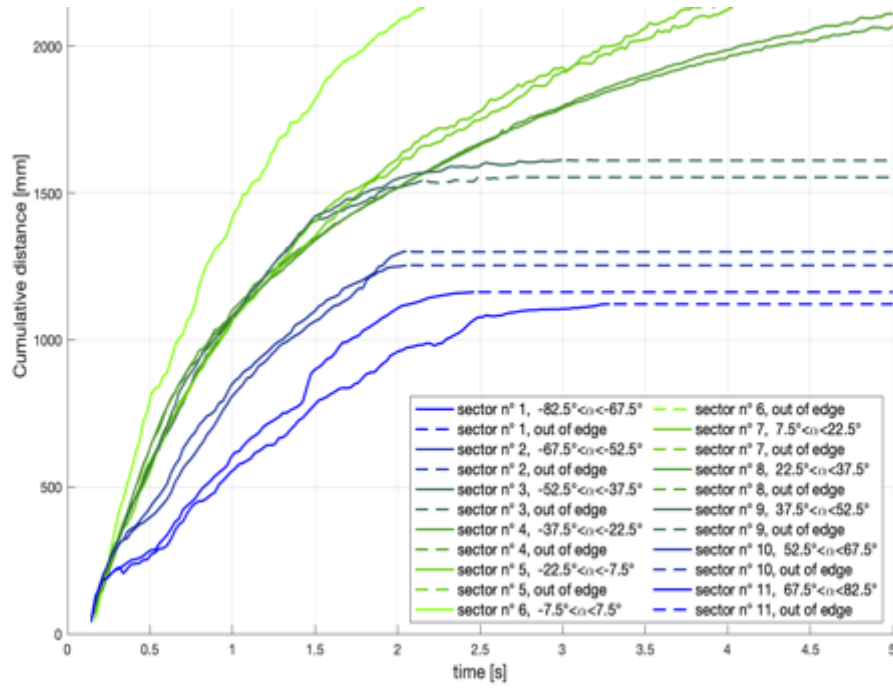


Figure 4.12: Comparison of cumulative distance in all sectors for test with mesh 5x5 with 0°

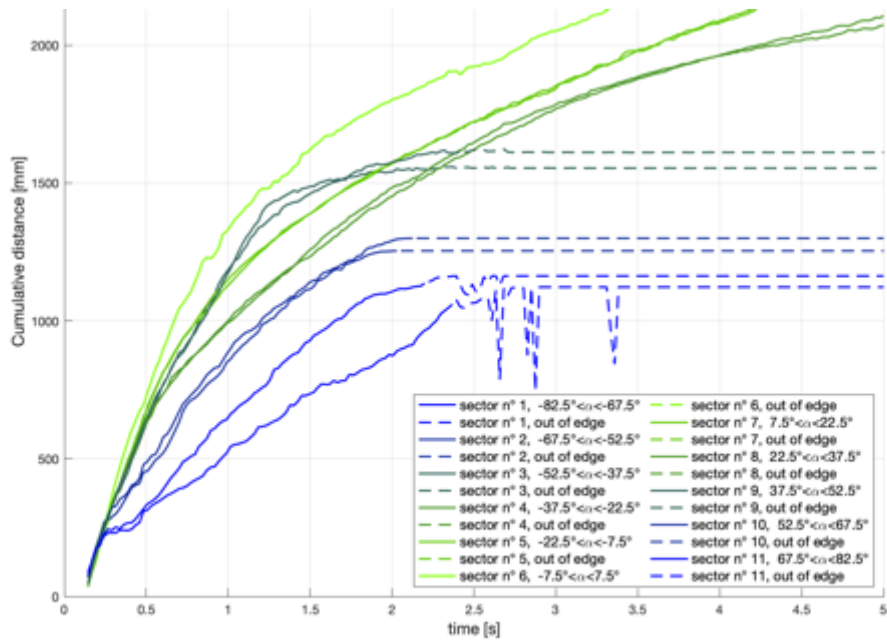


Figure 4.13: Comparison of cumulative distance in all sectors for test with mesh 5x5 with 45°

As a result of the cumulative distance, the sector number 6 reaches the highest values of distance in all the cases. After that, the sectors that are between 22.5° and 37.5° grow up faster than the others. It can be noticed that the distance does not start from 0 but from the impact point.

From the distances, it is possible to evaluate the velocity of the wave fronts. Its values of velocity are represented in the Figure 4.14, 4.15, 4.16, 4.17. The values obtained are the rolling average in seven different points.

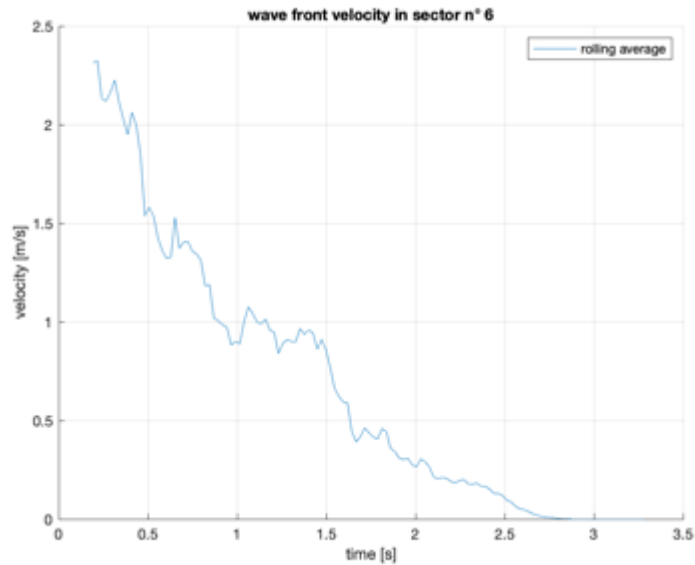


Figure 4.14: Velocity in sector 6 for test with mesh 10x10 with 0°.

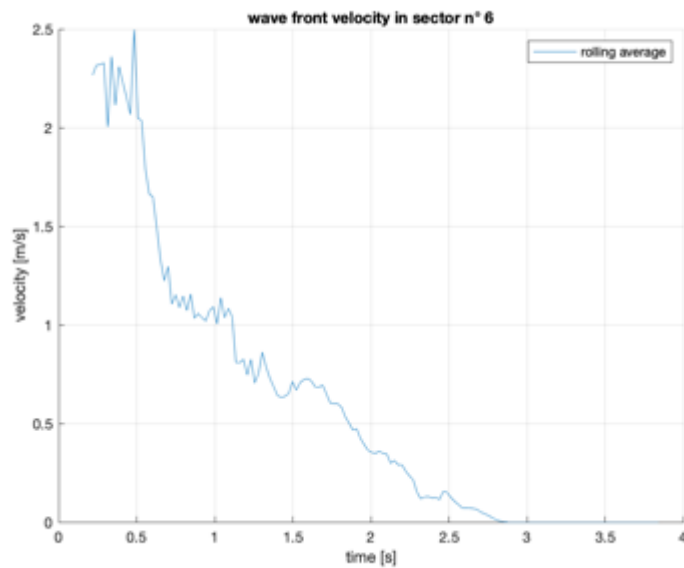


Figure 4.15: Velocity in sector 6 for test with mesh 10x10 with 45°.

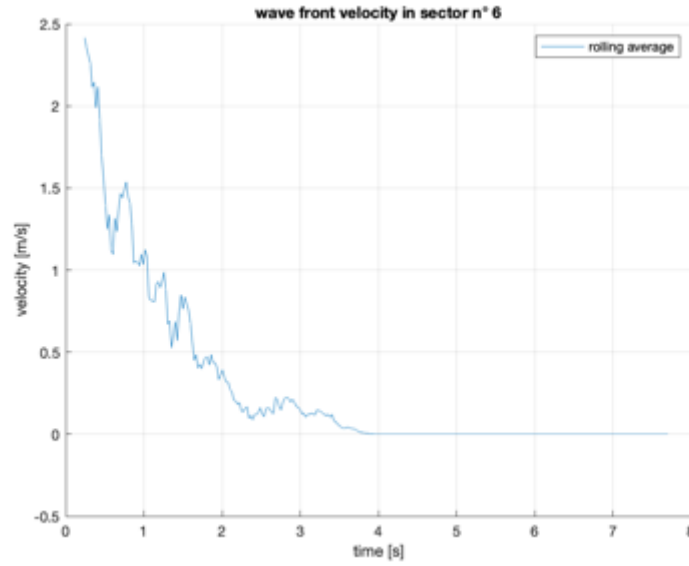


Figure 4.16: Velocity in sector 6 for test with mesh 5x5 with 0°.

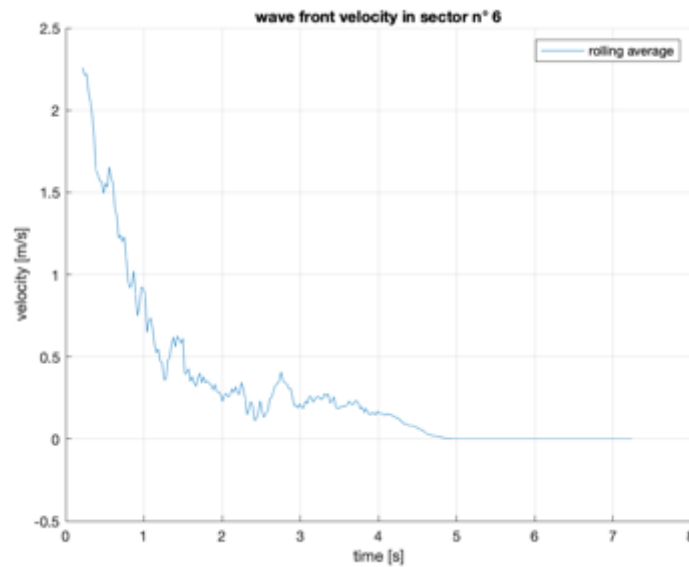


Figure 4.17: Velocity in sector 6 for test with mesh 5x5 with 45°.

As expected from results of distances, the central sector (sector n°6) is the one with the highest velocities. The values reach a maximum of 2.5 m/s in the first instants near the point of impact. After that, there is a fall that reaches the 0 m/s in 3 seconds in the case of the mesh 10x10 and 4 seconds in the case of mesh 5x5. This difference is due to the fact that the initial splitting of the wave leads to the creation of main channels through the metallic rods.

4.4 Lambert-Beer law and the evaluation of heights

The Lambert-Beer law describes the propagation of light in a medium considering the chemical properties of the medium and the light absorbed. Mainly used in chemistry, the law is used to describe all the phenomena that the ray theory is not able to mark out.

The empiric law was initially discovered by Pierre Bouguer (Bouguer, 1729) but it is granted to Lambert because it is described in his work *Photometria* (Lambert 1760). In the middle of the Eighteenth, Beer modified and improved the law saying that the absorbance is correlated to the concentration of the solute.

Nowadays, the Lambert-Beer law can be written as:

$$\ln\left(\frac{I}{I_0}\right) = -k \cdot h \quad 4.1$$

Where:

- I [cd] is the local intensity due to the light signal;
- I_0 [cd] is the initial intensity of the background;
- $k(\lambda)$ is a parameter that is function of the wavelength;
- h [m] is the path in the medium made by the light signal.

This represents the starting point for the water depth analysis.

In order to use the Lambert-Beer law for the purpose of the detection of the water depth, it is necessary to carry out two different measurements. This campaign leads to the evaluation of the coefficient k using a spectrometer.

The first one is the measurement on a bedground with a known level of red water.

The second kind of measurements is done in an aquarium with the same water at different heights.

The law can be written as:

$$k(\lambda) = -\left(\frac{\ln\left(\frac{I}{I_0}\right)}{h}\right) \quad \left[\frac{1}{m}\right] \quad 4.2$$

In particular, the term λ is the wavelength measured by the spectrometer.

As a result of the measurement campaign, see Figure 4.18.

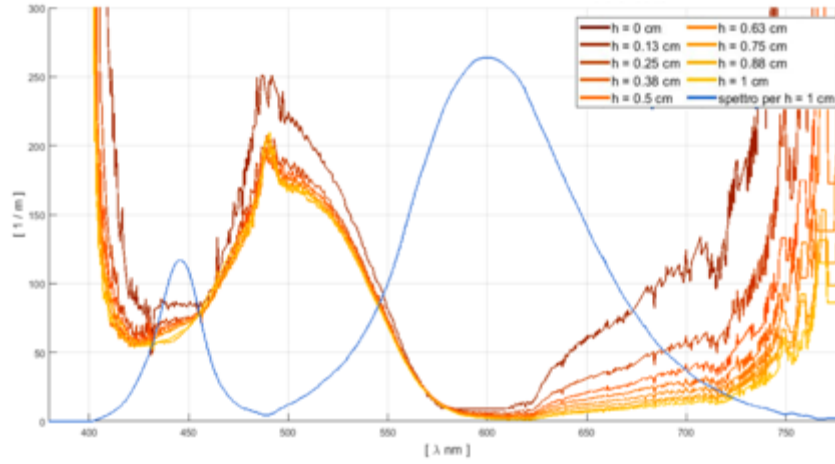


Figure 4.18: Measurements of the spectrometer of the k in function of the wavelength λ within 1 cm. Source: Briano, 2019.

As can be seen in Figure 4.18, the k has a high variability after 600 nm. This means that if this method would be used, the value of k should be refreshed step by step.

In order to avoid this problem, a new coefficient k' is searched. This coefficient takes into account the intensity ratio, given by the images of the Zyla camera, and the depth of water.

The sensor of the camera registers the energy of the light signal that is visible in the downstream area. The intensity is then dependent from the wavelength and the path.

Equation 4.1 can be written as:

$$\frac{I(\lambda, h)}{I_0(\lambda, h)} = \frac{\int_0^\infty I(\lambda, h) d\lambda}{\int_0^\infty I_0(\lambda, h) d\lambda} = e^{-k(\lambda) \cdot h} \quad 4.3$$

Equation 4.3 is valid in every pixel of the images.

For the purpose of the study, all the results between 600-780 nm do not take into account the dependence of the wavelength from heights, because all the heights after 0.13 cm tend to the same values.

Equation 4.2 is then written as:

$$k_i = - \left(\frac{\ln \left(\frac{A_i}{A_0} \right)}{h} \right) \quad \text{where } A_i = \int_0^\infty I(\lambda) d\lambda \quad 4.4$$

It can be noticed that the dependence from the water depth is loosen in equation 4.4.

The results of the analysis in the aquarium are shown in Figure 4.19.

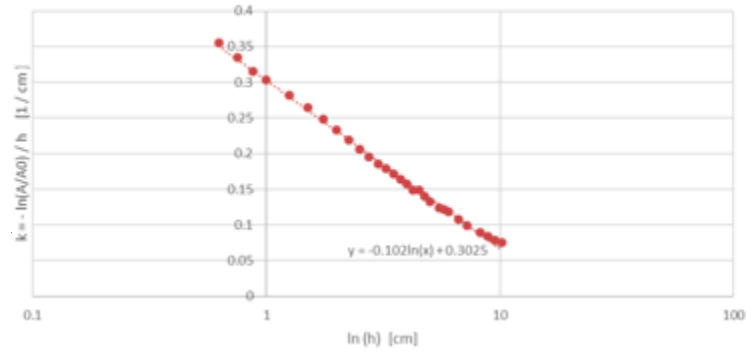


Figure 4.19: Trend of the parameter k' in dependence of $\ln(h)$ in the aquarium. Source: Briano, 2019.

The equation that describes the curve is:

$$k' = a \ln(h) + b = -0.102 \cdot \ln(h) + 0.3025 \quad 4.5$$

The attention is then moved to the measurements in the downstream area. In order to fit the results of the aquarium campaign, it is necessary to multiply the results by 2.3 for the test with the cone and 1.5 for the test without the cone.

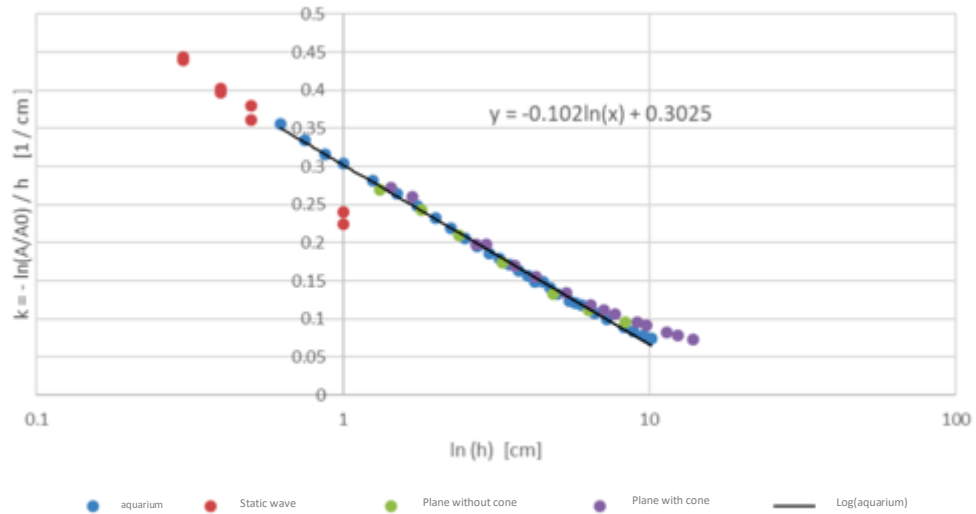


Figure 4.20: Trend of the parameter k' in dependence of the height h for all the different campaigns. Source: Briano, 2019.

With the results obtained, it is possible to use the Lambert-Beer law and the parameter k' for all the tests made with the physical model.

It is possible to build a graph in which, entering with the intensity values pixel per pixel, they are known the correspondent values of water depth.

The equation is:

$$\frac{I}{I_0} = e^{-h \cdot k'} = e^{-h \cdot (-0.102 \cdot \ln(h) + 0.3025)} \quad 4.6$$

The results are shown in Figure 4.21.

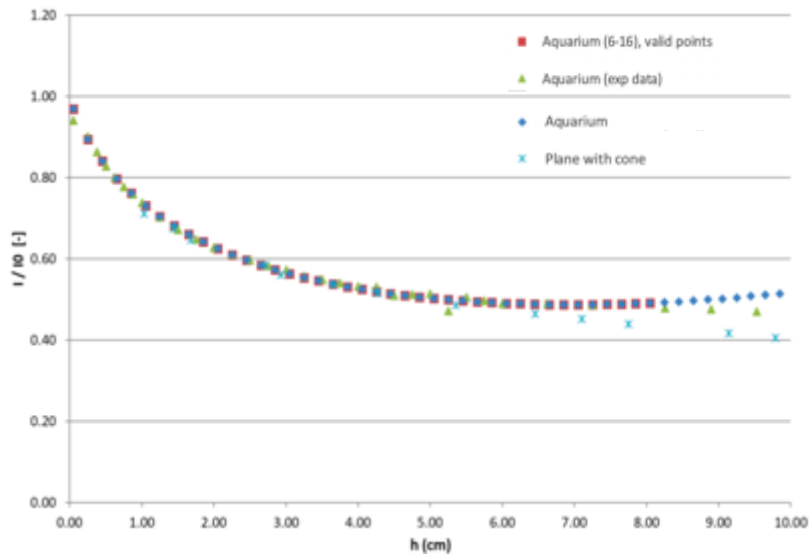


Figure 4.21: Conversion curve from intensity to depth. Source: Briano 2019.

4.5 Theoretical analysis of the upper part of the free surface profile in proximity of a rectangular orifice

In order to describe the behaviour of water in proximity of the sluice gate, it is necessary to start from the Torricelli theorem. He stated that:

“The velocity of a fluid passing through an orifice in the side of a reservoir is the same as that which would be acquired by a heavy body falling freely through the vertical height measured from the surface of the fluid in the reservoir to the centre of the orifice.”

The flow leaving a weir can be studied considering a series of orifices along the wall where each flow is independent, as shown in Figure 4.22. This was the study of Horton (Horton, 1907), in which the Torricellian theorem was applied to a spillway obtained through a high number of orifices along the wall.

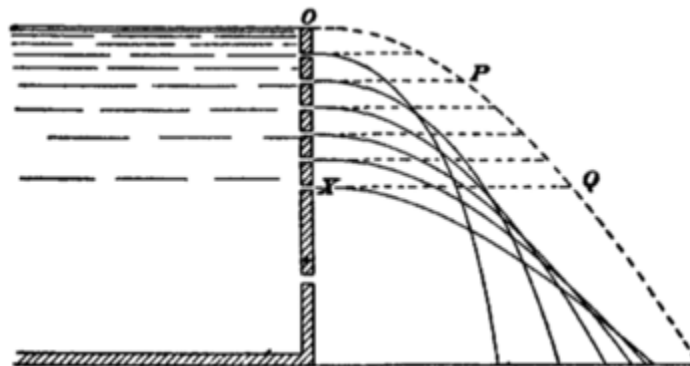


Figure 4.22: Independent flows from orifices. Source: Horton, 1907.

The total flow, considering the contribution of each orifice, is given by the formula:

$$Q = M\sqrt{2g} \left[A_1 H_1^{\frac{1}{2}} + A_2 H_2^{\frac{1}{2}} + \dots + A_n H_n^{\frac{1}{2}} \right] \quad 4.7$$

Where:

- M is a coefficient that it needs to be evaluated in each case;
- g is the gravity;
- A_i is the area of the generic orifice i ;
- H is the head.

In the application of Horton, the orifices are considered as increments of the head. In that case, the flow is given by the summation of each term as stated in the formula 4.8.

$$Q = \frac{MLH}{n} \sqrt{2g} \left[\sqrt{\frac{H}{n}} + \sqrt{\frac{2H}{n}} + \sqrt{\frac{3H}{n}} + \dots \right] \quad 4.8$$

Where:

$\frac{LH}{n} = A_1 + A_2 + \dots + A_n$ in the case of a rectangular weir.

The series under the square root can be written as: $\sqrt{1} + \sqrt{2} + \sqrt{3} + \dots + \sqrt{n} = \frac{2}{3} n^{\frac{3}{2}}$.

Equation 4.9 can be written as:

$$Q = \frac{MLH}{n} \sqrt{2g} \sqrt{\frac{H}{n}} \cdot \frac{2}{3} n^{\frac{3}{2}} = \frac{2}{3} MLH \sqrt{2gH} \quad 4.9$$

Focusing on the trajectories of the flows from the orifices, the equation that describes the trajectories is the one of the falling bodies:

$$y = z_0 - \frac{gt^2}{2} \quad 4.10$$

Considering the equation of velocity:

$$v = \frac{x}{t} \quad 4.11$$

Considering the equation of the velocity in a point near the orifice, as obtained from the Bernoulli analysis:

$$v = \sqrt{2gh} \quad 4.12$$

Making a system of equations 4.10, 4.11 and 4.12, it is obtained:

$$y = z_0 - \frac{x^2}{4h} \quad 4.13$$

Where:

- x is the distance from the reservoir;
- z_0 is the height of the orifice considered;
- h is the difference between the total head (H and z_0).

Defining the function $F(x, y, z_0)$ as the function which describes the family of curves (equation 4.13) in a plane (x, y), the envelope can be found using the two following conditions:

$$F(x, y, z_0) = 0$$

$$\frac{\delta F(x, y, z_0)}{\delta z_0} = 0$$

Substituting the terms:

$$F(x, y, z_0) = y - z_0 - \frac{x^2}{4(H - z_0)}$$

$$F(x, y, z_0) = 4yH - 4yz_0 - 4Hz_0 + 4z_0^2 + x^2$$

Using the second condition:

$$\frac{\delta F(x, y, z_0)}{\delta z_0} = -4y - 4H + 8z_0 = 0$$

The previous passage gives:

$$z_0 = y + \frac{y + H}{2} \quad 4.14$$

Substituting the 4.14 in 4.13, it can be obtained:

$$y = z_0 - \frac{x^2}{2H - z_0}$$

$$x^2 + 4(y - z_0)(H - z_0) = 0$$

$$x = H - y \quad 4.15$$

The equation 4.15 describes a line with a slope of -1 and an angle of 45° . The envelope is shown in Figure 4.23.

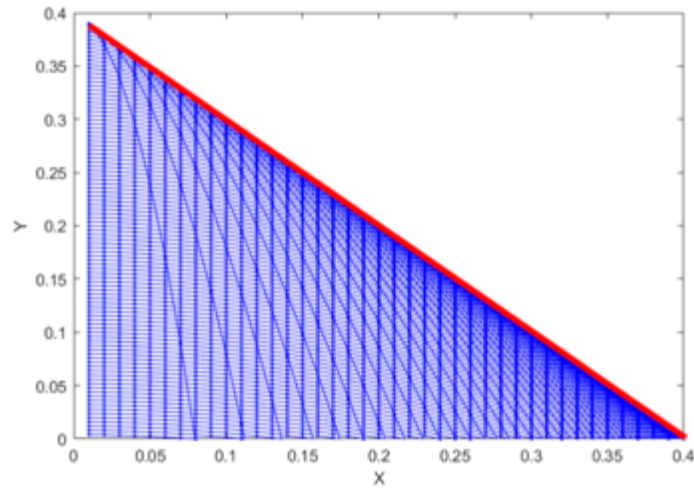


Figure 4.23: Envelope of the flows passing through parallel orifices

Chapter 5

The numerical model

The numerical model is a useful instrument in the engineering and science fields, that allows us to solve complex problems. On one hand, it is possible to reproduce numerical tests in order to simulate real past events, with registered human loss, and to recreate the scenarios that are difficult or impossible to build on a physical model. On the other hand, it is possible to obtain several information that are not possible to measure during the experimental observation, which is a great advantage when the investigation does not look for the evaluation of variables related to the flow (like velocity, pressure, etc.).

The equations related to numerical models can be solved with a mesh using a Eulerian description or can be solved without any mesh with a Lagrangian description. All the methods based on mesh (finite elements, finite differences and finite volumes) are robust methods, well developed and with a great variety of applications carrying good results. The mesh-based methods are powerful in the case of fixed boundaries and restricted domain. But, as soon as the boundaries have a high variation in terms of velocity or the system is complex, results cannot be considered as reliable.

The work of this thesis is focused on the use of the meshfree method (and Lagrangian), which is widely adopted in solid mechanics and fluid dynamics. For ages, the computational fluid dynamics CFD had used a mesh-based method (finite volumes). Passing to a meshfree method means a change in the distribution of the nodes, that are placed in an arbitrary manner. In this way, there is a search for a flexible and versatile model if compared to the mesh-based ones. The meshfree method is a good improvement for all the applications with complex geometry, discontinuity and high displacements in the flow. In particular, the meshfree method used to simulate the dam-break is Smoothed Particle Hydrodynamics (SPH).

5.1 Smoothed Particle Hydrodynamics Method

Smoothed Particle Hydrodynamics (SPH) is a Lagrangian meshfree method that has been developed in the last 50 years and widely used in the field of fluid dynamics. Starting from the 1970s, this method was first developed by Gingold and Monaghan, 1977, Lucy, 1977, for the purpose of studying the astrophysics and cosmology.

After that, this method has been applied in different situations, showing its robustness in different fields of astrophysics, magneto-hydrodynamics and solid mechanics. In the last years the application has covered even the field of waves and coastal structures and their interactions, floating objects, wave propagation and industrial applications in different fields. Related to dam-break, there is a great variety of case studies and in 2004 a study conducted by Gómez-Gesteira and Dalrymple, 2004, led to the 3D analysis.

In SPH, the continuum is discretized as a group of points or nodes called particles. In SPH, when it is used for simulations of fluid dynamics the resolution of the Navier-Stokes equations leads to the evaluation of the representative physical variables (like velocity, position, density and pressure) for each particle, as an interpolation of the surrounding particles. The Navier-Stokes equations are the momentum equation (to evaluate the variation ratio of velocity or acceleration) and the continuity equation (to evaluate the variation ratio of density).

In SPH, the conservation laws are written in the differential form, instead of the integral, and using an interpolation function. In this way, the equations can deal with the particles used for describing the reality at a certain point of the domain.

In the integral form, any function $A(\mathbf{r})$ is defined in \mathbf{r}' as:

$$A(\mathbf{r}) = \int_{\Omega} A(\mathbf{r}') W(\mathbf{r} - \mathbf{r}', h) d\mathbf{r}' \quad 5.1$$

Where:

- \mathbf{r} is the position vector
- W is the kernel function
- h is the distance of interaction

The approximation of the previous equation in the discrete form is written as:

$$A(\mathbf{r}) = \sum_{j=1}^N A(\mathbf{r}_j) W(\mathbf{r} - \mathbf{r}_j, h) \frac{m_j}{\rho_j} \quad 5.2$$

The summation takes into account all the neighbouring particles j that are in the region defined by the kernel function W . Moreover, in the discretized equation there are the mass m_j and density ρ_j of the neighbouring particles respectively. Their ratio represents the volume of the neighbouring particles Δv_j .

In this way from the equation (5.1) to (5.2) is possible to pass from the continuum to the discrete notation, from integral to discrete.

5.1.1 The smoothing kernel

In order to consider a limited domain in which it is possible to evaluate the behaviour of the particle of interest, the kernel function W is used for the purpose.

In general, kernels are considered as a part of a non-dimensional distance q , related to the smoothing length h and the distance between the particle of study and one other particle r : $q = \frac{r}{h}$.

The kernel chosen for the analysis is the quintic (Wendland, 1995)

$$W(r, h) = \alpha_D \left(1 - \frac{q}{2}\right)^4 \quad 0 \leq q \leq 2 \quad 5.3$$

where α_D is equal to $7/4\pi h^2$ in 2-D and $21/16\pi h^3$ in 3-D. The trend of the kernel and its derivative is shown in Figure 5.1.

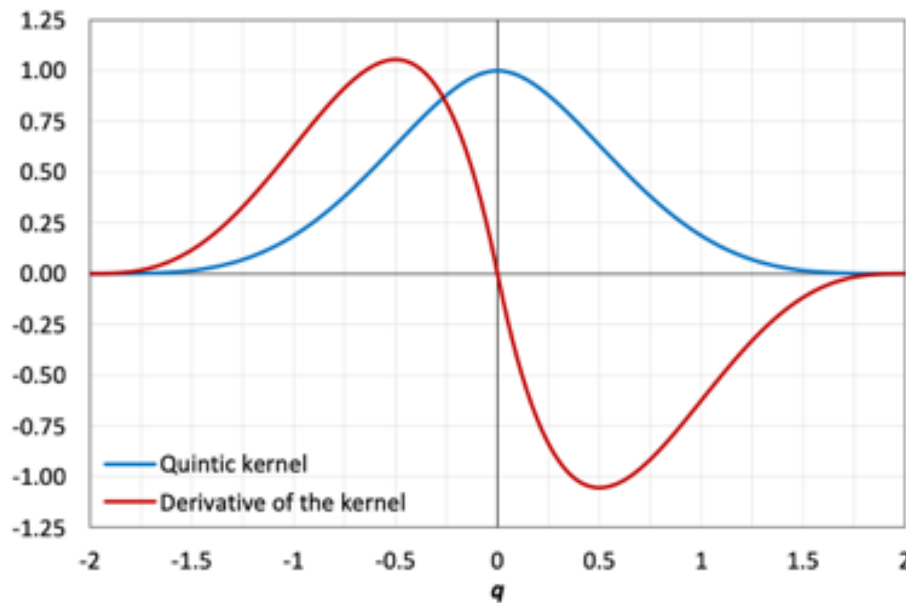


Figure 5.1: Quintic kernel and the derivative divided by the factor α_D . Source: Domínguez, 2014.

This function has different properties:

- Positivity: $W(r - r_j, h) \geq 0$ in the domain
- Function defined in a limited domain: $W(r - r_j, h) = 0$ out of the domain
- Standardization: $\int W(r - r_j, h) dr' = 1$
- The limit that tends to zero: $\lim_{h \rightarrow 0} W(r - r_j, h) dr' = \delta(r - r')$
- Decreasing monotonic behaviour of $W(r - r_j, h)$

In the Figure 5.2, it is shown the interaction domain in relation with the kernel function (W). All the particles that are at a distance that is less than $2h$ (double of the smoothing length) are the neighbouring particles which interact with the particle of interest. As can be seen the trend is represented by a normal distribution of probability and less is the distance, more is the contribution.

In particular the s represents the coefficient that multiplies the smoothing length and it is equal to 2. This leads to consider an upper domain of interaction to describe the behaviour of the particle of interest.

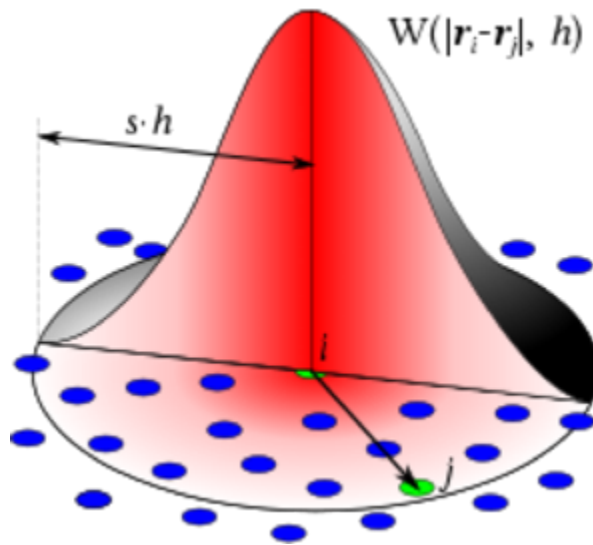


Figure 5.2: Kernel function (W) and smoothing length (h).

5.1.2 Momentum Equation

The Navier-Stokes equation of the moment conservation leads to the evaluation of the fluid velocity:

$$\frac{Dv}{Dt} = -\nabla \frac{P}{\rho} + g + \nu_0 \nabla^2 v \quad 5.4$$

where P is the pressure, ρ is the density, v is the velocity, g is the gravity and $\nu_0 \nabla^2 v$ is the viscosity term. Passing to SPH, the (5.4) can be written as:

$$\frac{dv_a}{dt} = - \sum_b m_b \left(\frac{P_b}{\rho_b^2} + \frac{P_a}{\rho_a^2} + \Pi_{ab} \right) + \nabla_a W_{ab} - g \quad 5.5$$

This equation is used to evaluate the velocity of the particle a (v_a) from the sum of the interactions with all the neighboring particles b , using the kernel function W_{ab} that is evaluated starting from the distance between particles a and b . In this case the viscosity term is Π_{ab} .

In detail, the viscosity term is equal to

$$\Pi_{ab} = \begin{cases} -\frac{\alpha \overline{c_{ab}} \mu_{ab}}{\overline{\rho_{ab}}} & v_{ab} \cdot r_{ab} < 0 \\ 0 & v_{ab} \cdot r_{ab} > 0 \end{cases} \quad 5.6$$

Where:

- $\overline{\rho_{ab}} = 0.5(\rho_a + \rho_b)$ is the mean density between two different particles
- $r_{ab} = r_a - r_b$ is the distance between two particles
- $v_{ab} = v_a - v_b$ is the difference of velocity between two particles
- $\mu_{ab} = \frac{h v_{ab} \cdot r_{ab}}{(r_{ab}^2 + \eta^2)}$
- $\overline{c_{ab}} = 0.5(c_a + c_b)$ is the mean value of the speed of sound
- α is a coefficient that takes dissipation according to its value. The value considered in the analysis proposed in this work are with a value of $\alpha = 0.1$
- $\eta^2 = 0.001 h^2$ is a factor that avoids the divergence when the distance between particles is next to zero.

5.1.3 Continuity Equation

The continuity equation of Navier-Stokes (or mass conservation equation) is:

$$\frac{1}{\rho} \frac{D\rho}{Dt} + \nabla \cdot \mathbf{v} = 0 \quad 5.7$$

In the SPH form, the previous equation can be written:

$$\frac{d\rho_a}{dt} = \sum_b m_b \mathbf{v}_{ab} \cdot \nabla_a W_{ab} \quad 5.8$$

Moreover, in DualSPHysics can be applied a δ -SPH formulation that introduce a diffusive term (Molteni and Colagrossi, 2009) in order to reduce the density fluctuations:

$$\frac{d\rho_a}{dt} = \sum_b m_b \mathbf{v}_{ab} \cdot \nabla_a W_{ab} + 2\delta h \sum_b m_b \overline{c_{ab}} \left(\frac{\rho_a}{\rho_b} - 1 \right) \frac{1}{r_{ab}^2 + \eta^2} \cdot \nabla_a W_{ab} \quad 5.9$$

Where:

- $\overline{c_{ab}} = 0.5(c_a + c_b)$ is the mean value of the speed of sound
- δ is the *delta*-SPH coefficient.

In particular, for the aim of this thesis, δ -SPH is not applied.

5.1.4 State Equation

The fluid in the SPH formulation is assumed as weakly compressible (Monaghan, 1994) and the pressure is evaluated starting from the density. The compressibility is handled in order to use lower values of the speed of sound: in this way the time step size can be maintained at low values. Anyway, this leads to the constriction to have the speed of sound at least ten times faster than the velocity of the particles, density variation less than 1%.

According to Monaghan et al., 1999, and Batchelor, 1974, the state equation is:

$$P = B \left[\left(\frac{\rho}{\rho_0} \right)^\gamma - 1 \right] \quad 5.10$$

Where:

- $\gamma = 7$
- $\rho_0 = 1000 \text{ kg/m}^3$ is the density
- $c_0 = c(\rho_0) = \sqrt{\partial P / \partial \rho}_{\rho_0}$ is the speed of sound for a specific density
- $B = c_0^2 \rho_0 / \gamma$.

Considering the equations written above, the values of dv/dt and $d\rho/dt$ are evaluated starting from the equations (5.5) and (5.8). With these values and at the next temporal step (Δt), the values of velocity and density of all of the particles are estimated. From the velocity is possible to evaluate the position of the particles and from the density the pressure is found using the state equation.

5.1.5 Time Stepping

In DualSPHysics is possible to choose between different numerical integration schemes. In particular, the one used in the numerical tests is the Symplectic Scheme.

Considering the following equalities:

$$\frac{dv_a}{dt} = F_a \quad 5.11a$$

$$\frac{d\rho_a}{dt} = D_a \quad 5.11b$$

$$\frac{dr_a}{dt} = v_a \quad 5.11c$$

5.1.5.1 Symplectic Scheme

This scheme is represented by a time reversible algorithm in the absence of friction or viscous effects. It maintains the energy time-reversal symmetry that can be found in the motion equations, which leads to a major resolution in long term solution behaviour. This scheme has an accuracy of $o(\Delta t^2)$ and presents predictor and corrector steps.

Considering the predictor steps, acceleration and density are determined at half of the time step:

$$r_a^{n+\frac{1}{2}} = r_a^n + \frac{\Delta t}{2} v_a^n \quad \rho_a^{n+\frac{1}{2}} = \rho_a^n + \frac{\Delta t}{2} D_a^n \quad 5.12$$

In the corrector stage the term $dv_a^{n+\frac{1}{2}}/dt$ is used to evaluate the value of the velocity, and then the position, at the end of the time step through:

$$v_a^{n+1} = v_a^{n+\frac{1}{2}} + \frac{\Delta t}{2} F_a^{n+\frac{1}{2}} \quad r_a^{n+1} = r_a^{n+\frac{1}{2}} + \frac{\Delta t}{2} v_a^{n+\frac{1}{2}} \quad 5.13$$

In the end the true value of density $d\rho_a^{n+1}/dt = D_a^{n+1}$ is evaluated using the values v_a^{n+1} and r_a^{n+1} just updated (Monaghan, 2005).

5.1.5.2 Variable Time Step

The other scheme is represented by the variable time step which is subject to the Courant-Friedrich-Levy (CFL) condition, force terms and viscous diffusion term. The variable time step Δt can be calculated as proposed (Monaghan and Kos, 1999)

$$\begin{aligned}
 \Delta t &= 0.2 \cdot \min(\Delta t_f, \Delta t_{cv}) \\
 \Delta t_f &= \min\left(\sqrt{\frac{h}{|f_a|}}\right) \\
 \Delta t_{cv} &= \min_a \frac{h}{c + \max_b \left| \frac{h v_{ab} \cdot r_{ab}}{(r_{ab}^2 + \eta^2)} \right|}
 \end{aligned} \tag{5.14}$$

where Δt_f is related to the force per unit mass ($|f_a|$) and Δt_{cv} is related to the Courant and viscous time step controls.

5.1.6 Boundary Conditions

Boundary conditions are represented by particles that are the same as the ones of the fluid but with different behaviour. In fact, it is possible to assign to a group of particles as boundary particles. Furthermore, it is possible to distinguish between different boundary conditions as described below.

5.1.6.1 Dynamic Boundary Conditions

The Dynamic Boundary Conditions (DBC) is the default method used in DualSPHysics (Crespo et al., 2007). Using this boundary condition, all the particles that create the system are divided in two main groups: the first group of particles represents the fluid and they are moved by force applied on them; the second group is the boundary particles that are fixed or moving according a predefined motion. It allows simulating gates or wave-makers.

During the execution of the numerical model, when two different kinds of particles interact the distance between them is less than $2h$, that is twice the smoothing length. Moreover, the density reaches higher value than the standard due to this interaction and the pressure increases too. This leads to generate repulsive forces that interest the fluid particles, according to the pressure term in the moment equation.

The stability of this method is guaranteed by the choice of the time step, that should be relatively short so that is possible to deal with the highest velocity of the fluid. In fact, this can be a trouble if considering how the time step is evaluated.

5.1.6.2 Pre-imposed Boundary Motion

In DualSPHysics it is also possible to set a pre-imposed motion to a group of boundary particles. Various movements can be assigned considering their availability in the code and third part motions from different files can be added to the code.

The behaviour of this kind of particles is the same as described above (DBC), but they move according to the imposed motion and the forces acting on them. This is a good way to recreate complex cases, such as the ones in which the boundaries make an influence on the fluid.

5.2 DualSPHysics code

The Ephyslab group of the University of Vigo (Spain) has developed a code called *DualSPHysics*, in collaboration with researchers from different universities University of Manchester (United Kingdom), Università degli Studi di Parma (Italy), Instituto Superior Técnico de Lisboa (Portugal) and the Universiteit Gent (Belgium). The work was initially focused on the wave propagation and the interaction with the coastal structures (Crespo et al., 2015, Altomare et al., 2015 and Altomare et al., 2017).

Prof. Peter Stansby

Dr Benedict D. Rogers
Dr Athanasios Mokos
Dr Georgios Fourtakas

Prof. Moncho Gómez Gesteira

Dr Alejandro J.C. Crespo
Dr Jose M. Domínguez
Dr José González Cao
Orlando G. Feal

Prof. Rui Ferreira

Dr Ricardo Canelas
Dr Moisés Brito



Prof. Peter Troch

Dr Vasiliki Stratigaki
Dr Tomohiro Suzuki
Dr Tim Verbrugghe

Prof. Paolo Mignosa

Dr Renato Vacondio

Prof. Agustín Sánchez

Dr Xavier Gironella
Dr Corrado Altomare

Figure 5.3: Institutions involved in the DualSPHysics project.

DualSPHysics is an open-source code that can be downloaded freely from the web page www.dual.sphysics.org (see Figure 5.4). The politic of the research group is that anyone can deal with the code, improving it and reaching new goals.

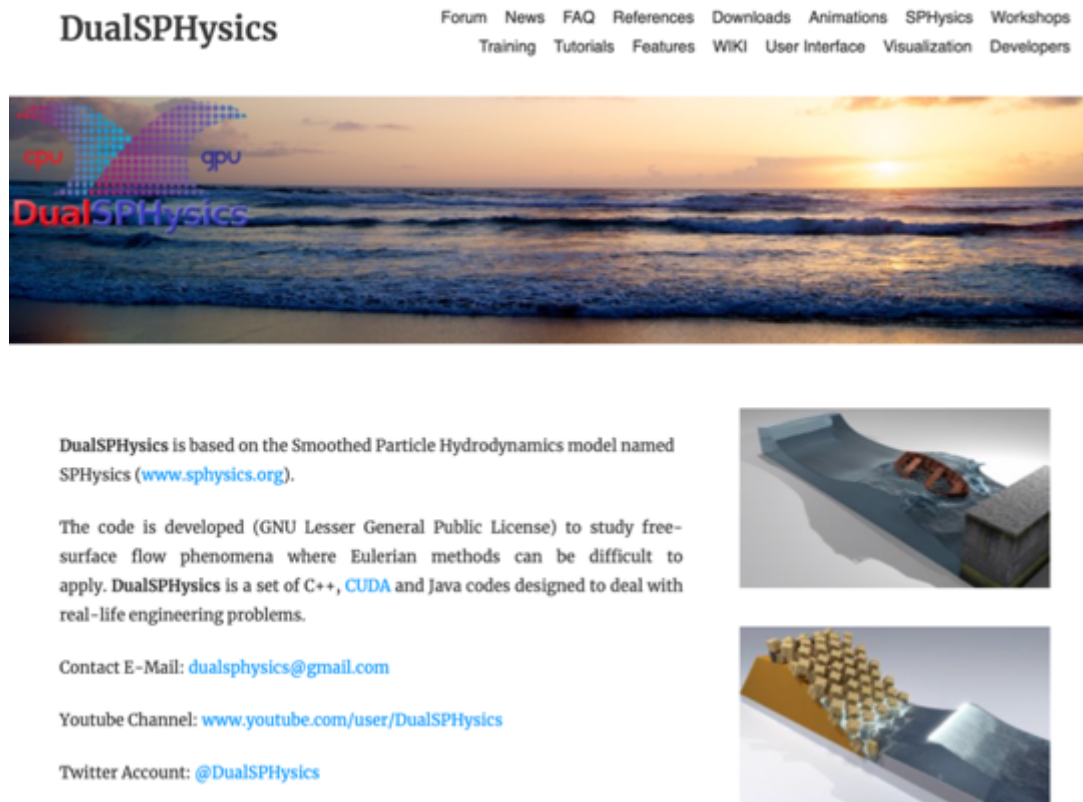


Figure 5.4: Webpage of DualSPHysics. Source: dual.sphysics.org

The code can deal with every kind of test, but the main problem is related to the high computational costs. This leads to avoid the use of the code for some real engineering problems. In particular, in some cases describing the problem, the number of particles representing the system increases a lot, leading to high computational costs. Instead of having a limit in the time domain, there is a limit in the number of particles that can be processed. For this reason, the High-Performance Computation (HPC) is a necessary instrument to solve this kind of problems.

The code has been implemented both on CPU, using C++, and GPU, using CUDA (Domínguez et al., 2013). Moreover, multiple CPUs simulation can be run nowadays, with the aim of running on multiple GPUs in the future.

It is well known in the scientific community that the GPU (Graphics Processing Unit) are a good alternative to speed up some processes: the same is for SPH, using a great programming potential in parallel, where the graphic units are used to run the simulations.

As a result of implementing the run on the GPU, it is demonstrated that the cases run in GPU are up to 100 times faster than the ones run in the CPU (Crespo et al, 2011).

In this way is possible to run complex cases with millions of particles and using a high-resolution, maintaining reasonable time executions.

All the simulations for the purpose of this thesis are executed on a computer using a GPU *GeForce GTX1080*.

5.3 Initial Conditions & Pre-processing

The generation of the initial condition in DualSPHysics is the creation of the particles with their initial position, velocity and density, etc. As already said in the previous paragraphs, SPH is a numerical mesh-free method where no mesh is used to describe the interactions between particles and to solve the fluid dynamics equations. But, at the starting point it is necessary to create the particles in an exact position and to do that is necessary to use a mesh. After that, all the particles can move freely in the domain.

To detect the initial position where all the particles can be created, a cartesian tridimensional mesh is used and all the particles will be created in the nodes of the mesh. The distance between each node is called dp . In order to represent 3D objects is just necessary to use the nodes that are close to the geometry of the objects.

In Figure 5.5 is shown how is possible to discretize a triangle in particles.

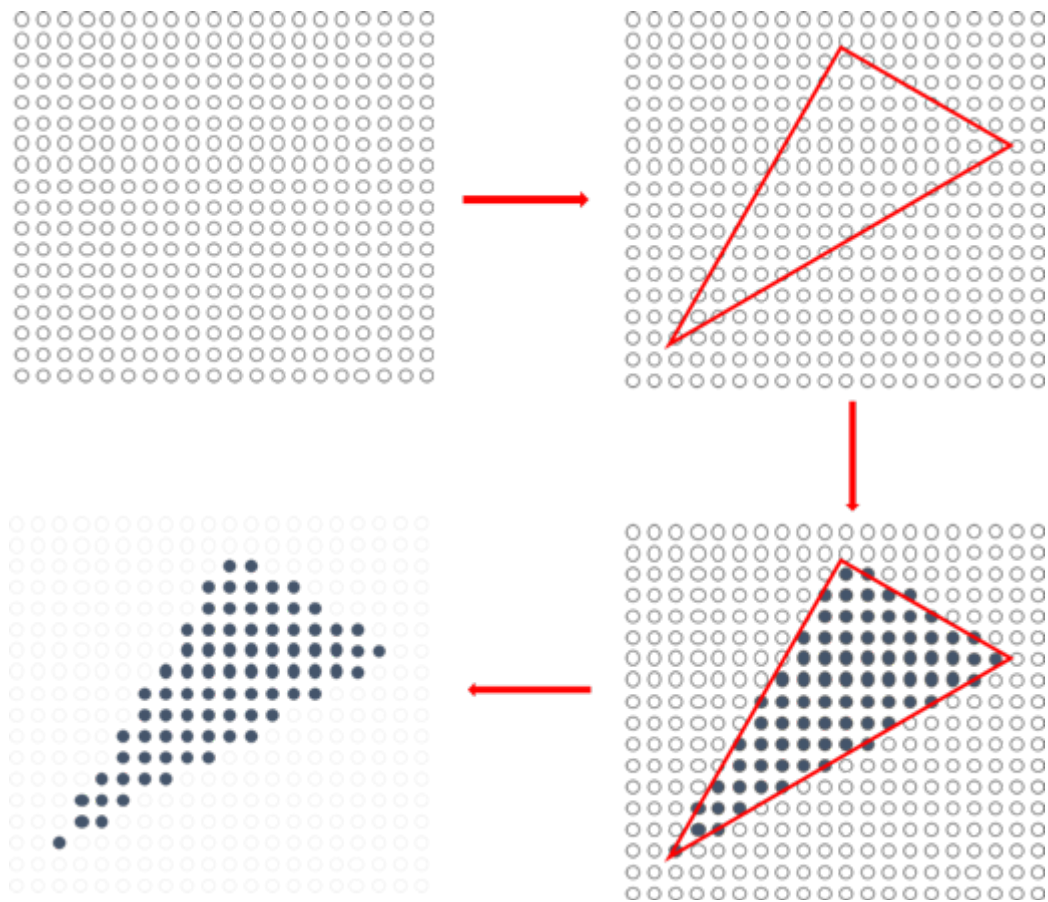


Figure 5.5: Creation of a triangle using particles. Source: XML Guide for DualSPHysics v4.4.

Once the object is defined using particles, can be noticed that there always be a lack of information and it is related to the resolution. Lower the dp is, higher precision there is.

This is how the *GenCase* works in order to recreate the geometry, and in general the setup of the case. The user is able to do that using the existing *.xml* example files and modifying them as preferred. Every *.xml* file is considered as divided in different sections, which allows an easier use of it at the users.

A brief description of the main sections is given to the reader below.

```

name app"molcdm v4.0.100 (27-06-2023)" data"08-06-2013 04:25:50"

constantsdef
<define bound"1" fluid"0" />
<gravity w"0" yw"0" xw"0.81"/>
<stop value"1000"/>
<hole value"0" auto"true"/>
<open value"0"/>
<seedopen value"0"/>
<seedround value"20"/>
<seedround value"0"/>
<seed value"0.5"/>
<dp value"1"/>
<number value"0.2"/>
</constantsdef>

<define bound"2" fluid"0" />
<geometry>
<definition dp"0.005" units_comment"metres (m)">
<pointmin x"2" yw"0" xw"1 />
<pointmax x"4" y"3.8" xw"0.5" />
</definition>
<command>
<initlist>
<newer GateWidth"0.0375" gate"true" rem"Gate hole" />
<newer Gate"0.32" gate"true" rem"Initial position of gate" />
<newer dp"0.2" gate"true" rem"Half of dp" />
<setshapebox"actual 1 dp 1 bound"/setshapebox>
<setround mode"full" />
<!-- Tank for fluid -->
<setabound ab"0" />
</define>
<!-- Wall tank -->
<define>
<setfill"wall"right/top/boxfill>
<layer wdp"1" />
<point xw"1.5" yw"0.75" xw"0" />
<size xw"1.5" yw"1.5" xw"0.42" />
</define>
<!-- Wall tank -->
<setabound ab"1" />
</define>
<define>
<setfill"wall"boxfill>
<point xw"0" yw"0.75-dp"2" xw"0" />
<size xw"0dp"2" yw"0.75dp"2" xw"0.42" />
</define>
<!-- Wall tank -->
<setabound ab"2" />
</define>
<define>
<setfill"wall"boxfill>
<point xw"0" yw"0dp"2" xw"0.75dp"2" xw"0.42" />
</define>
<!-- Output area -->
<setabound ab"3" />
</define>
<define>
<setfill"bottom/boxfill>
<layer wdp"1" />
<point xw"0" yw"1.5" xw"0" />
<size xw"4" yw"2" xw"0.10" />
</define>
<!-- Fills the fluid tank -->
<setabound ab"0" />
<fillbox xw"0.05" yw"0.01" xw"0.1" />
<modefill"void"/modefill>
<point xw"0" yw"0.8" xw"0.1" />
<size xw"1.0" yw"1.3" xw"0.5" />
</fillbox>
<shapeout file"" />
<!-- Gate -->
<setabound ab"0" />
</define>
<define>
<setfill"wall/boxfill>
<point xw"0.0001" yw"0.03" xw"0dp" />
<size xw"0dp"2" yw"0.06" xw"0.42" />
</define>
<shapeout file"Gate" />
</initlist>
</command>
</geometry>

<subreal ref"5">
<begin new"1" start"0.5798664" />
<newest lib" duration"0.0015" />
<real w"0" yw"0" xw"0.154" units_comment"m/s" />
</newest>
</subreal>
</define>
</initlist>

<move abbound"0" xw"0" yw"0dp" xw"0" />
<move abbound"1" xw"0" yw"0dp" xw"0" />
<move abbound"2" xw"0.0001" yw"0dp" xw"0" />
<move abbound"3" xw"0" yw"0.0001-dp"2" xw"0" />
<move abbound"0" xw"0" yw"0.0001-dp"2" xw"0" />
<move abbound"0" xw"0" yw"0dp" xw"0dp"2" />
</initlist>
</define>

<parameters>
<parameter key"Postionable" value"1" comment"Precision in particle interaction 0:simple, 1:boxlike, 2:time and space double (default=0)" />
<parameter key"StepAlgorithm" value"2" comment"Step Algorithm 1:Verlet, 2:symplectic (default=1)" />
<parameter key"VerletSteps" value"40" comment"Verlet only: Number of steps to apply Euler timestepping (default=40)" />
<parameter key"Kernel" value"2" comment"Interaction Kernel 1: cubic spline, 2:Woodward (default=1)" />
<parameter key"Viscosity" value"0" comment"Viscosity formulation 1:Artificial, 2:anisotropic (default=1)" />
<parameter key"Viscos" value"0.01" comment"Viscosity value" />
<parameter key"ViscosityFactor" value"1" comment"Multiply viscosity value with boundary (default=1)" />
<parameter key"DeltaDP" value"0" comment"DeltaDP value, 0.1 is the typical value, with 0 disabled (default=0)" />
<parameter key"Shift" value"0" comment"Time to freeze the flootage at simulation start (warmup (default=0) units_comment"seconds" />
<parameter key"ShiftCoeff" value"2" comment"Coefficient for shifting computation (default=2)" />
<parameter key"ShiftTP" value"1.5" comment"Threshold to detect free surface. Typically 1.5 for 2D and 2.75 for 3D (default=0)" />
<parameter key"ShiftAlgorithm" value"1" comment"Shift Algorithm 1:SPM, 2:SRM (default=1)" />
<parameter key"FlowRate" value"0.5" comment"Flow rate to freeze the flootage at simulation start (warmup (default=0) units_comment"seconds" />
<parameter key"FlowRateCoeff" value"0.05" comment"Coefficient to calculate minimum time step dtime=coeff*min(h/speedsound (default=0.05)" />
<parameter key"FlowRate" value"0.0001" comment"Initial time step (default=h/speedsound) units_comment"seconds" />
<parameter key"FlowRate" value"0.0001" comment"Minimum time step (default=coeff*min(h/speedsound) units_comment"seconds" />
<parameter key"FlowRateCoeff" value"0.05" comment"Coefficient for shifting computation (default=2)" />
<parameter key"FlowRate" value"0.0001" comment"Initial time step (default=h/speedsound) units_comment"seconds" />
<parameter key"FlowRate" value"0.0001" comment"Minimum time step (default=coeff*min(h/speedsound) units_comment"seconds" />
<parameter key"FlowRateCoeff" value"0.05" comment"Coefficient for shifting computation (default=2)" />
<parameter key"FlowRate" value"0.0001" comment"Initial time step (default=h/speedsound) units_comment"seconds" />
<parameter key"FlowRate" value"0.0001" comment"Minimum time step (default=coeff*min(h/speedsound) units_comment"seconds" />
<parameter key"FlowRateCoeff" value"0.05" comment"Coefficient for shifting computation (default=2)" />
<parameter key"FlowRate" value"0.0001" comment"Initial time step (default=h/speedsound) units_comment"seconds" />
<parameter key"FlowRate" value"0.0001" comment"Minimum time step (default=coeff*min(h/speedsound) units_comment"seconds" />
<parameter key"FlowRateCoeff" value"0.05" comment"Coefficient for shifting computation (default=2)" />
<parameter key"FlowRate" value"0.0001" comment"Initial time step (default=h/speedsound) units_comment"seconds" />
<parameter key"FlowRate" value"0.0001" comment"Minimum time step (default=coeff*min(h/speedsound) units_comment"seconds" />
<parameter key"FlowRateCoeff" value"0.05" comment"Coefficient for shifting computation (default=2)" />
<parameter key"FlowRate" value"0.0001" comment"Initial time step (default=h/speedsound) units_comment"seconds" />
<parameter key"FlowRate" value"0.0001" comment"Minimum time step (default=coeff*min(h/speedsound) units_comment"seconds" />
<parameter key"FlowRateCoeff" value"0.05" comment"Coefficient for shifting computation (default=2)" />
<parameter key"FlowRate" value"0.0001" comment"Initial time step (default=h/speedsound) units_comment"seconds" />
<parameter key"FlowRate" value"0.0001" comment"Minimum time step (default=coeff*min(h/speedsound) units_comment"seconds" />
<parameter key"FlowRateCoeff" value"0.05" comment"Coefficient for shifting computation (default=2)" />
<parameter key"FlowRate" value"0.0001" comment"Initial time step (default=h/speedsound) units_comment"seconds" />
<parameter key"FlowRate" value"0.0001" comment"Minimum time step (default=coeff*min(h/speedsound) units_comment"seconds" />
<parameter key"FlowRateCoeff" value"0.05" comment"Coefficient for shifting computation (default=2)" />
<parameter key"FlowRate" value"0.0001" comment"Initial time step (default=h/speedsound) units_comment"seconds" />
<parameter key"FlowRate" value"0.0001" comment"Minimum time step (default=coeff*min(h/speedsound) units_comment"seconds" />
<parameter key"FlowRateCoeff" value"0.05" comment"Coefficient for shifting computation (default=2)" />
<parameter key"FlowRate" value"0.0001" comment"Initial time step (default=h/speedsound) units_comment"seconds" />
<parameter key"FlowRate" value"0.0001" comment"Minimum time step (default=coeff*min(h/speedsound) units_comment"seconds" />
<parameter key"FlowRateCoeff" value"0.05" comment"Coefficient for shifting computation (default=2)" />
<parameter key"FlowRate" value"0.0001" comment"Initial time step (default=h/speedsound) units_comment"seconds" />
<parameter key"FlowRate" value"0.0001" comment"Minimum time step (default=coeff*min(h/speedsound) units_comment"seconds" />
<parameter key"FlowRateCoeff" value"0.05" comment"Coefficient for shifting computation (default=2)" />
<parameter key"FlowRate" value"0.0001" comment"Initial time step (default=h/speedsound) units_comment"seconds" />
<parameter key"FlowRate" value"0.0001" comment"Minimum time step (default=coeff*min(h/speedsound) units_comment"seconds" />
<parameter key"FlowRateCoeff" value"0.05" comment"Coefficient for shifting computation (default=2)" />
<parameter key"FlowRate" value"0.0001" comment"Initial time step (default=h/speedsound) units_comment"seconds" />
<parameter key"FlowRate" value"0.0001" comment"Minimum time step (default=coeff*min(h/speedsound) units_comment"seconds" />
<parameter key"FlowRateCoeff" value"0.05" comment"Coefficient for shifting computation (default=2)" />
<parameter key"FlowRate" value"0.0001" comment"Initial time step (default=h/speedsound) units_comment"seconds" />
<parameter key"FlowRate" value"0.0001" comment"Minimum time step (default=coeff*min(h/speedsound) units_comment"seconds" />
<parameter key"FlowRateCoeff" value"0.05" comment"Coefficient for shifting computation (default=2)" />
<parameter key"FlowRate" value"0.0001" comment"Initial time step (default=h/speedsound) units_comment"seconds" />
<parameter key"FlowRate" value"0.0001" comment"Minimum time step (default=coeff*min(h/speedsound) units_comment"seconds" />
<parameter key"FlowRateCoeff" value"0.05" comment"Coefficient for shifting computation (default=2)" />
<parameter key"FlowRate" value"0.0001" comment"Initial time step (default=h/speedsound) units_comment"seconds" />
<parameter key"FlowRate" value"0.0001" comment"Minimum time step (default=coeff*min(h/speedsound) units_comment"seconds" />
<parameter key"FlowRateCoeff" value"0.05" comment"Coefficient for shifting computation (default=2)" />
<parameter key"FlowRate" value"0.0001" comment"Initial time step (default=h/speedsound) units_comment"seconds" />
<parameter key"FlowRate" value"0.0001" comment"Minimum time step (default=coeff*min(h/speedsound) units_comment"seconds" />
<parameter key"FlowRateCoeff" value"0.05" comment"Coefficient for shifting computation (default=2)" />
<parameter key"FlowRate" value"0.0001" comment"Initial time step (default=h/speedsound) units_comment"
```

Figure 5.6: Xml code for defining the case.

In Section 1 there are all the constants used to describe the problem in the numerical model and all the properties of the particles, such as the gravity, speed of sound, gamma, etc.

Section number 2 is for creating the geometry of the case in the numerical model and the most important choice, the dp . Moreover, another task left to the user is the definition of the domain: it is important to define the correct dimensions of the domain because particles will be created only inside that domain. Once the domain is defined, is possible to create all the elements that the user needs to reproduce the geometry of the case. For each element an identification number is given, and it is called mk . This is an easy way to differentiate from fluid to boundary particles in the moment of their creation.

The Section 3 includes the motion of the gate and the initial motions of particles. In particular, the motion of the gate is assigned detecting the particles by the mk . The motions that can be assigned are various and all of them are described in the xml guide that can be found in the folder. In the case of the image above, there is a uniform rectilinear motion, defining just the height of the motion, time and velocity. The initial motions (<initials>) represent the movement of group of particles, selected by their mk . These groups move before starting the tests, changing their initial position by the defined value.

Section 4 deals with the execution parameter used by DualSPHysics like: kernel, integration scheme, viscosity, shifting, duration of the simulation, etc. Most of them have been described in the previous paragraph.

In order to launch the *GenCase*, it is necessary to use the terminal, in the case of Windows computers. In fact, there is a *file.bat* that run in the terminal of the computer. The .bat file can be edited in a Text Editor. In particular, the one used for the purpose is Notepad++.

As a result of the *GenCase*, see the figure attached below.

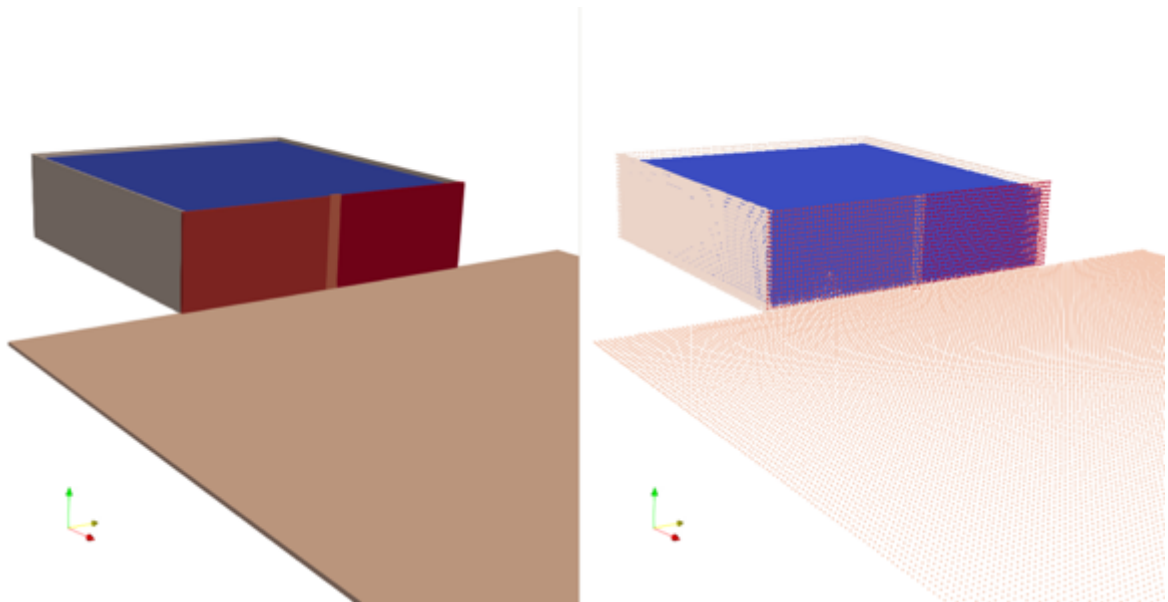


Figure 5.7: Geometry of the tank with planes (left) and particles (right).

5.4 Running DualSPHysics & Post-processing

Once the *GenCase* has been run by the user, several files will be created both in *VTK* format (*Case_All*, *Case_Bound*, *Case_Fluid*, *Case_Actual*, *Case_Dp*), *XML* (*Case.xml*, with information about particles created) and the *bi4* (*Case.bi4*, with information about the particles at the first instant).

Starting from all this data, then is possible to run the *DualSPHysics* code. This phase is launched in the terminal and the SPH solver starts to deal with all the interactions between particles: different kind of particles interact, such as, fluid-fluid, fluid-solid and solid-solid. As a result of the *DualSPHysics* all the binary files with the information about the particles and their properties will be created. In particular, in each binary file there will be information about position, velocity, density and id.

Furthermore, *Run.out* file with the information about the run of *DualSPHysics*, *Part_Head.ibi4* with information useful to execute the post-processing tools and *PartOut.obj4* with all the particles excluded in the simulation are created.

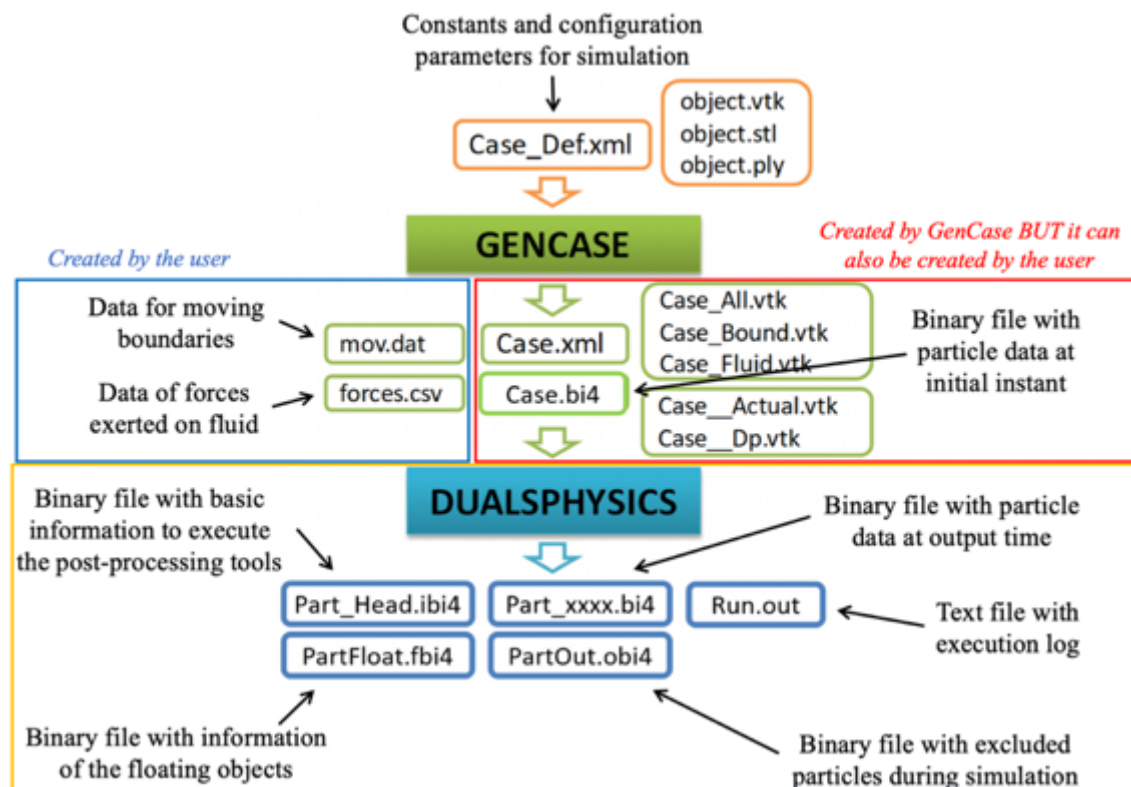


Figure 5.8: Workflow of DualSPHysics. Source: XML Guide for DualSPHysics v4.4.

After *DualSPHysics* is possible to run all the post-processing tools, useful to transfer all the information from the binary format into different ones, that are described below.

5.4.1 PartVTK

Once all the binary files are created, is possible to convert them into files that can be used for the visualization in third part programs like ParaView, Octave, etc. This is a useful instrument that lets the users look at the results of the simulation. The choice of the results can be various. In fact, the user can choose to visualize for example by mk, id, type, position of particles, velocity and a lot more.

Moreover, it is possible to save a file containing the visualization of all the particles leaving the domain. This is a useful tool to recognize if in the domain there are some empty spaces that can become holes for losing particles. Other cases that can lead to lose particles are related to density (usually set between values of 700 and 1300) or velocity (if a particle has a motion in one-time step higher than 0.9 the size of the cell).

To do this, from the terminal is possible to launch the command selecting the .bat file of PartVTK.

5.4.2 MeasureTool

In order to compare the numerical results with the experimental data, MeasureTool is the executable that transfer the information from the binary files into CSV or ASCII files. All the data are obtained from the mean of the values of the neighboring particles in a given position. Three different quantities can be measured: pressure, heights, velocity. The user can select before launching the post-processing tool, all the positions in which evaluate the physical quantities. In this case, the positions must be written in a .txt file as shown in the Figure 5.9.

"POINTS"	"#POINTS LIST"
x1 y1 z1	#BeginX BeginY BeginZ
x2 y2 z2	#StepX StepY StepZ
x3 y3 z3	#CountX CountY CountZ

Figure 5.9: How to set the positions for measuring quantities in MeasureTool.

5.4.3 Flow computation (FlowTool)

Another useful tool is FlowTool, that lets the user to evaluate quantities that are difficult to measure during the experiments. To do so, it is necessary to define a *box* with the coordinates of the points in a .txt file, generally called FileBoxes. Running in the terminal the MeasureTool tool is possible to obtain all the information in CSV or VTK-binary formats. Considering the CSV format, that is the one mainly used for the purpose of this thesis, in the first rows there are the information about the box created and after that, in each column there are the saved quantities gained by the binary files.

This is a useful instrument to evaluate for example, the inflow ratio or the discharge ratio in the created box.

BOX @name
x1 y1 z1
x2 y2 z2
x3 y3 z3
x4 y4 z4
x5 y5 z5
x6 y6 z6
x7 y7 z7
x8 y8 z8

Figure 5.10: How to create the box in FlowTool.

Moreover, according to the pieces of information of particles it is possible to have an estimation of the entering/leaving volume of the fluid or the entering particles velocity.

These are the main tools often used in the analysis of the 3D Dam-break.

In Figure 5.11 is shown the .bat file used to launch the complete simulation, or just a part of it, in Notepad++.

```
set name=CaseDamBreak
set dirout=%name%_out
set diroutdata=%dirout%\data

rem "executables" are renamed and called from their directory

set dirbin=../../bin/windows
set gencase=%dirbin%/GenCase4_win64.exe"
set dualphysicscpu=%dirbin%/DualSPHysics4.4CPU_win64.exe"
set dualphysicsgpu=%dirbin%/DualSPHysics4.4_win64.exe"
set boundaryvtk=%dirbin%/BoundaryVTK4_win64.exe"
set partvtk=%dirbin%/PartVTK4_win64.exe"
set partvtkout=%dirbin%/PartVTKOut4_win64.exe"
set measuretool=%dirbin%/MeasureTool4_win64.exe"
set computeforces=%dirbin%/ComputeForces4_win64.exe"
set isosurface=%dirbin%/IsoSurface4_win64.exe"
set flowtool=%dirbin%/FlowTool4_win64.exe"
set floatinginfo=%dirbin%/FloatingInfo4_win64.exe"

rem "dirout" to store results is removed if it already exists
if exist %dirout% rd /s /q %dirout%

rem CODES are executed according the selected parameters of execution in this testcase

rem Executes GenCase4 to create initial files for simulation.
%gencase% %name%_Def %dirout%/name% -save:all
if not "%ERRORLEVEL%" == "0" goto fail

rem Executes DualSPHysics to simulate SPH method.
%dualphysicsgpu% -gpu %dirout%/name% %dirout% -diroutdata %dirout% -svres
if not "%ERRORLEVEL%" == "0" goto fail

rem Executes PartVTK4 to create VTK files with particles.
set dirout2=%dirout%\particles
%partvtk% -dirin %diroutdata% -savevtk %dirout2%/PartFluid -onlytype:-all,+fluid
if not "%ERRORLEVEL%" == "0" goto fail

rem Executes PartVTKOut4 to create VTK files with excluded particles.
%partvtkout% -dirin %diroutdata% -savevtk %dirout2%/PartFluidOut -SaveResume %dirout2%/ResumeFluidOut
if not "%ERRORLEVEL%" == "0" goto fail

set dirout2=%dirout%\boundary
%boundaryvtk% -loadvtk AutoDp -motiondata %diroutdata% -savevtkdata %dirout2%/Gate.vtk -onlymk:16
if not "%ERRORLEVEL%" == "0" goto fail

set dirout2=%dirout%\measuretool
%measuretool% -dirin %diroutdata% -points heights.txt -onlytype:-all,+fluid -height:0.4 -savecsv %dirout2%/heights -savevtk %dirout2%/heights
if not "%ERRORLEVEL%" == "0" goto fail

REM rem Executes FlowTool4 to create VTK files with particles assigned to different zones and a CSV file with information of each zone.
set dirout2=%dirout%\flow
%flowtool% -dirin %diroutdata% -fileboxes CaseDamBreak_FileBoxes.txt -savecsv %dirout2%/ResultFlow.csv -savevtk %dirout2%/Boxes.vtk
if not "%ERRORLEVEL%" == "0" goto fail
```

Figure 5.11: Screenshot of the .bat file.

5.5 Validation

In this section a case of validation is included to analyse the capabilities of *DualSPHysics* to simulate dam-breaks. The experiment of Fraccarollo and Toro (1995) will be reproduced with the numerical tool.

5.5.1 Experiment

In the experiment of Fraccarollo and Toro (1995) (Figure 5.12) the behaviour of a fluid confined in a tank was studied. The initial volume of water is of 2m x 1m and 0.6m high. In the middle of the front wall of the reservoir there is a gate (0.4m wide) that rotates with an angle of 90° in 0.10 s and releases the water that will move along the downstream area.

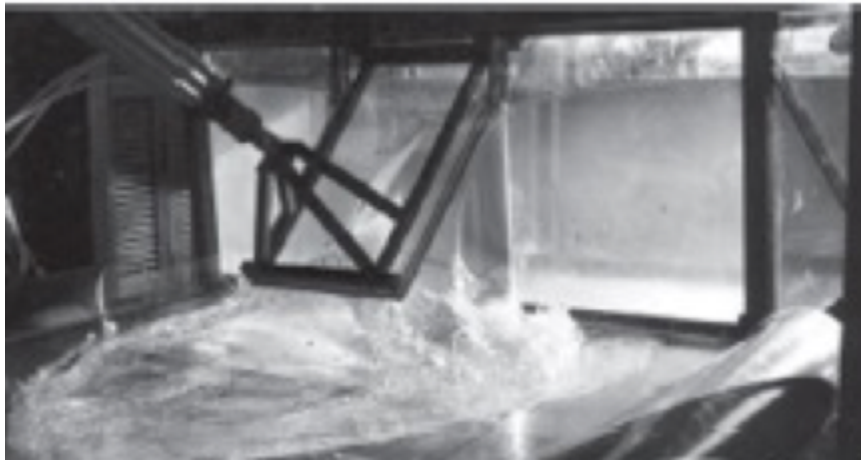


Figure 5.12: Image of the experiment of the dam-break. Source: Fraccarollo and Toro (1995).

5.5.2 Numerical setup

The dimensions of the experiment are represented in the numerical tank as shown in Figure 5.13. In addition, a downstream area is created with a squared shape with no lateral walls of 2m x 2m. The gate opens so fast that it can be considered as a sudden removal, however the motion of the gate will be included in the simulations.

The experimental data includes the time series of water elevation at six different positions. Therefore, the same six positions were used in *DualSPHysics* to obtain the numerical time results: 2 inside the reservoir, 2 in the location of the gate and 2 in the downstream area. The positions of the gauges are included in Table 5.1. The coordinates X and Y correspond to the axis shown in Figure 5.12.

Table 5.1: Position of the water gauges to measure the elevation of the water column.

Position	5A	C	0	4	4A	8A
X (m)	0.18	0.51	1	1	1.32	1.72
Y(m)	1	0.35	1	1.16	1	1

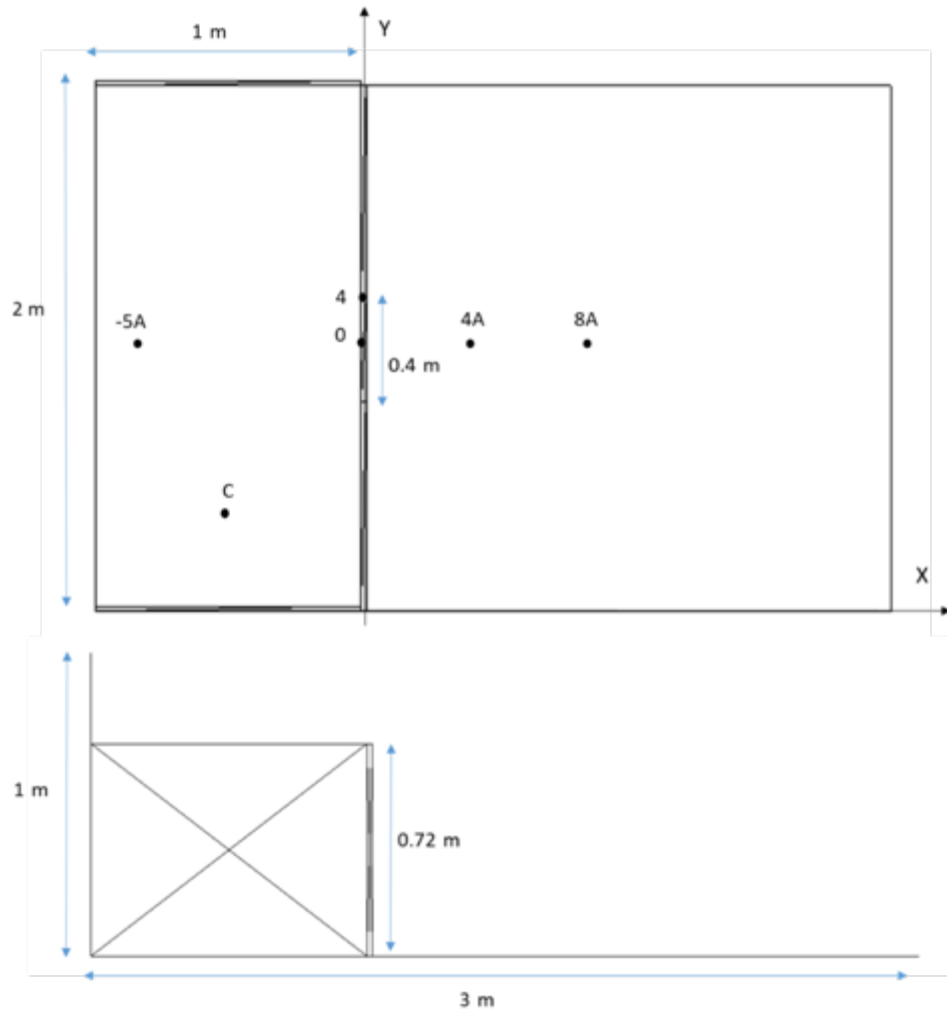


Figure 5.13: Numerical setup of the dam-break including dimensions and position of the gauges.

As mentioned, before, Figure 5.13 includes all the dimensions of the numerical tank and the positions of the gauges to measure the water elevation during the simulation.

The physical time to be simulated here is 10 seconds. In DualSPHysics, the execution time depends on the resolution, so that on the number of particles. Three different resolutions will be simulated here using different initial particle spacing (dp). By changing this parameter, different number of particles (np) will be initially created. Table 5.2 shows the different resolutions and the runtimes using NVIDIA GeForce GTX 1080. It can be observed how decreasing dp the number of particles np increases and therefore the execution time increases as well.

Table 5.2: Different resolutions and execution times with DualSPHysics.

case name	dp	np	Runtime
TestFT1	0.02 m	172,995	0.37 h
TestFT2	0.01 m	1,291,389	4.04 h
TestFT3	0.0075 m	2,992,221	12.00 h

5.5.3 Results

Different instants of the simulation of TestFT3 ($dp=0.0075$ m) are plotted in the Figure 5.14. The colour of the particles corresponds to the velocity magnitude.

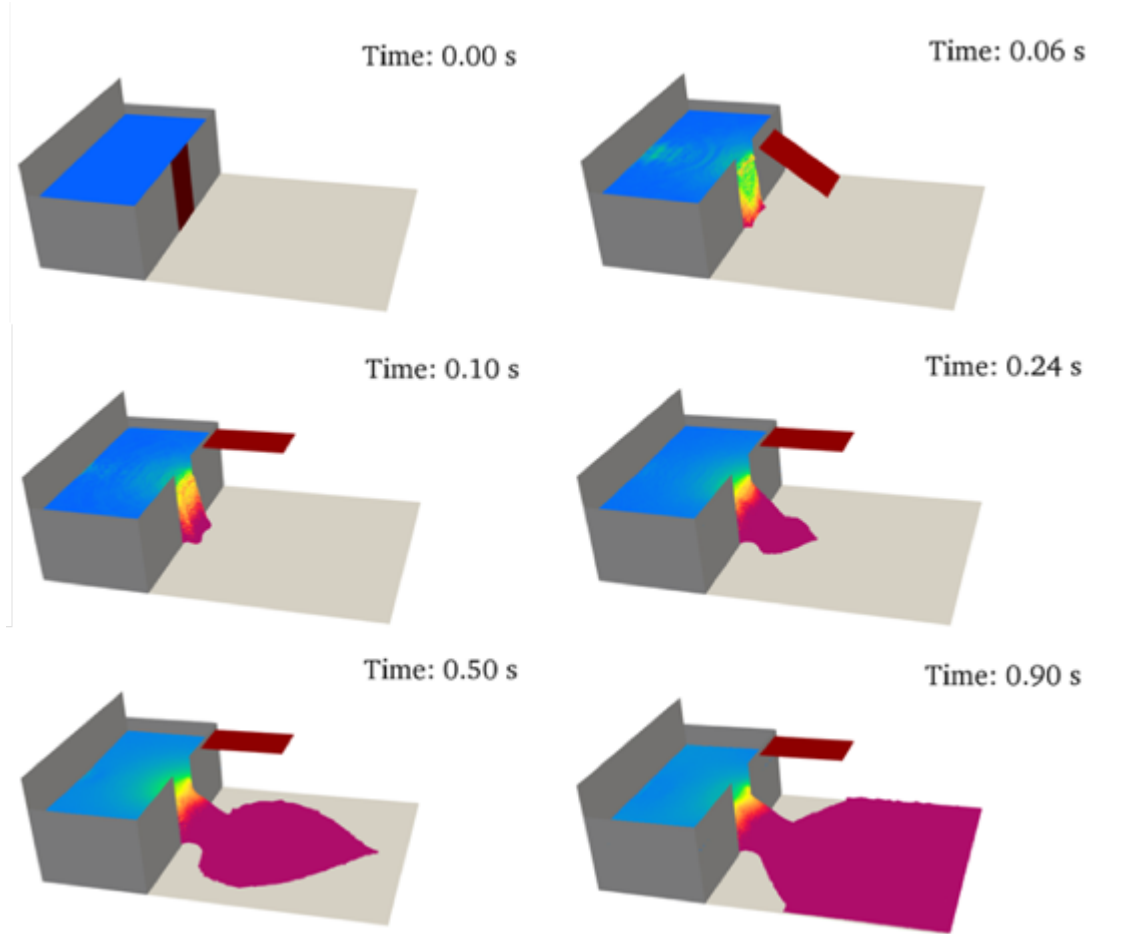


Figure 5.14: Different instants of the TestFT3 ($dp=0.0075$ m) using DualSPHysics.

The experimental data is compared with the numerical results in Figure 5.15. This figure shows the values of water elevation at the six gauges (Table 5.1). The numerical results are obtained for the three different resolutions (Table 5.2).

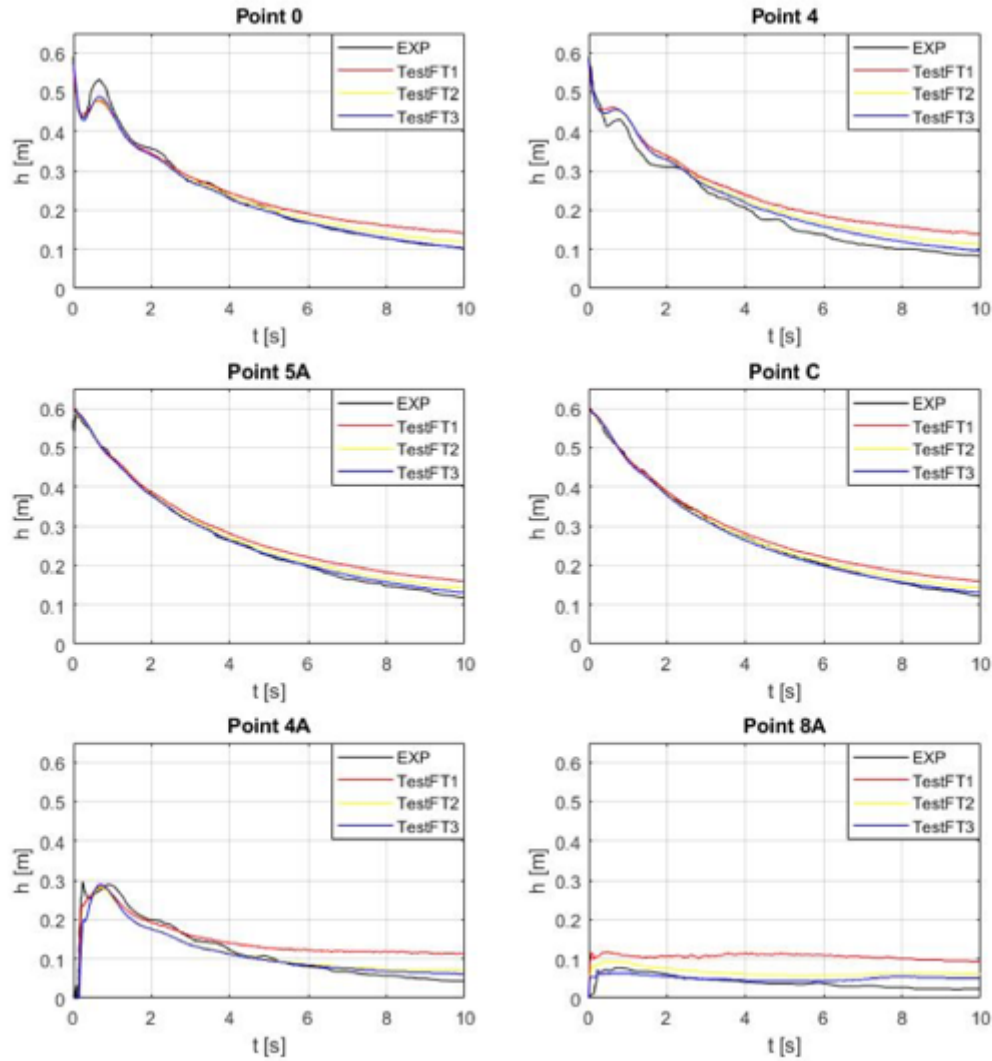


Figure 5.15: Comparison of experimental and numerical water elevation for different resolutions.

The agreement between experimental and numerical data is good. For the gauges located inside the structure (-5A and C), the height of the fluid decreases with time once the gate is opened and the water flows to the outside bottom. For the points 0 and 4, located at the initial position of the gate, the water elevation decreases initially when opening the gate, then an upward rebound is observed and then the elevation decreases again. This rebound is due to the fact that the fluid confined behind the gate, once it has been completely opened, acquires a higher emptying speed (this behaviour is properly reproduced in the simulation). By analysing the behaviour of the fluid at the gauges outside the dam (4A and 8A), an initial absence of water is observed until the fluid reaches these positions. After an initial sudden water elevation, the water column decreases as the water confined is released and then leaves the domain since there are no lateral walls. This decrease of the

water column can be better observed in gauge 4A since the water column fluid is higher than in 8A where the water level is more constant during the first 10s.

For all the gauges, it can be observed that with a higher resolution of the simulation (higher number of particles) the results are closer to the experimental ones. The worst results are obtained for gauge 8A because this is the furthest away and where the resolution has a high impact in order to measure the water elevation with accuracy.

Finally, the inflow was measured in the downstream area. This magnitude is very difficult to measure in the experiments of laboratory, but easy to compute using the post-processing tools of the DualSPHysics software (in particular with FlowTool). Figure 5.16 shows the inflow for the three different resolutions. Note that the trend of the inflow, between the different tests and especially with different resolution, can be considered the same.

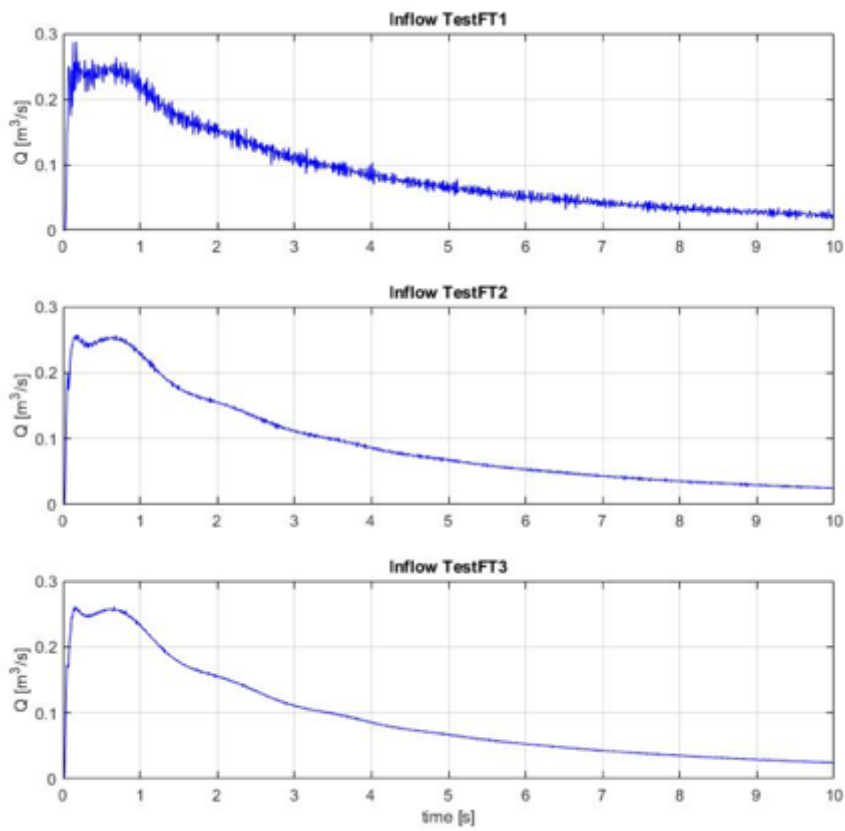


Figure 5.16: Time series of the numerical inflow for different resolutions with DualSPHysics.

It can be concluded that DualSPHysics is a reliable tool for reproducing the interaction between fluid and structures to study the dam-break evolution.

Chapter 6

Numerical study of the Dam-Break

In this chapter are described all the choices that have led to the numerical analysis in SPH of the dam-break in an area with vegetation. To do this, it has been necessary to validate the SPH code in the case of the dam-break with flat bottom downstream area. Different sizes of the sluice gate and different values of viscosities have been tried in order to have the same discharge ratio measured by the twelve sensors placed in the experimental facility.

After the validation is possible to improve the efficiency of the numerical model applying several changes but trying to reproduce the same discharge ratio in each case. The height of the water in the upstream reservoir is set equal to 40 cm, that is the same height in all the tests with vegetation.

Several results will be presented and comparison in terms of discharge ratio and wave front.

Once the validation with flat bottom has given good results, is then possible to start the analysis of the downstream area in the presence of vegetation, that is represented by the different configuration of metallic rods described in Chapter 3.

In the case of vegetated area all the choices made in the case of flat bottom will be maintained and once the code is updated case per case, is possible to run SPH with the new configurations.

6.1 Test with Flat Bottom

The analysis of the dam-breaks related to the physical model built in Turin starts with the analysis of the one with flat bottom. The physical experiment follows all the steps already described in Chapter 4, with the exception of leaving the downstream area free from the polycarbonate panels with rods. In this way the surface is represented by the white PVC layer that covers the framework.

Only after the validation of this case, it is then possible run all the cases with the vegetation in the downstream area.

6.1.1 Numerical setup

In the numerical model is possible to recreate the exact geometry that has been built in the *Giorgio Bidone* Laboratory in Turin as can be seen in Figure 6.1. At the starting point, the value of the dp is set to 0.005m. In addition, in grey there are all the boundary particles. The reservoir has a height of 42 cm instead of the 50 cm of the physical model. In red can be seen the sluice gate, which movement is regulated by the motion in the xml file; its height is set equal to 42 cm. In blue are represented the particles of fluid at a height of 40 cm.

The opening of the gate is set to 0.0375 m as a starting value in accord to the dp .

The viscosity chosen is 0.1.

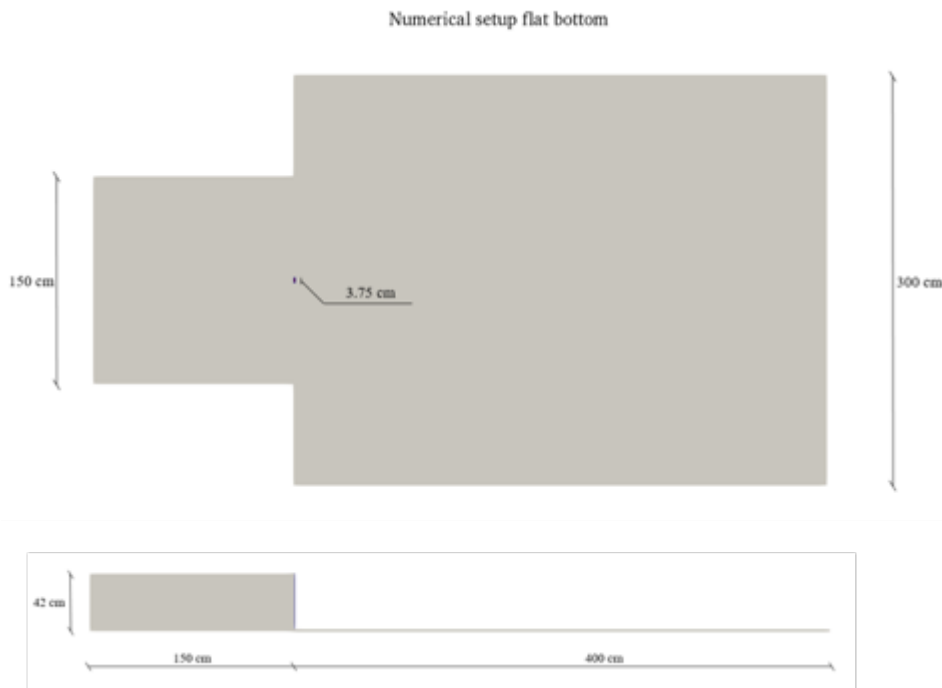


Figure 6.1: Numerical SPH setup.

In order to compare the two different experiments, physical and numerical, it is necessary to compare the elevation in the weir during the tests. As already described, in the physical model there are twelve sensors that are placed just above the upstream reservoir.

Whereas in the numerical code it is possible to place in the same positions the twelve gauges in the *Case_Def.xml* file. In fact, after running the DualSPHysics, it is already possible to have information about the decreasing height of water in the reservoir.

In Figure 6.2 are shown all the gauges in the upstream reservoir.

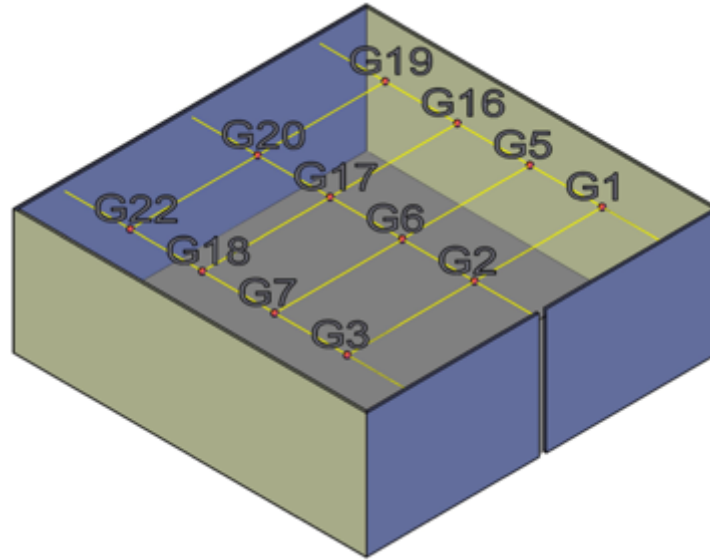


Figure 6.2: Representation of the upstream reservoir with gauges.

In particular, one row is on the axis of symmetry in the centre of the gate. The gauge 2 has a distance of 0.282 m from the gate; gauge 6 has 0.594 m; gauge 17 has 0.906 m and gauge 21 has 1.218 m from the gate. The other two rows are at the same distance and equal to 0.55 m in the y direction, one in the positive direction and the other in the negative.

In a table, assuming the origin of the axis in the middle of the gate:

Table 6.1: Position of the wave gauges in the upstream reservoir.

Gauge id	x [m]	y [m]
G1	-0.282	0.55
G2	-0.282	0
G3	-0.282	-0.55
G5	-0.594	0.55
G6	-0.594	0
G7	-0.594	-0.55
G16	-0.906	0.55
G17	-0.906	0
G18	-0.906	-0.55
G19	-1.218	0.55
G20	-1.218	0
G22	-1.218	-0.55

6.1.2 Results (VALIDATION)

Once the gauges are placed in the exact position, it is then possible to start to compare the results between the two tests. In particular, considering the physical model, all the data collected during the experiments have been post-processed in order to have the discharge curves of the upstream reservoir and the wave front. To obtain the wave front, it is necessary to post-process the photos collected by the Andor Zyla camera, running the MATLAB code and extrapolating from the matrix all the values. In Figure 6.3 the wave fronts from both models are shown.

Considering that the frame rate of the camera is set to 41.388 Hz , between each instant there is a temporal step of 0.02416 s .

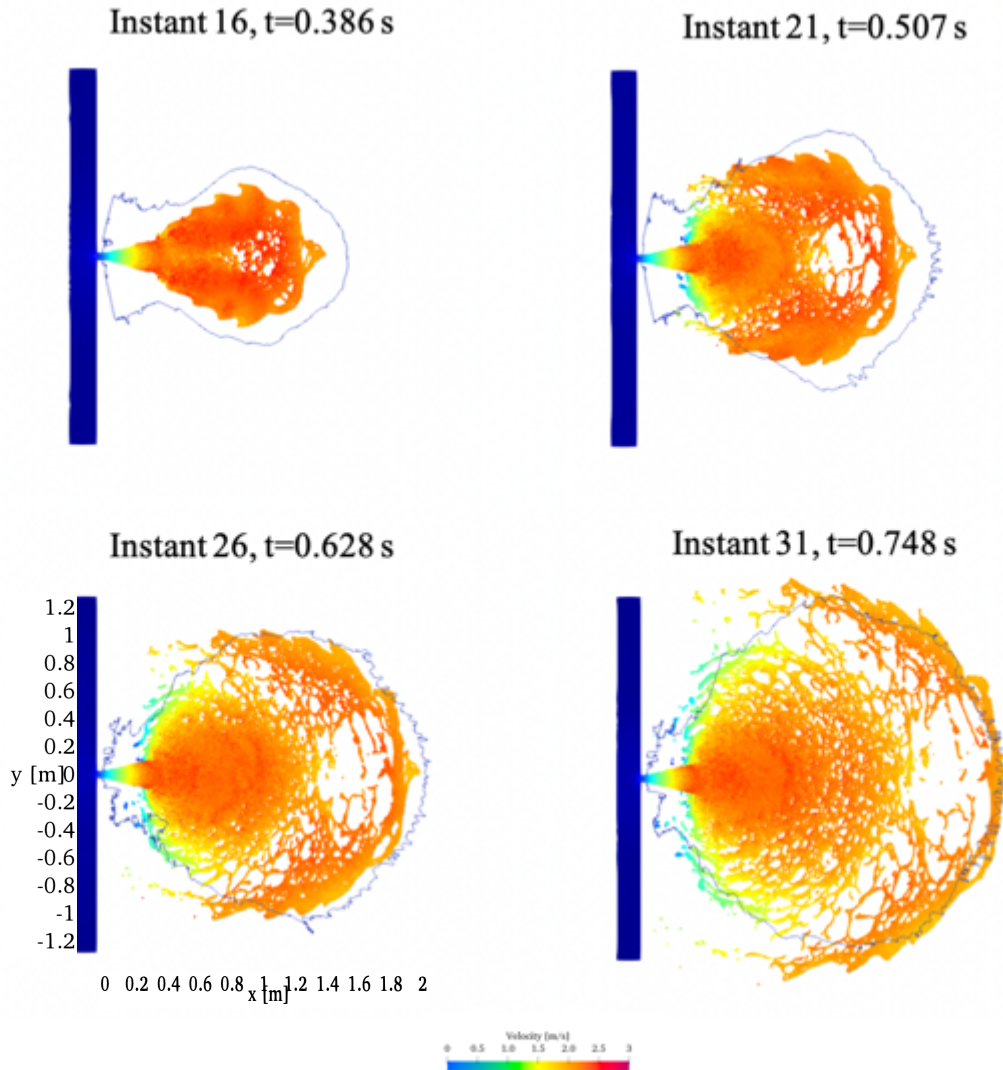


Figure 6.3: Different instants of the simulation. Comparison between the experimental data (blue line) and numerical model (coloured particles).

In the numerical model, for a more precise detection of the wave front at the same instant, a time saving of 0.02416 has been set.

The wave fronts are not enough to validate the case, in fact it is necessary to compare all the results given by the water gauges from the two different models.

The free surface elevation is evaluated in 2 seconds and the results are plot below.

All the results of the experimental data are represented in black and the ones of the numerical model in red. To let the readers have a better comprehension of the results, bounds of error are added to the graphics. In particular, the red dot lines are only moved by half of the dp .

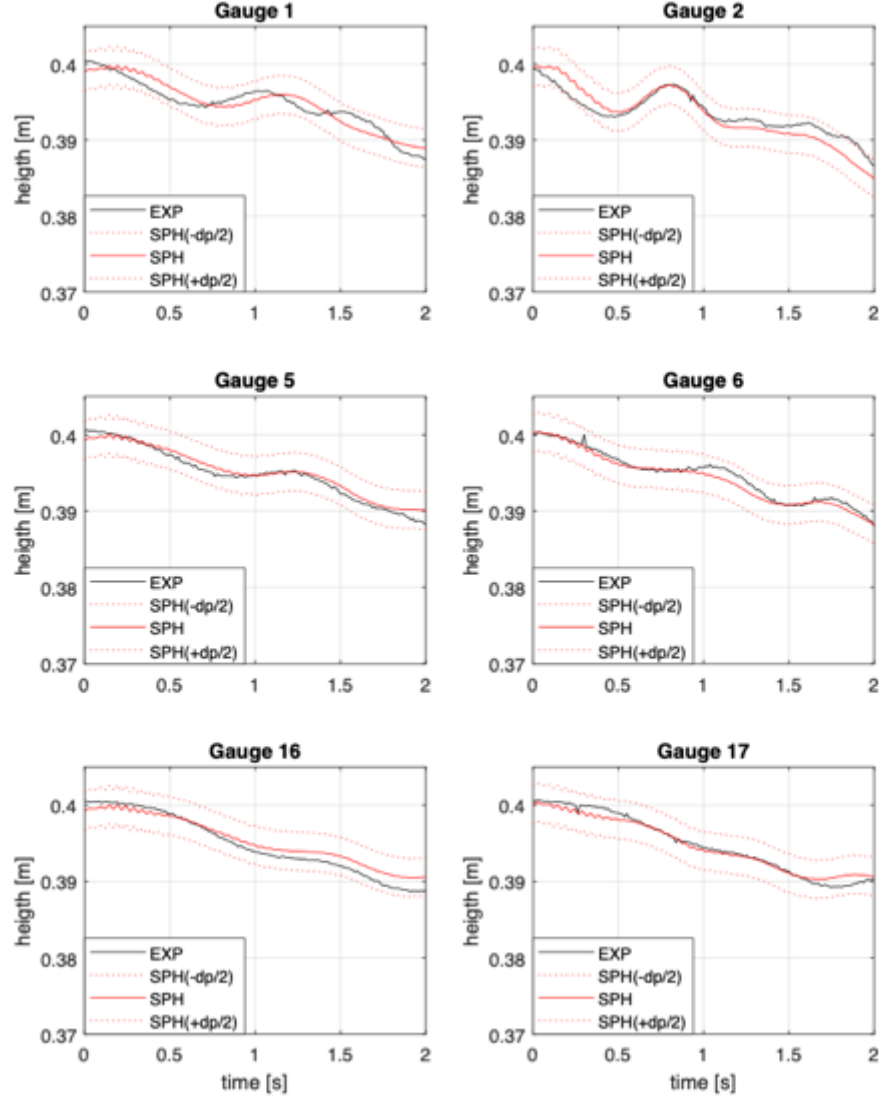


Figure 6.4: Comparison of free surface elevation both in physical and numerical model.

As can be seen in the figure above, results are good enough to consider this case valid. All the lines, experimental and SPH, in the two seconds of test are inside the bounds and can be concluded that the values of viscosity, viscosity bound factor and dp are acceptable.

6.1.3 Improving efficiency

Although the results obtained are good enough to validate the case, it is then necessary improve the efficiency of the numerical model.

There are three different ways to do this.

- i. Applying symmetry
- ii. Reducing the reservoir dimensions
- iii. Increasing resolution

The need of using symmetry is due to the fact that in the numerical model is then possible increase the resolution in order to approach the real case of the physical model. To do this, it is necessary to modify the *Case_Def.xml* and setting the parameter of symmetry equal to 1. Furthermore, the user needs to limit the domain just in the part that wants to be seen. Before launching the code, it is necessary to take into account one important thing: all the particles around the axis of symmetry need to be moved by half of dp in order to describe in a proper way the behaviour around that axis.

As a result of this changes, see Figure 6.5.

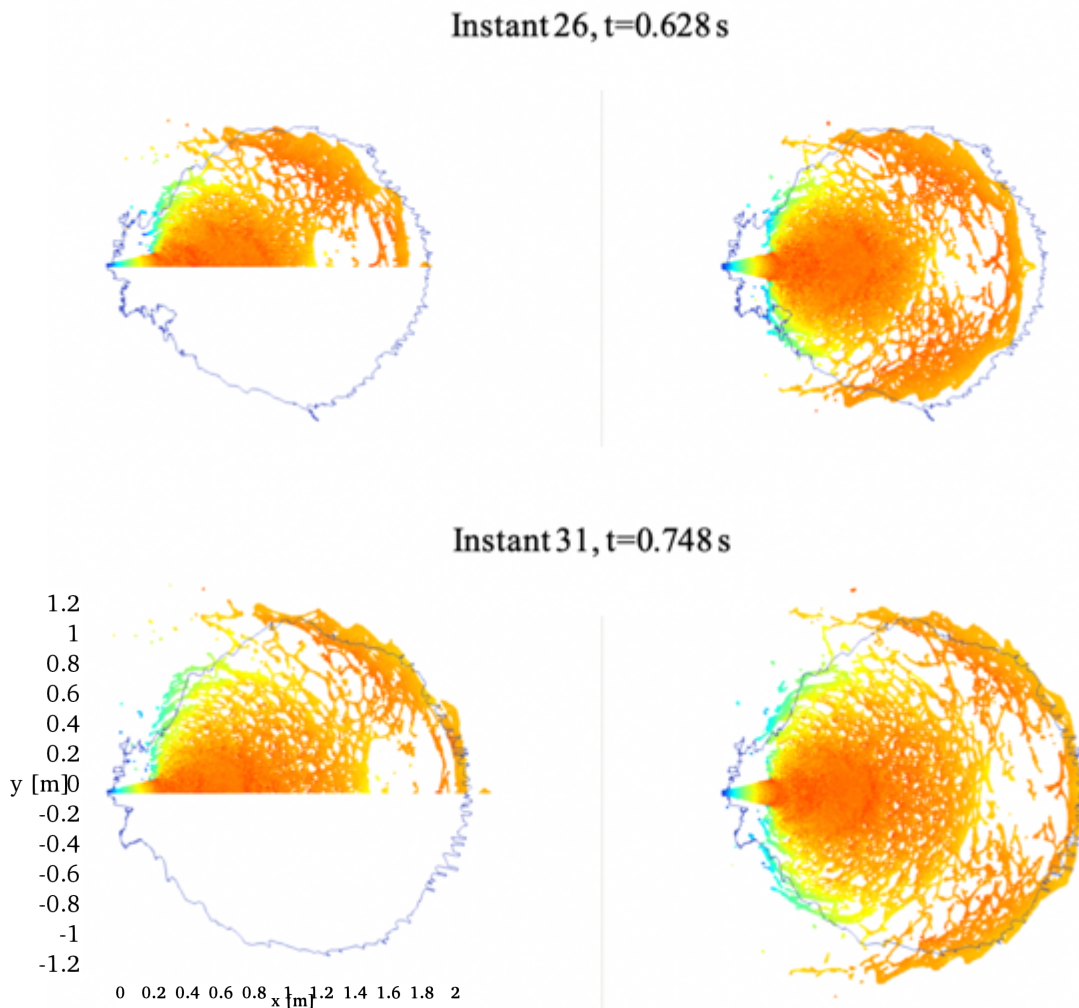


Figure 6.5: Comparison between symmetric and non-symmetric wave fronts at two instants.

It can be concluded that the symmetry does not affect the result.

Once the symmetry gives good results, the next step is the reduction of the reservoir to reduce in a significant way the number of particles used in the simulations. The research of the new reservoir pass through the identification of the best discharge ratio in correspondence of the twelve water gauges.

The new geometry for the reservoir has a double slope in the nearby of the gate and a flat zone with a thin layer in the back. In the following image, there are the reservoir with the complete geometry and its symmetric case and the reservoir with the new geometry and its symmetric case. In the bottom there is the lateral view of the reservoir with the new geometry.

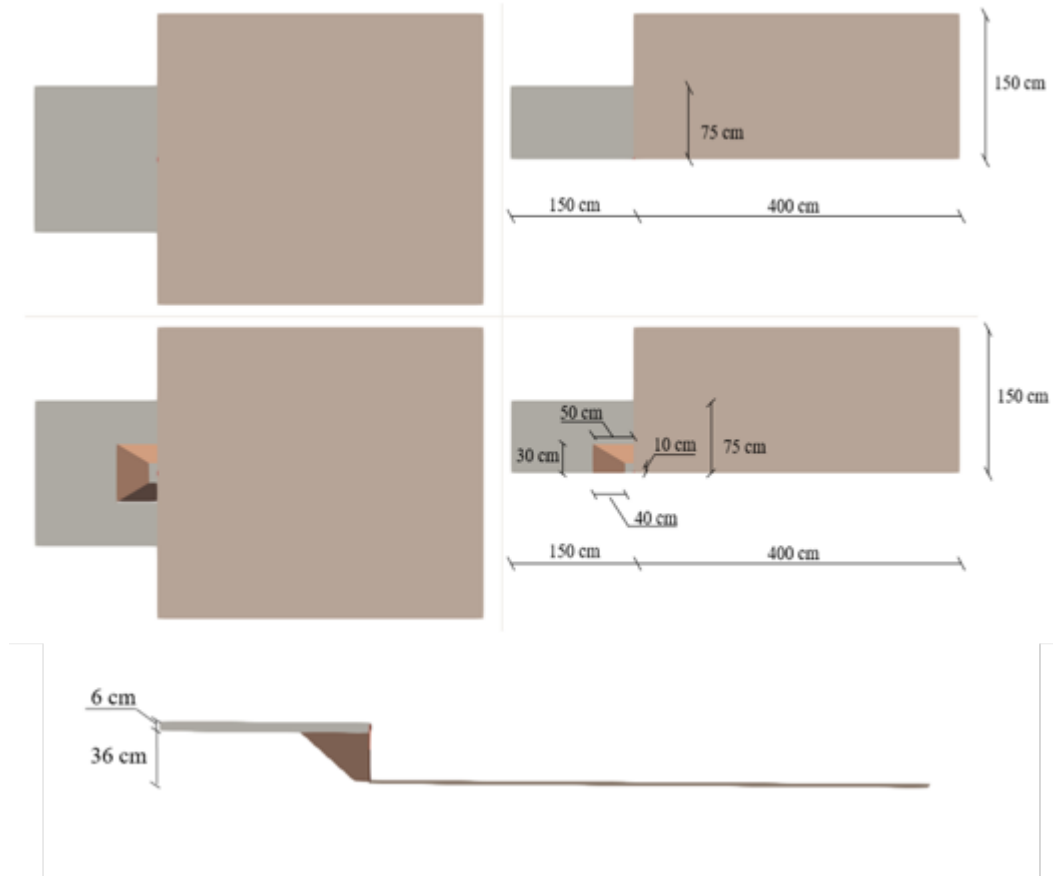


Figure 6.6: Numerical models in case of complete tank (left) and reduced tank (right) with their sizes. The first row is the bottom view in the case of complete geometry; the second is the bottom view for the reduced tank and the third is the lateral view of the reduced tank.

The last step is the increase of resolution of the numerical model using two further different values of dps . According to this, the reader has to consider that the reduction of half dp from the starting value leads to the increasing by 8 times the number of particles. This is why all the previous steps were necessary before this.

Considering that the radius of interaction changes as soon as the value of dp changes, remembering that in these numerical models the value of h is equal to dp , it is necessary to review the size of the gate in each case. The analyzed case presents a value of viscosity of 0.1 and viscosity bound factor of 1.

The final choices of the sluice gates are reached after a numerical campaign in which there was paid attention to the inflow. In particular, for $dp=0.005\text{m}$ the gate is 0.0375m ; for $dp=0.0025\text{m}$ gate is 0.0325m and for $dp=0.0020\text{m}$ gate is 0.0320m .

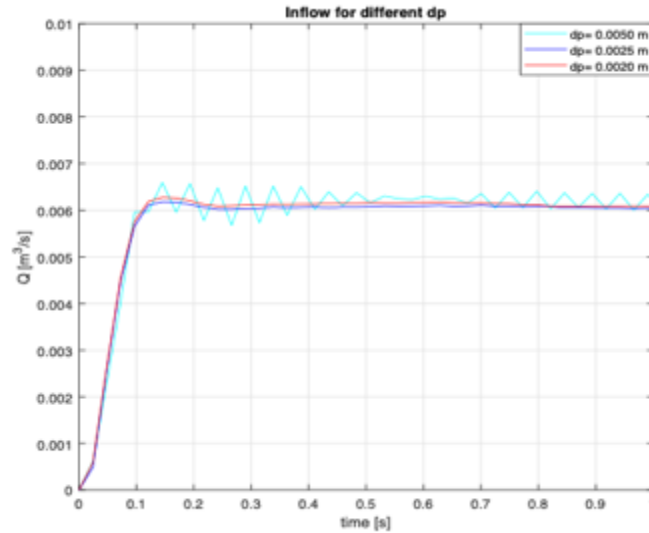


Figure 6.7: Inflow for different resolution.

Also, in this case it can be concluded that the dp does not affect the results.

Once all the previous passages have been accomplished, it is possible to represent the wave front at different instants and for the different values of dp , always remembering that the value of viscosity is fixed to 0.1.

As a conclusion of this analysis in the case of flat bottom, the wave front from the experimental data is well represented by the one from the numerical model. In particular it can be noticed that, increasing the value of the dp , the wave front is more compact. Looking at the different instants in Figure 6.8, in the case of $dp=0.005$ just after few instants there are some voids in the wave front. To overcome this problem the only way is to increase the resolution and in fact, as can be seen for the $dp=0.0025$ and $dp=0.002$, the voids appear after more than half a second. Even in the lower value of dp the wave front starts to have some voids inside, due to the fact that the resolution should be lowered even more. However, the number of particles and the execution time should be too high.

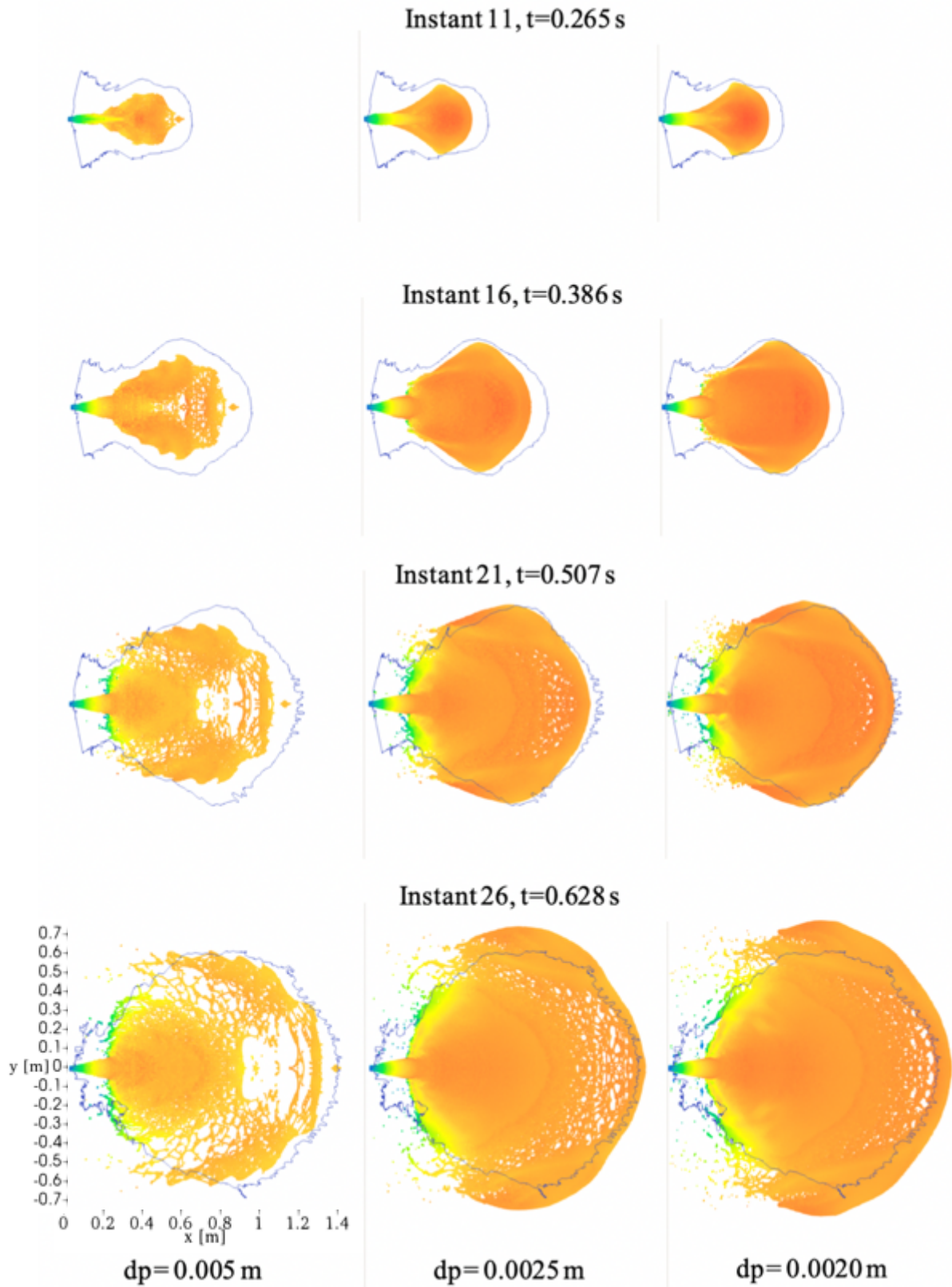


Figure 6.8: Comparison between experimental data and SPH wave front for different resolutions.

6.1.4 Evaluation of the water depth

A direct consequence of the wave front analysis is the possibility to evaluate the water depth. Considering the results represented in Figure 6.8, the analysis is carried just using the lower resolution for particles, 0.002m. This choice is due to the fact that the wave is similar to the experimental one, avoiding problems related to voids.

The evaluation is done along three main longitudinal directions, that are represented in Figure 6.9.

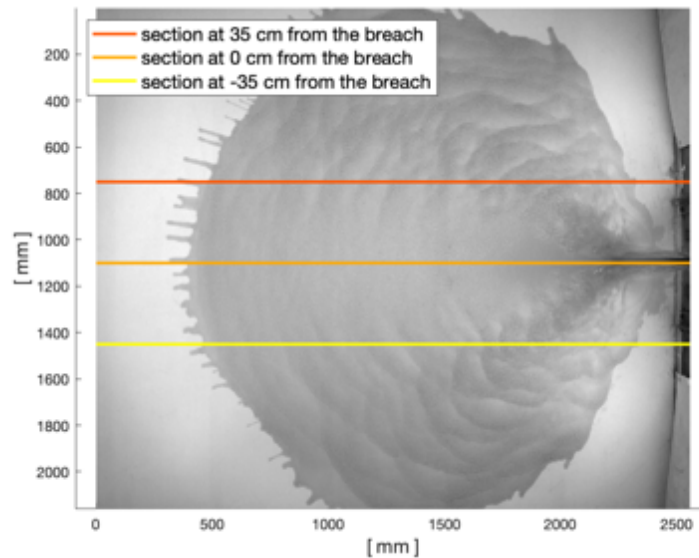


Figure 6.9: Position of the longitudinal directions for the evaluation of the water depth

The analysis of the experimental data is done using the Lambert-Beer law and representing the results using a MATLAB script.

In SPH the *MeasureTool* tool is used for the purpose, considering a band of 1.5 cm, with a step of 0.2 cm, and evaluating the means on eight points.

In Figures 6.10, 6.11 and 6.12 are represented the results of this analysis.

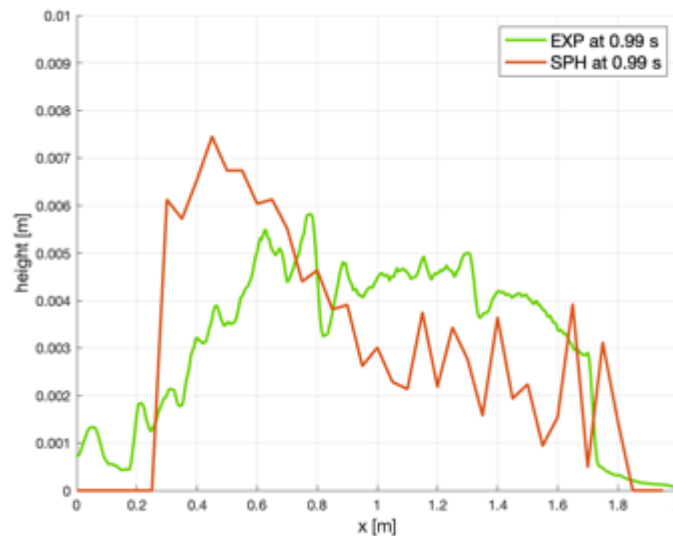


Figure 6.10: Water depth at a distance of -35 cm from the breach. The red line is SPH and the green the EXP.

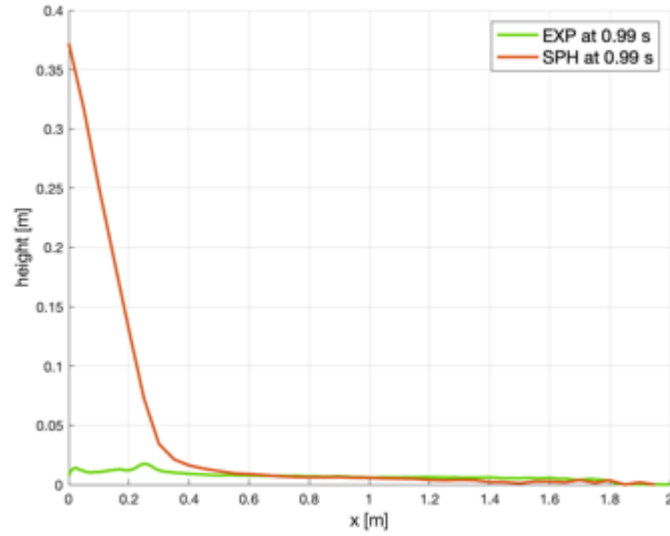


Figure 6.11: Water depth at a distance of 0 cm from the breach. The red line is SPH and the green the EXP.

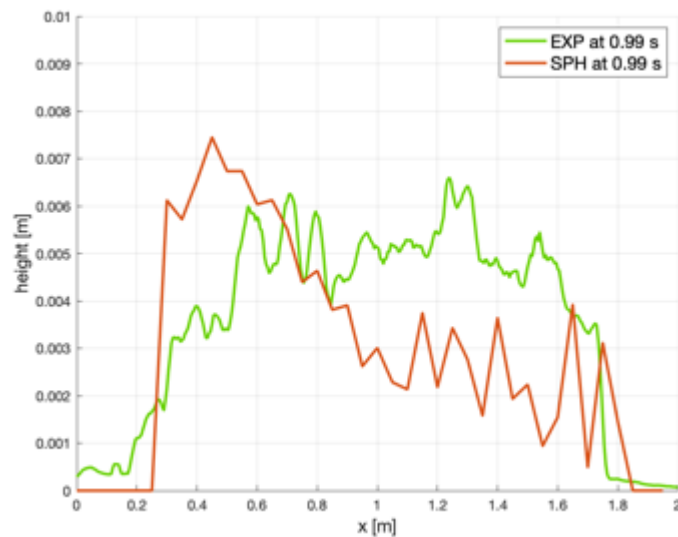


Figure 6.12: Water depth at a distance of 35 cm from the breach. The red line is SPH and the green the EXP.

It can be noticed that in the cases at a distance of -35 and 35 cm, results almost agree between them. In particular the peak detected from SPH is in accordance with the one from the experimental data, at a distance of 0.41 m.

Considering Figure 6.11, it can be seen that in the experimental data does not figure the triangular shape near the sluice gate. After 0.5 m, results are in agreement.

6.2 Tests with different roughness

The last part of this thesis is related to the numerical tests in the case of roughness in the downstream area. Its presence is due to the desire to simulate the behaviour when the downstream area is plenty of vegetation, represented by metallic rods, that is the aim of the RESBA in the work assigned at the Politecnico di Torino.

Once the flat bottom case is validated, then it is possible to take as starting point the results just reached. In particular, the viscosity value is equal to 0.1. According to the results obtained in the previous paragraph, the analysis is conducted with the three different values of δp : 0.005 m, 0.0025 m and 0.002 m.

6.2.1 Numerical setups

The possibility to recreate the metallic rods in the numerical models is given through the addition of list of commands in the *Case_Def.xml*. All the four different configurations are created, and each rod is represented by a line.

```
<list name="Rod">
  <drawlines>
    <point x="0" y="0" z="0" />
    <point x="0" y="0" z="0.05" />
  </drawlines>
  <move x="0" y="0.10" z="0" />
</list>
<list name="Rods5">
  <runlist name="Rod" />
  <runlist name="Rod" />
  <runlist name="Rod" />
  <runlist name="Rod" />
  <runlist name="Rod" />
</list>
<list name="Rods25">
  <matrixsave />
  <runlist name="Rods5" />
  <runlist name="Rods5" />
  <runlist name="Rods5" />
  <runlist name="Rods5" />
  <runlist name="Rods5" />
  <matrixload />
  <move x="0.10" y="0" z="0" />
</list>
```

Figure 6.13: How to create rods in SPH.

As a result of the *GenCase*, it is possible to give a look at the *.vtk* files, in which are represented the four different configurations. The new geometries for the downstream are represented in Figure 6.14. These are the starting geometries for the new tests.

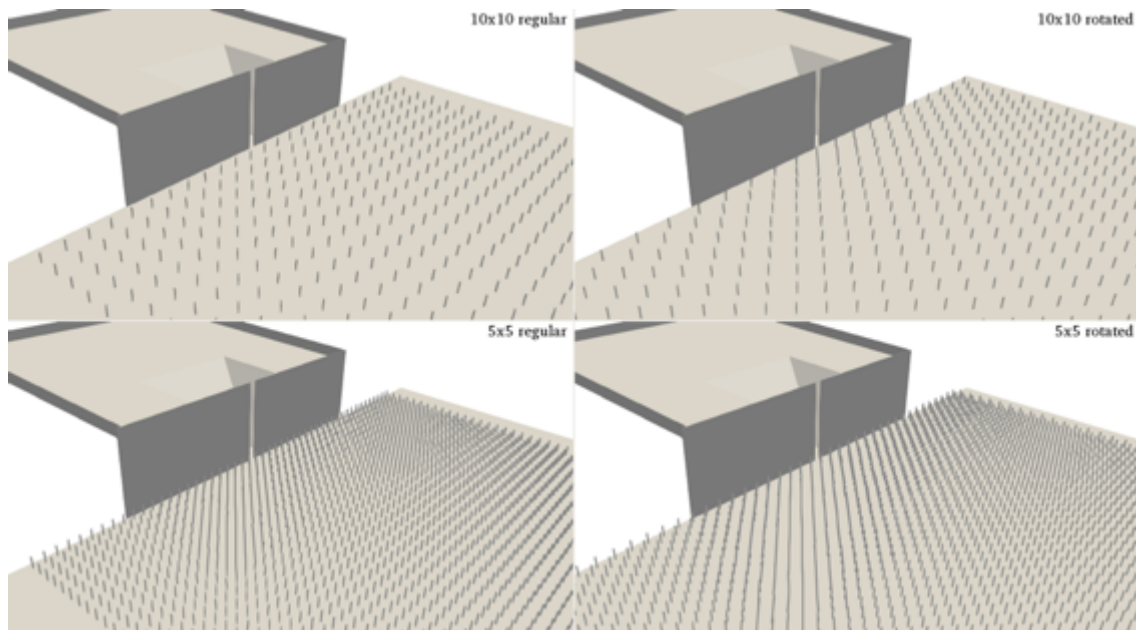


Figure 6.14: Four different configurations for downstream area with rods. On the left there are the regular geometries (0°) for mesh 10x10 (up) and 5x5 (down). On the right there are the rotated geometries (45°) for mesh 10x10 (up) and 5x5 (down).

The analysis is conducted with the three different resolutions. In this case the presence of the metallic rods mitigates the development of the wave front along the downstream area.

6.2.2 Results of the wave fronts

Then it is possible to run the *DualSPHysics* in order to create the binary files for particles and from that the *PartVTK* for all the instants of the simulations. The results can be seen using ParaView. All the instants considered are plotted for the three different resolutions and compared with the experimental data.

The results are shown in the following order: Regular 10x10, Rotated 10x10, Regular 5x5, Rotated 5x5.

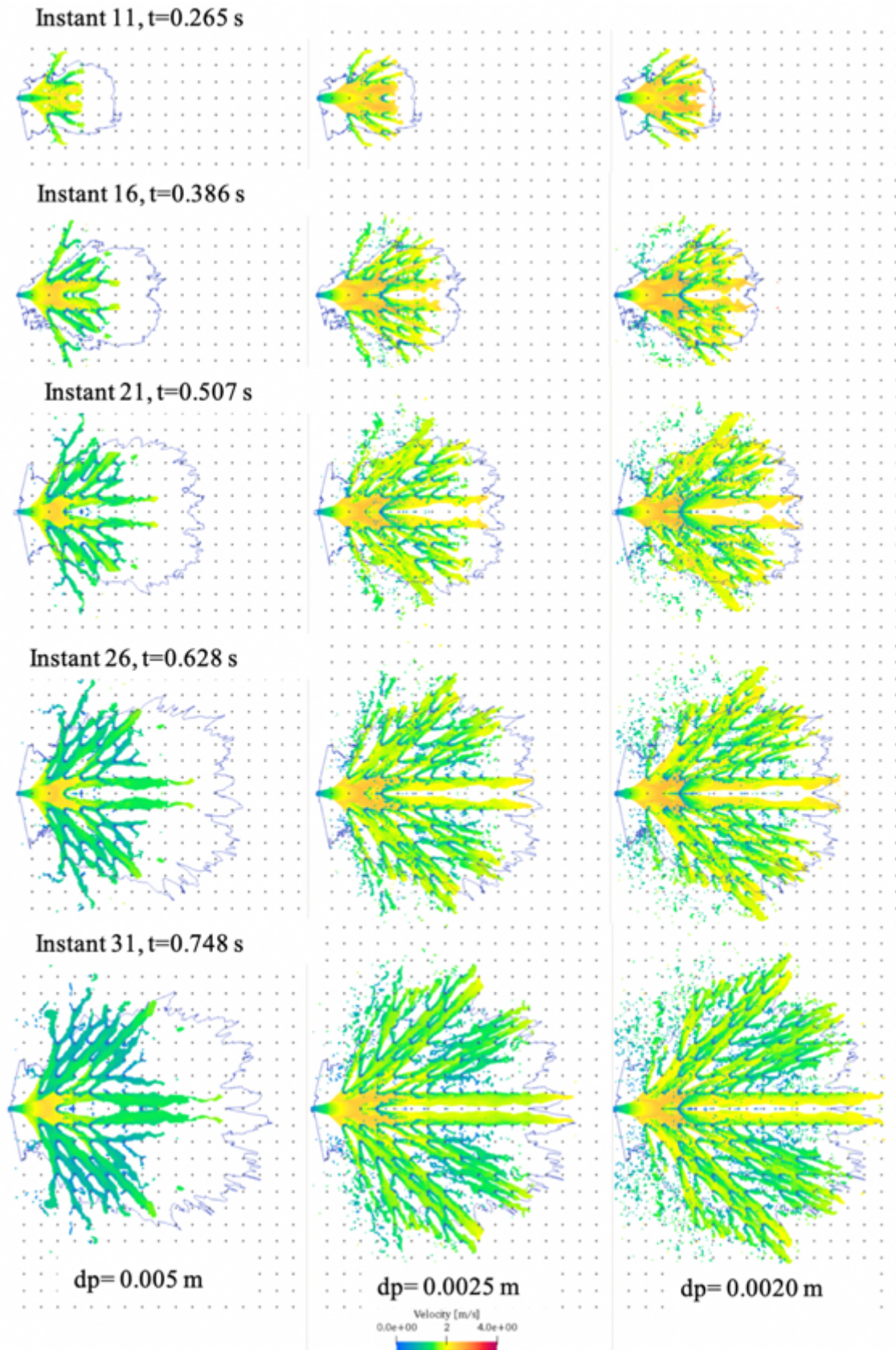


Figure 6.15: Comparison of experimental (blue lines) and SPH (coloured particles) wave fronts for different resolutions with 10x10 regular mesh. The black dots represent the metallic rods.

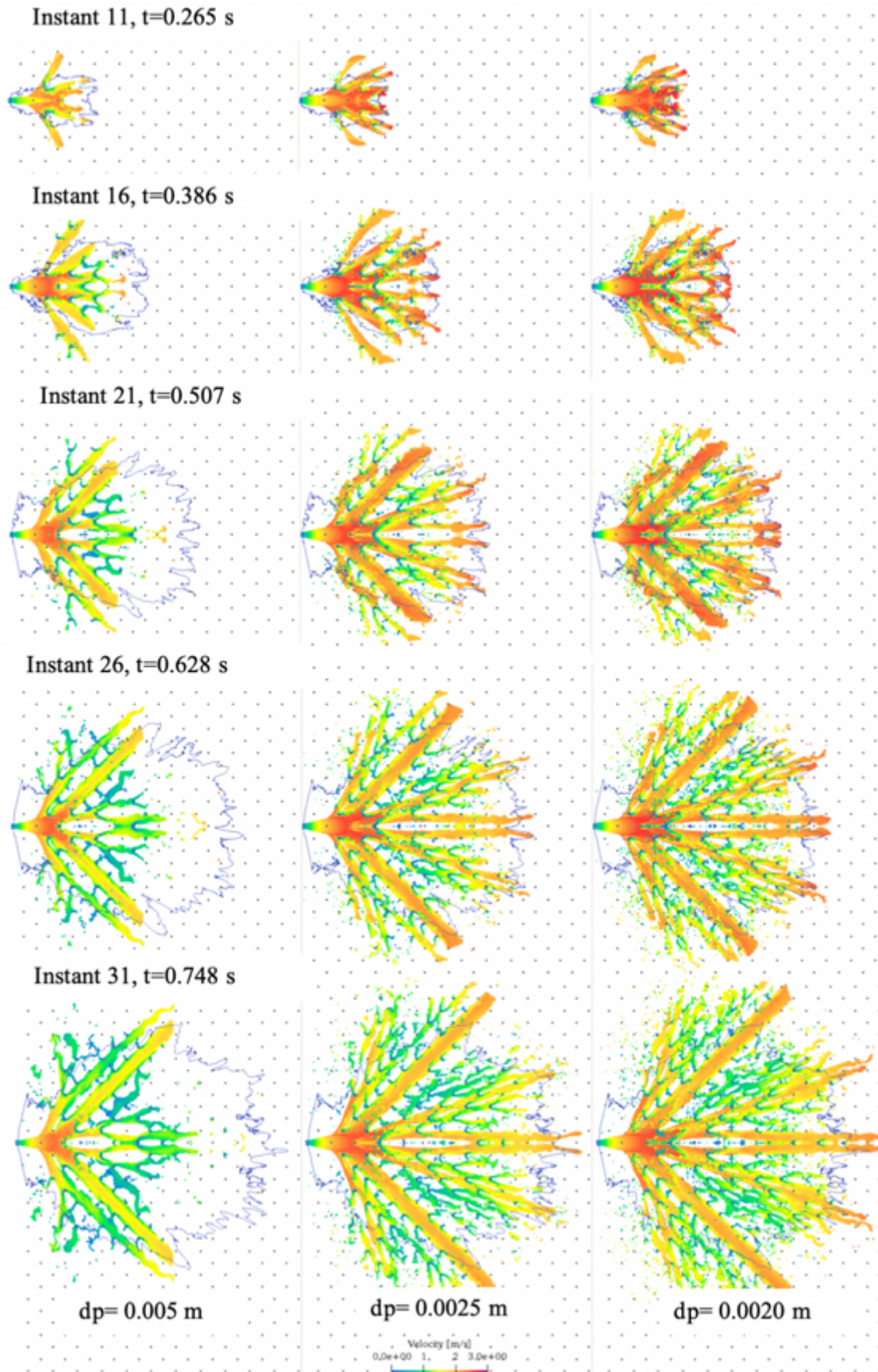


Figure 6.16: Comparison of experimental (blue lines) and SPH (coloured particles) wave fronts for different resolutions with 10x10 rotated mesh. The black dots represent the metallic rods.

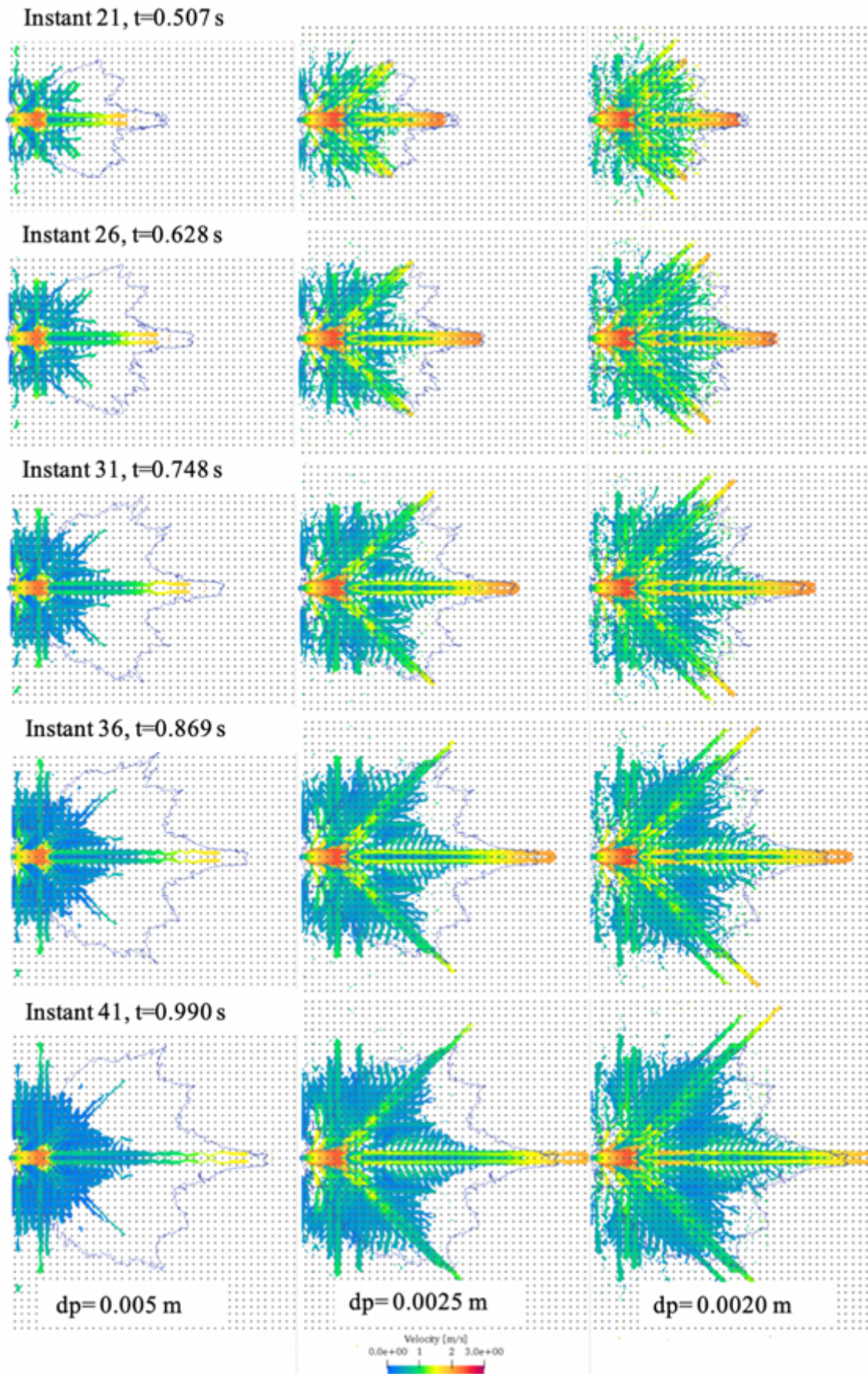


Figure 6.17: Comparison of experimental (blue lines) and SPH (coloured particles) wave fronts for different resolutions with 5x5 regular mesh. The black dots represent the metallic rods.

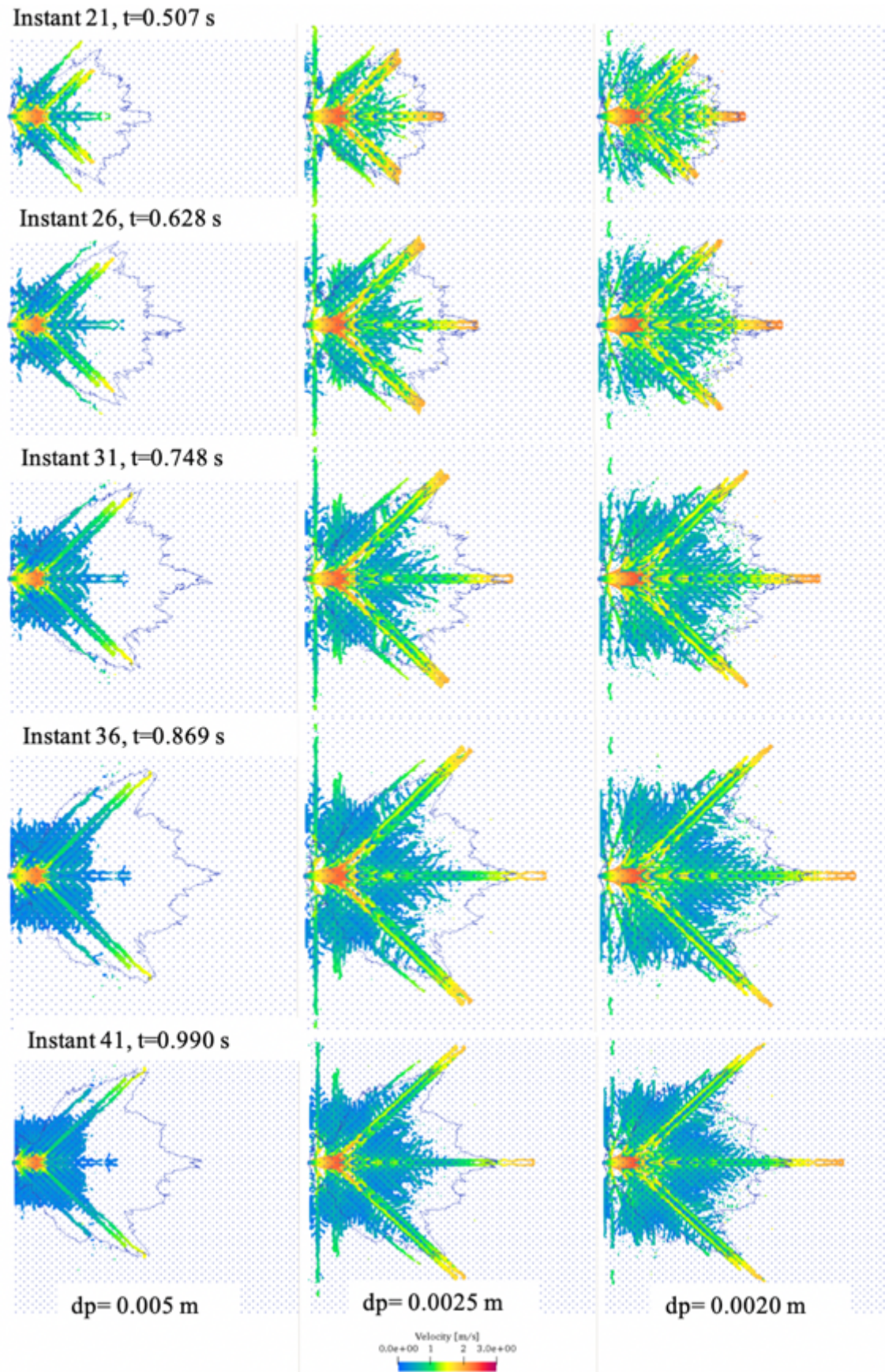


Figure 6.18: Comparison of experimental (blue lines) and SPH (coloured particles) wave fronts for different resolutions with 5x5 rotated mesh. The black dots represent the metallic rods.

According to Figure 6.15, it can be said that the wave front is badly represented by the lower resolution starting from the first instants. In fact, there is a gap almost by 20 cm (considering that the space between two rods is 10 cm). Moving to higher resolutions, SPH is able to reproduce in a proper way the wave fronts of the first 31 instants. The main directions of the water fronts are identified as can be seen in the central area and in the two directions at 45 degrees. Although these good results at the first instants, after 0.748s the wave front starts to increase more than in the experimental data. This is due to lack of resolution on the numerical model. According to the velocity, this is the setup in which the highest velocities are reached from the fluid.

In Figure 6.16 the results are almost as described before. Six main directions can be identified in which the fluid flows reaching velocity of 3m/s. This is the setup in which there are the highest velocities due to the fact that the fluid, in the case of SPH particles, finds preferential runaways. According to the wave front, the experimental results are well represented in the cases of high resolution. Even in this case, only the first 31 instants can be considered as a good result reached by the SPH code. After that, the wave front in the numerical model increases more than the one in the experiment.

Passing to Figure 6.17, the wave front changes its shape due to the change of setup. In fact, in this case it is possible to notice that there are three main directions instead of the five of the past two cases. The wave front is well represented in these three directions whereas it starts to lose information in the areas between the main directions. The lower resolution, $dp=0.005$ m, can be considered as not representative of the experiment. The other two resolutions are quite good and there are not too many differences between them. The highest velocities are reached in correspondence of the impact area and in some areas where the wave front develops. But as can be seen in instants 36 and 41, particles in the front are losing velocity after the impact between them and the rods.

In the end, in Figure 6.18 is shown how SPH is able to reproduce the wave fronts in the cases of high resolution. The low resolution is not even able to reproduce the main directions of the wave front. Passing to the higher resolutions, the numerical wave front reaches good results and it is almost able to represent the experimental one. As before, the highest velocities are in the area of impact and in the fronts.

As a conclusion of this analysis, SPH is able to represent in a really good way the development of the wave front in the case of dam-breaks with this particular configuration of roughness in most of the time of the experiment. The wave fronts represented by the numerical model are good to describe the experimental ones, considering that the white area could be just thin layers that cannot be reproducible in the numerical model. This is due to the value of resolution used in SPH, that is quite high it can be considered that is just 2 mm.

A mention must be done on the running time of these four cases. Considering the steps done for improving efficiency, the cases are studied as symmetric and only for the representation the symmetric part has been created using a code in windows and implemented for the occasion. In this way, the next table represents the running time and number of particles for $dp=0.002$ m and in the case of symmetry.

Table 6.2: Information about the four different cases with rods for a $dp=0.002$ m

case name	np	Runtime
10x10 regular	11,549,517	14.13 h
10x10 rotated	11,550,267	14,30 h
5x5 regular	11,578,767	14.60 h
5x5 rotated	11,579,667	14.52 h

6.2.3 Comparison of the upper part of the free surface profile in proximity of the gate for experiment and different numerical models

One further analysis regarding the experimental data and, in this case, numerical models is the study of the free surface upper shape near the sluice gate. In particular, the numerical models used to compare the experimental results are ParBrezo and Ansys. The experimental analysis was made by D'Oria, 2019. The detection of the profile is shown in Figure 6.19. This is possible using an action camera fixed and through a post-processing MATLAB script.



Figure 6.19: Detection of the free surface profile. Source: D'Oria, 2019.

The other two numerical models are described in Natali, 2019. The cases considered are the dam-breaks with flat bottom for a height of 30 cm in the weir. The results are shown in Figure 6.20.

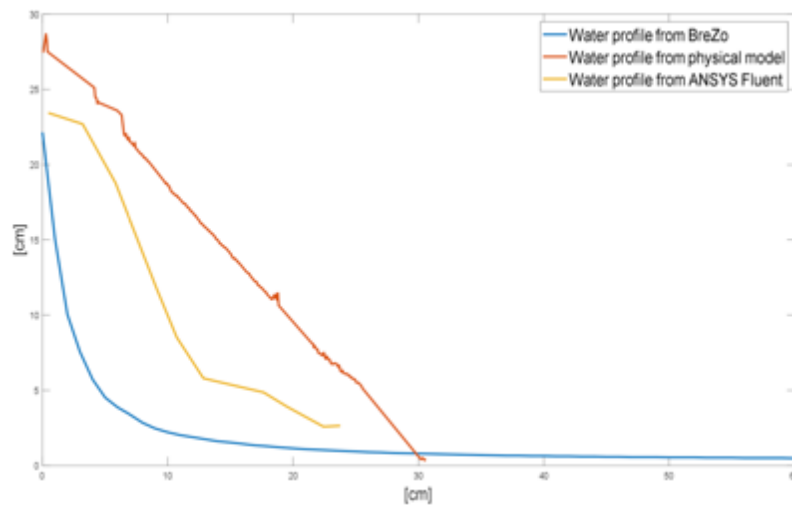


Figure 6.20: Comparison of the upper part of the free surface profile at 1 second for EXP (red line), BreZo (blue line) and Ansys (yellow line). Results are in centimetres. Source: Natali, 2019.

Focusing on Figure 6.20, it can be seen that BreZo cannot be considered reliable to describe the free surface profile. This inability is due to the shallow water approximation, that is at the base of this numerical model.

Differently, results given by Ansys can be considered closer to the experimental ones.

According to SPH, the analysis of the free surface is done using the post-processing tool *MeasureTool*, already described in the previous chapter. In this case the *.txt* file is changed in order to save information every 0.01 m in the *x* direction and with a precision in the *z* direction of 0.0025 m. Considering that SPH is a Lagrangian model, the detection of the free surface is detected through the neighbouring particles at every position along the *z* direction. All the information to run the *MeasureTool* tool are saved in the binary files obtained after running *DualSPHysics*.

The case of study for the detection of the free surface upper profile is the one in absence of roughness, used for validating SPH and described in Chapter 6.

The comparison between SPH and EXP is shown in the Figure 6.21.

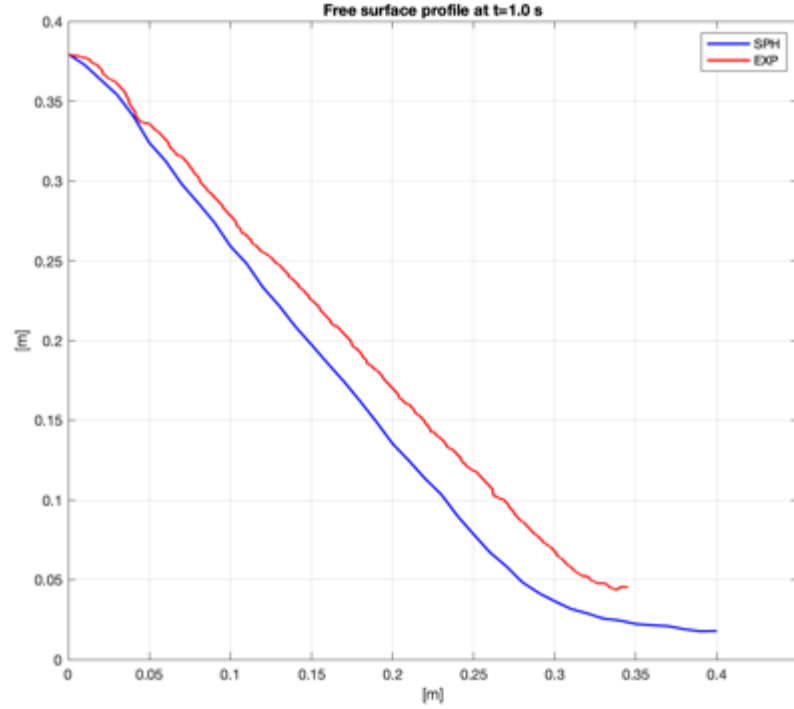


Figure 6.21: Comparison of the upper part of the free surface profile for EXP (red line) and SPH (blue line) at 1.0 second.

The results from SPH can be considered as reliable in the description of the free surface profile. The gap between the two curves is due to the resolution used for the tests, even though it is just 0.002 m.

In the cases of roughness results are exactly the same, with some differences near 0.35 m along the x-axis because of the presence of rods.

6.3 Evaluation of the vulnerability for flat bottom test

The last step that represents one of the aims of this thesis is the evaluation of vulnerability in the downstream area. The model is studied as Froude constant model. This means that:

$$\left\{ \begin{array}{l} \text{Geometric scale: } \lambda = \frac{1}{30} \\ \text{Velocity scale: } \lambda_u = \lambda^{\frac{1}{2}} \\ \text{Time scale: } \lambda_t = \lambda^{\frac{1}{2}} \\ \text{Roughness scale: } \lambda_n = \lambda^{\frac{1}{6}} \\ \text{Reynolds scale: } \lambda_{Re} = \lambda^{\frac{3}{2}} \\ \text{Flow scale: } \lambda_Q = \lambda^{\frac{1}{2}} \end{array} \right.$$

Remembering Equation 1.2, the quantities evaluated from the model can be used to measure the vulnerability in the real case using the following equation:

$$V = u \cdot y = u_m \cdot \lambda^{-\frac{1}{2}} \cdot y_m \cdot \lambda^{-1} = u_m \cdot y_m \cdot 164.31 \quad \left[\frac{m^2}{s} \right] \quad 6.1$$

The analysis of the vulnerability is carried out along the longitudinal direction at 0 cm from the breach in five different points and in the case of flat bottom. The time considered for both of the experiments is 0.99 s.

Table 6.3: Height and velocity in the real case starting from the EXP in five different points.

Position in the EXP [m]	Mean velocity in EXP [m/s]	Mean height in EXP [m]	Position in the real [m]	Velocity in the real [m/s]	Height in the real [m]
0.30	5.80	0.01212	9.00	31.73	0.36
0.50	3.81	0.007849	15.00	20.86	0.23
0.70	3.02	0.007428	21.00	16.52	0.22
0.90	2.28	0.006991	27.00	12.47	0.21
1.00	2.05	0.005977	30.00	13.09	0.18

Table 6.4: Height and velocity in the real case starting from SPH in five different points.

Position in SPH [m]	Mean velocity in SPH [m/s]	Mean height in SPH [m]	Position in the real [m]	Velocity in the real [m/s]	Height in the real [m]
0.30	2.61	0.03431	9.00	12.05	1.02
0.50	2.45	0.0114	15.00	13.41	0.34
0.70	2.44	0.006979	21.00	13.36	0.21
0.90	2.41	0.00633	27.00	13.20	0.19
1.00	2.39	0.005699	30.00	13.09	0.17

Table 6.5: Evaluation of the vulnerability from the EXP data (left) and SPH (right).

Real position [m]	Vulnerability from EXP [m ² /s]	Real position [m]	Vulnerability from SPH [m ² /s]
9.00	11.55	9.00	12.40
15.00	4.91	15.00	4.59
21.00	3.68	21.00	2.80
27.00	2.62	27.00	2.48
30.00	2.01	30.00	2.23

Chapter 7

Conclusion and future perspective

This work of thesis has reached good results in terms of validations. The work is made up of two main parts: the experimental model and the numerical model.

Focusing on the physical model, it can be said that the model itself is at an early stage. This step is necessary before approaching to more complex and closer to real situations. It is reminded that the model is a Froude constant model. It has been demonstrated its validity, through the evaluation of the Reynolds number. This has led to the consideration that the behaviour is not influenced by the viscosity and surface tension.

After this, the next steps are mainly focused on the framework of the model. In fact, the model has a flat downstream area and all the tests are carried out on the flat plane. In the future what can be changed could be the slope of the plane in order to simulate tests closer to real cases.

Another element is the shape of the sluice gate. The collapse of a dam can be various, with a straight dependence on the materials that they are made. Focusing on the case of earthfill dams, the collapse is generated by the progressive enlargement of a triangular shaped hole on the crest. In order to approach to real cases, future tests can be done with new shapes of the sluice gate.

The case presented is based on a medium of all the reservoirs built in the province of Cuneo. The aim is to study the general behaviour of these dams and it is not a specific case. Future implementations can take into account different kinds of vegetation that are in the downstream area.

A further change can be the use of water with different density in order to simulate floods.

Moving to the numerical model, extremely good results are reached. The conclusion is that SPH is able to reproduce the cases under study and it can be considered as valid.

In SPH, the study started with the validation of the case with flat bottom. This test has requested a long campaign in order to find the best solution in terms of discharge ratio and wave fronts. The use of particles has led to a new dimension of the gate, that differs just 2.5 mm from the one used in the physical model. In fact, for a resolution of 0.002 m, the orifice is 3.25 x 40 cm. In terms of wave fronts the result can be considered as reliable just in few instants, but after that the wave fronts increase more that the experimental ones.

Once the flat bottom test was validated, then the attention was paid to the tests with roughness. The presence of rods has incremented the time resolution of the tests, although the wave fronts from the numerical tests fit even better the experimental ones.

In the future a great implementation can be the use of multi GPUs in order to run even more complex tests with lower runtimes. At the moment the results reached are obtained with a single GPU.

The thing that can be done now is the use of a different geometry for the reservoir, always considering that the discharge ratio should fit the one from the experimental data.

The results of the upper part of the free surface profile in proximity of the gate are valid. In order to increase these results, the resolution should be lowered even more. At the moment this passage is not possible because of the time.

In the end, the results about vulnerability are in accordance between the two tests. It is clear that the higher values of vulnerability are in proximity of the gate, where there is the impact between water and surface. Although in the experimental test the water depth near the gate is not correct, results are in agreement. In the next points considered, results of vulnerability are close enough that can be considered reliable.

The choice of a meshfree method has reached really good results, compared to the experiments, and even better results than the mesh-based methods.

Table of figures

Figure 1.1: Nature of dam ownership in the USA. Data taken from the FEMA.	2
Figure 1.2: Main uses of the American Dams documented by the FEMA.....	3
Figure 1.3: Database of the NPDP of main twenty countries in number of dams.....	3
Figure 1.4: Two Australian States with contrasting dam management practices: Tasmania and South Australia Source: Tingey-Holyoak et al., 2012.....	4
Figure 1.5: Definition of the risk and representation of the terms. Image taken from the work of Cordero, S., 2013.....	6
Figure 2.1: Picture of the facility built at the University of Parma and a reconstruction of the facility with the main dimensions. Source: Aureli et al., 2008.....	10
Figure 2.2: Experimental (left) and numerical (right) water depths for test n° 4 at $t=0.40$ s; $t=0.75$ s; $t=1.45$ s; $t=2.16$ s and $t=2.86$ s. Source: Aureli et al., 2008.....	11
Figure 2.3: Set-up of the experimental test and initial conditions for the Dam-break wave over a triangular bottom sill. The pieces of information about the experiment are evaluated at the gauges 1-3. Source: Robb et al., 2015	12
Figure 2.4: Comparison between the experimental and numerical results, for the case of a Dam-break over a dry bed and over a triangle bottom sill. Source: Robb et al., 2015	13
Figure 2.5: Experimental setup in the dam-break wave simulation with an isolated rotated obstacle. All the pieces of information are evaluated at the gauges 1-6. Source: Robb et al., 2015	13
Figure 2.6: Comparison of the results between the numerical and experimental data at the five gauges downstream. Source: Robb et al., 2015	14
Figure 2.7: Information about the free-surface elevation from 0 m (blue) to 0.4 (red) at different times: $t=1.0$ s, $t=3.0$ s, $t=10$ s. Source: Robb et al., 2015.....	14
Figure 2.8: Facility of the experimental model, scale 1:40, made at the Università degli Studi della Basilicata in order to simulate the downstream behaviour after a dam-break event. Source: Albano et al., 2014.	15
Figure 2.9: Time evolution for the up-stream height of the fixed body (h_1) and the same for the down-stream body (h_2). Source: Albano et al., 2014.....	16
Figure 2.10: Time evolution of the x-coordinate for the centre of mass of the bodies (up) and the evolution on the z-coordinate of the centre of mass of the bodies (down). Source: Albano et al., 2014.....	17
Figure 2.11: A brief comparison between the numerical model and the experimental test at the time $t=1.00$ s, $t=1.35$ s, $t=1.40$ s and $t=1.95$ s. Source: Albano et al., 2014.	18
Figure 2.12: Experimental set-up for the dam-break analysis. Source: Turhan et al., 2019	19
Figure 2.13: Measure points in the experimental setup. Source: Turhan et al., 2019...	20
Figure 2.14: Evolution of the free surface at different instants for experiment, RANS and SPH. Source: Turhan et al., 2019.	20
Figure 2.15: Evolution of the free surface in case of reflection of the wave at different instants for experiment, RANS and SPH. Source: Turhan et al., 2019.	21
Figure 2.16: Flow depth variation during the 3 s of the experiment considered. Source: Turhan et al., 2019.	21
Figure 3.1: Position of the physical model in the Hydraulics Laboratory in Turin.	24
Figure 3.2: General overlook over the physical model with the correct dimensions (left) and a section of the model (right).	25
Figure 3.3: Upstream reservoir in the Hydraulics laboratory in Turin.	26

Figure 3.4: Technical description of the twelve Balluff sensors that are used in the physical model taken from the manual.	27
Figure 3.5: Variation of the water surface during an experimental test, obtained after processing the sensors' data. It represents just the variation of the water in the correct dimensions of the reservoir.	28
Figure 3.6: Picture of the sliding gate on which is possible to recognize the two magnets both on the reservoir and on the gate. Source: Natali, M., 2019.	28
Figure 3.7: Photo taken into the physical model to show the led lightning and the PVC matte white stratus.	30
Figure 3.8: Image of the Andor Zyla 5.5 sCMOS camera. Source: https://andor.oxinst.com	31
Figure 3.9: Global shutter mode. Source: https://andor.oxinst.com	31
Figure 3.10: Images of the Nikon DSLRD810 camera and lens. Source: official website of Nikon https://www.nikon.it	32
Figure 3.11: Photos taken in the configuration with panels 100 mm x 100 mm with angle of 0° (left) and 45° (right).	34
Figure 3.12: Photos taken in the configuration with panels 50 mm x 50 mm with angle of 0° (left) and 45° (right).	34
Figure 4.1: Overview of the layout of the physical model.	36
Figure 4.2: Binary images for mesh 10x10 0° (left) and 45° (right)	39
Figure 4.3: Binary images for mesh 5x5 0° (left) and 45° (right)	39
Figure 4.4: Wave front detection for mesh 10x10 at 0° (left) and 45° right at instant 41	40
Figure 4.5: Wave front detection for mesh 5x5 at 0° (left) and 45° right at instant 41 .	40
Figure 4.6: Temporal evolution of the wave front in the case of mesh 10x10 0° (left) and 45° (right).	41
Figure 4.7: Temporal evolution of the wave front in the case of mesh 5x5 0° (left) and 45° (right).	41
Figure 4.8: Representation of the eleven sectors in the tests with mesh 10x10 with 0° (left) and 45° (right).	42
Figure 4.9: Representation of the eleven sectors in the tests with mesh 5x5 with 0° (left) and 45° (right).	42
Figure 4.10: Comparison of cumulative distance in all sectors for test with mesh 10x10 with 0°	43
Figure 4.11: Comparison of cumulative distance in all sectors for test with mesh 10x10 with 45°	43
Figure 4.12: Comparison of cumulative distance in all sectors for test with mesh 5x5 with 0°	44
Figure 4.13: Comparison of cumulative distance in all sectors for test with mesh 5x5 with 45°	44
Figure 4.14: Velocity in sector 6 for test with mesh 10x10 with 0°	45
Figure 4.15: Velocity in sector 6 for test with mesh 10x10 with 45°	45
Figure 4.16: Velocity in sector 6 for test with mesh 5x5 with 0°	46
Figure 4.17: Velocity in sector 6 for test with mesh 5x5 with 45°	46
Figure 4.18: Measurements of the spectrometer of the k in function of the wavelength λ within 1 cm. Source: Briano, 2019.	48
Figure 4.19: Trend of the parameter k' in dependence of $\ln(h)$ in the aquarium. Source: Briano, 2019.	49
Figure 4.20: Trend of the parameter k' in dependence of the height h for all the different campaigns. Source: Briano, 2019.	49

Figure 4.21: Conversion curve from intensity to depth. Source: Briano 2019.....	50
Figure 4.22: Independent flows from orifices. Source: Horton, 1907.....	50
Figure 4.23: Envelope of the flows passing through parallel orifices	53
Figure 5.1: Quintic kernel and the derivative divided by the factor αD . Source: Domínguez, 2014.....	57
Figure 5.2: Kernel function (W) and smoothing length (h).....	58
Figure 5.3: Institutions involved in the DualSPHysics project.....	63
Figure 5.4: Webpage of DualSPHysics. Source: dual.sphysics.org	64
Figure 5.5: Creation of a triangle using particles. Source: XML Guide for DualSPHysics v4.4.....	65
Figure 5.6: Xml code for defining the case.....	66
Figure 5.7: Geometry of the tank with planes (left) and particles (right).	67
Figure 5.8: Workflow of DualSPHysics. Source: XML Guide for DualSPHysics v4.4.	68
Figure 5.9: How to set the positions for measuring quantities in MeasureTool.	69
Figure 5.10: How to create the box in FlowTool.....	69
Figure 5.11: Screenshot of the .bat file.....	70
Figure 5.12: Image of the experiment of the dam-break. Source: Fraccarollo and Toro (1995).	71
Figure 5.13: Numerical setup of the dam-break including dimensions and position of the gauges.	72
Figure 5.14: Different instants of the TestFT3 ($dp=0.0075$ m) using DualSPHysics....	73
Figure 5.15: Comparison of experimental and numerical water elevation for different resolutions.	74
Figure 5.16: Time series of the numerical inflow for different resolutions with DualSPHysics.	75
Figure 6.1: Numerical SPH setup.	78
Figure 6.2: Representation of the upstream reservoir with gauges.....	79
Figure 6.3: Different instants of the simulation. Comparison between the experimental data (blue line) and numerical model (coloured particles).	80
Figure 6.4: Comparison of free surface elevation both in physical and numerical model.	81
Figure 6.5: Comparison between symmetric and non-symmetric wave fronts at two instants.	82
Figure 6.6: Numerical models in case of complete tank (left) and reduced tank (right) with their sizes. The first row is the bottom view in the case of complete geometry; the second is the bottom view for the reduced tank and the third is the lateral view of the reduced tank.	83
Figure 6.7: Inflow for different resolution.....	84
Figure 6.8: Comparison between experimental data and SPH wave front for different resolutions.	85
Figure 6.9: Position of the longitudinal directions for the evaluation of the water depth	86
Figure 6.10: Water depth at a distance of -35 cm from the breach. The red line is SPH and the green the EXP.....	86
Figure 6.11: Water depth at a distance of 0 cm from the breach. The red line is SPH and the green the EXP.	87
Figure 6.12: Water depth at a distance of 35 cm from the breach. The red line is SPH and the green the EXP.....	87
Figure 6.13: How to create rods in SPH.	88

Figure 6.14: Four different configurations for downstream area with rods. On the left there are the regular geometries (0°) for mesh 10x10 (up) and 5x5 (down). On the right there are the rotated geometries (45°) for mesh 10x10 (up) and 5x5 (down).....	89
Figure 6.15: Comparison of experimental (blue lines) and SPH (coloured particles) wave fronts for different resolutions with 10x10 regular mesh. The black dots represent the metallic rods.....	90
Figure 6.16: Comparison of experimental (blue lines) and SPH (coloured particles) wave fronts for different resolutions with 10x10 rotated mesh. The black dots represent the metallic rods.....	91
Figure 6.17: Comparison of experimental (blue lines) and SPH (coloured particles) wave fronts for different resolutions with 5x5 regular mesh. The black dots represent the metallic rods.....	92
Figure 6.18: Comparison of experimental (blue lines) and SPH (coloured particles) wave fronts for different resolutions with 5x5 rotated mesh. The black dots represent the metallic rods.....	93
Figure 6.19: Detection of the free surface profile. Source: D'Oria, 2019.....	95
Figure 6.20: Comparison of the upper part of the free surface profile at 1 second for EXP (red line), BreZo (blue line) and Ansys (yellow line). Results are in centimetres. Source: Natali, 2019.....	96
Figure 6.21: Comparison of the upper part of the free surface profile for EXP (red line) and SPH (blue line) at 1.0 second.....	97

Bibliography

- Albano, R., Mirauda, D., Sole, A., 2014. N.d. Experimental validation of a 3D SPH model for the simulation of a dam-break event involving multiple fixed and mobile bodies. *Engineering Geology* 8.
- Altomare, C., Crespo A.J.C., Domínguez, J.M., Gómez-Gesteira, M., Suzuki, T., Verwaest, T., 2015. Applicability of Smoothed Particle Hydrodynamics for estimation of sea wave impact on coastal structures. *Coastal Engineering*, 96: 1-12. doi:10.1016/j.coastaleng.2014.11.001.
- Altomare, C., Domínguez, J.M., Crespo, A.J.C., González-Cao, J., Suzuki, T., Gómez-Gesteira, M., Troch, P., 2017. Long-crested wave generation and absorption for SPH-based DualSPHysics model. *Coastal Engineering*, 127: 37-54 doi: 10.1016/j.coastaleng.2017.06.004.
- Aureli, F., Maranzoni, A., Mignosa, P., Ziveri, C., 2008. Dam-Break Flows: Acquisition of Experimental Data through an Imaging Technique and 2D Numerical Modeling. *J. Hydraul. Eng.* 134, 1089–1101.
- Batchelor, G.K., 1974. *Introduction to fluid dynamics*. Cambridge University Press.
- Beer, A., 1852. Determination of the absorption of red light in coloured liquids, in *Annalen der physik und Chemie*, pp. 78-88.
- Black, R.D., 1975. Flood Proofing Rural Residences. A Project Agnes Report, Department of Agricultural Engineering, Cornell University, New York.
- Bouguer, P., 1729. *Essai d'optique sur la gradation de la lumière*. Parigi, Claude Jombert, pp. 16-22.
- Briano, J., 2019, “Analisi sperimentale dell’onda di dam break su superfici lisce e vegetate” *Circ. Min. LL.PP.* 19 aprile 1995, n. US/482, 1995. 5.
- Clausen, L., Clark, P. B., 1990. "The development of criteria for predicting dambreak flood damages using modelling of historical dam failures." *International Conference on River Flood Hydraulics*, John Wiley & Sons Ltd.
- Cordero, S., Poggi, D., Grimaldi, S., 2013. “Modellazione numerica delle onde di dam-break, caso studio: gli sbarramenti in terra”
- Crespo, A.J.C., Gómez-Gesteira, M., Dalrymple, R.A., 2007. Boundary Conditions Generated by Dynamic Particles in SPH Methods. *CMC: Computers, Materials, & Continua*, 5(3): 173-184.
- Crespo, A.J.C., Domínguez, J.M., Barreiro, A., Gómez-Gesteira, M., Rogers, B.D., 2011. GPUs, a new tool of acceleration in CFD: Efficiency and reliability on Smoothed Particle Hydrodynamics methods. *PLoS ONE* 6 (6), e20685, DOI: 10.1371/journal.pone.0020685.
- Crespo, A.J.C., Domínguez, J.M., Rogers, B.D., Gómez-Gesteira, M., Longshaw, S., Canelas, R., Vacondio, R., Barreiro, A., García-Feal, O., 2015. DualSPHysics: open-source parallel CFD solver on Smoothed Particle Hydrodynamics (SPH). *Computer Physics Communications*, 187: 204-216. doi: 10.1016/j.cpc.2014.10.004.
- D’Oria, A.D., 2019, “Studio sperimentale di onde di collasso su superfici non confinate” *Dam Ownership in the United States | FEMA.gov [WWW Document]*, n.d. URL <https://www.fema.gov/dam-ownership-united-states> (accessed 5.27.19).
- Dlgs 112/98 <http://www.parlamento.it/parlam/leggi/deleghe/98112dl.htm>
- Domínguez, J.M., Crespo, A.J.C., Gómez-Gesteira, M., 2013. Optimization strategies for CPU and GPU implementations of a smoothed particle hydrodynamics method. *Computer Physics Communications*, 184(3): 617-627. doi:10.1016/j.cpc.2012.10.015.

- Domínguez, J.M., Crespo, A.J.C., Valdez-Balderas, D., Rogers, B.D., Gómez-Gesteira, M., 2013. New multi-GPU implementation for Smoothed Particle Hydrodynamics on heterogeneous clusters. *Computer Physics Communications*, 184: 1848–1860. doi:10.1016/j.cpc.2013.03.008.
- Domínguez, J.M., 2014 “DualSPHysics: Towards High Performance Computing using SPH technique”
- FLOW-3D® Version 12.0 User’s Manual (2018). FLOW-3D [Computer software]. Santa Fe, NM: Flow Science, Inc. <https://www.flow3d.com>
- Fraccarollo, L., Toro, E. F. 1995. Experimental and numerical assessment of the shallow water model for two-dimensional dam-break type problems. *Journal of Hydraulic Research*, 33(6), 843–864.
- Gingold, R.A., Monaghan, J.J., 1977. Smoothed particle hydrodynamics: theory and application to non- spherical stars. *Monthly Notices of the Royal Astronomical Society* 181, 375–389.
- Hager, W.H., Visher, D.L., 1998. “*Dam Hydraulics*”. Wiley.
- Horton, R. E., 1906. Weir Experiments, Coefficients, and Formulas. [U.S. Geological Survey Water Supply and Irrigation Paper No. 150. Series M, General Hydrographic Investigations, 16.]
- Horton, R. E., 1907. Weir Experiments, Coefficients and Formulas, Department of the Interior - United States geological survey, Washington.
- Ingle, J. D., Crouch, S. R., 1988. *Spectrochemical Analysis*, New Jersey: Prentice Hall.
- Lambert, J. H., 1760. *Photometria*. Augsburg, Germania: Eberhardt Klett.
- Lauber, G., Hager, W., 1998. Experiments to dam-break wave: horizontal channel. *Journal of Hydraulic Research* (3, 291-304).
- Lucy, L.B., 1977. A numerical approach to the testing of the fission hypothesis. *The Astronomical Journal* 82, 1013–1024, DOI: 10.1086/112164.
- Gómez-Gesteira, M., Dalrymple, R., 2004. Using a 3D SPH method for wave impact on a tall structure. *Journal of Waterway, Port, Coastal and Ocean Engineering* 130 (2), 63-69.
- MATLAB, «MATLAB release R2018b Documentation» 2018.
- Monaghan, J.J., 1994. Simulating free surface flows with SPH. *Journal of Computational Physics* 110, 399- 406, DOI: 10.1006/jcph.1994.1034.
- Monaghan, J.J., Kos, A., 1999. Solitary waves on a Cretan beach. *Journal of Waterway, Port, Coastal and Ocean Engineering* 125(3), 145-154.
- Monaghan, J.J., Cas, R.A.F., Kos, A.M., Hallworth, M., 1999. Gravity currents descending a ramp in a stratified tank. *Journal of Fluid Mechanics* 379, 39–70.
- Monaghan, J.J., 2005, Smoothed Particle Hydrodynamics. *Reports on Progress in Physics* 68(8), 1703-1759, DOI: 10.1088/0034- 4885/68/8/R01.
- Molteni, D., Colagrossi, A., 2009. A simple procedure to improve the pressure evaluation in hydrodynamic context using the SPH. *Computer Physics Communications* 180(6), 861–872, DOI: 10.1016/j.cpc.2008.12.004
- Natali, M., 2019, Experimental and numerical analysis of dam-break waves propagation on vegetated slopes.
- OpenFOAM User Guide: 4.1.
- Pisaniello, J.D., 2011. A Comparative Review of Environmental Policies and Laws Involving Hazardous Private Dams: “Appropriate” Practice Models for Safe Catchments 35, 67.
- Poggi, D., Cordero, S., 2015. Report Finale Azione 3.1. Metodi speditivi per la mappatura di aree vulnerabili per onde dovute al collasso di sbarramenti.

- Price, J, Lewis, B., Rutherford, I., 2003. Water Quality in Small Farm Dams, 28 INT'L HYDROLOGY & WATER RES.
- Ritter, A., 1892. "The propagation of water waves". V.D.I. Zeitscher (Berlino), 36(2), 947-954.
- Robb, D., Vasquez, J., 2015. Numerical simulation of dam-break flows using depth-averaged hydrodynamic and three-dimensional CFD models.
- Sakamoto, T., Yamaguchi, Y., n.d. Dams and Storage Reservoirs 9.
- Sangrey, D. A., Murphy, P. J., Nieber, J. L., 1975. *Evaluating the Impact of Structurally Interrupted Flood Plain Flows*. Technical Report No. 98, Cornell University Water Resources and Marine Sciences Center, Ithaca, New York, USA.
- Soares-Frazão, S., 2007. Experiments of dam-break wave over a triangular bottom sill. *Journal of Hydraulic Research*, 45(sup1), 19-26.
- Soares-Frazão, S., Zech, Y., 2007. Experimental study of dam-break flow against an isolated obstacle. *Journal of Hydraulic Research*, 45(sup1), 27-36.
- TELEMAC-2D • Version 4.0 – User's Manual.
- The Role of Dams in the XXI Century - Dam Engineering & Construction, 2013. Dams, Piano Keys Weirs, Tidal Energy & Energy Storage. URL <http://www.hydrocoop.org/the-role-of-dams-in-the-xxi-century/>
- Tingey-Holyoak, J.L., Pisaniello, J.D., Burritt, R.L., Spassis, A., 2013. Incorporating on-farm water storage safety into catchment policy frameworks: International best practice policy for private dam safety accountability and assurance. *Land Use Policy* 33, 61–70. <https://doi.org/10.1016/j.landusepol.2012.12.011>
- Turhan, E., Ozmen-Cagatay, H., Tantekin, A., 2019. MODELING FLOOD SHOCK WAVE PROPAGATION WITH THE SMOOTHED PARTICLE HYDRODYNAMICS (SPH) METHOD: AN EXPERIMENTAL COMPARISON STUDY. *Appl. Ecol. Env. Res.* 17, 3033–3047.
- Wendland, H., 1995. Piecewise polynomial, positive definite and compactly supported radial functions of minimal degree. *Advances in Computational Mathematics* 4, 389-396.
- Xml guide of DualSPHysics available in the package of DualSPHysics.

Acknowledgement

Alla fine di questo lavoro è doveroso ringraziare il Prof. Davide Poggi e Silvia Cordero per l'opportunità datami e per i loro chiarimenti e consigli durante questo lavoro di tesi, il quale ha finalmente ha condotto al raggiungimento della tanto desiderata laurea. Assieme a loro c'è sicuramente da ringraziare il gruppo EPhysLab di Ourense, un gruppo coeso e variegato che mi ha fatto passare momenti fantastici. In particolare, ci tengo a ringraziare Alex e Jose, professori e ricercatori fantastici che mi hanno messo sotto torchio per quasi due mesi e da cui ho imparato tantissimo.

Un GRAZIE va alla mia famiglia per il sostegno continuo in questi anni di università, non facendomi pesare e mancare nulla. Spero di ripagare un giorno tutti i vostri sacrifici. Ringrazio anche tanto mia sorella Alessia sempre pronta a sostenermi prima di un esame e a risollevare il morale nei tempi bui. Vi voglio bene.

Ringrazio Francesca, sempre presente e sempre pronta a sostenermi da quando è al mio fianco. Hai assecondato le mie scelte e di questo te ne sono infinitamente grato. Se ora siamo qui, il merito è anche tuo. Con la tua vicinanza e il tuo amore sei riuscita a tirare fuori il meglio di me.

Tutti gli amici, vicini e lontani, e tutte le persone conosciute durante questo lungo percorso universitario che sono diventate una seconda famiglia.

Infine, tutti i miei parenti, sempre pronti a informarsi e sostenermi.

A tutti voi dico ancora una volta GRAZIE.